ATTACHMENT 1

Appendix A

Review of Evidence Regarding the Mode of Action for the Carcinogenicity of Chromium

APPENDIX A

REVIEW OF EVIDENCE REGARDING THE MODE OF ACTION FOR THE CARCINOGENICITY OF CHROMIUM

A two year cancer bioassay was completed for Cr(VI) (i.e., sodium dichromate dihydrate) in drinking water by the US National Toxicology Program (NTP, 2008; Stout et al., 2008). The NTP study design resulted in the development of intestinal tumors in mice and oral mucosal tumors in rats at daily concentrations in excess of 85 mg/L. Qualitative evidence for the human carcinogenicity of chromium is strong following inhalation exposures: a number of epidemiological studies in several different chrome industries have demonstrated an increased incidence of lung cancer mortality in workers chronically exposed to chromium compounds. However, there are no epidemiological studies indicating carcinogenicity following oral exposures.

Chromium is a naturally occurring essential trace element and exists in oxidation states ranging from -2 to 6+; however, the trivalent (+3) and hexavalent (+6) states are the only forms which may be found in the environment (ATSDR 1989; Snow and Xu 1991; Fan and Harding-Barlow 1987; De Flora and Wetterhahn 1989; Tandon 1985), with Cr3+ being more stable than Cr6+ (Shi and Dalal 1988; Petrilli et al. 1986; IARC 1980; Bianchi et al. 1980). Further, Cr6+ and Cr3+, as well as other chromium valences, do not typically exist as simple ions, but rather as molecules compounded with oxygen and other elements (Jones 1990). However, for the purpose of clarity in this paper, we will refer to the various forms of chromium by their valence state, i.e., Cr6+, Cr3+, etc.

Cr6+ is produced through industrial processes in the manufacturing of steel and alloys, chrome plating, and wood and water treatments, while Cr3+ is naturally occurring in the environment (ATSDR 1989; IARC 1980). Cr6+ readily crosses cell membranes and is rapidly reduced to Cr3+ *in vivo* by numerous processes (Mertz 1969).

Cr3+ i an essential nutrient (ILSI 1990) required for the maintenance of normal glucose metabolism (Hopkins et al. 1968), and is essentially nontoxic (Connett and Wetterhahn 1985; NAS 1974). Cr3+ does not cross cell membranes under normal physiological conditions. However, Cr3+ can pass across the membrane if it is bound to ligands. Ligand-binding would allow Cr3+ to cross the cell membrane via passive diffusion, which is much slower than the rate of actively transported Cr6+ (Patierno 1996).

Inhalation exposure to Cr6+ has been associated with an increased incidence of lung cancer in occupational and animal studies (Standeven and Wetterhahn 1989; Rossi et al. 1988; Shi and Dalal 1988). However, the valence state of chromium responsible for the observed tumorigenicity has been the subject of much study, but with very little conclusive results. This dilemma results from the observation that it is Cr+6 (and not Cr+3) that crosses the cell membrane, but Cr6+ has not been shown to interact directly with genetic material, as will be discussed later. However, test results indicate that numerous forms of metabolic intermediates and the ultimate metabolic form, Cr3+, may be capable of interaction with intracellular nuclear material believed to initiate the carcinogenic process. Therefore, an understanding of the metabolic fate and behavior of chromium, both extra- and intracellularly, is critical to understanding possible mechanisms of action.

Effects of Chemical Form and Solubility on Carcinogenicity

Key issues regarding the dose-response for chromium exposure are the impact of the oxidation state (trivalent vs. hexavalent), the specific chromium compound (lead chromate, calcium chromate, chromic oxide, etc.) and solubility. In considering the properties and biological effects of chromium, the two principal oxidation states, Cr3+ (trivalent) and Cr6+ (hexavalent) must be distinguished. Trivalent chromium is by far the most stable form, both in the environment (Cotton and Wilkinson 1966) and in biological systems (Mertz 1969), and for practical purposes oxidation of trivalent to hexavalent does not occur in biological systems (WHO 1988). Hexavalent chromium, on the other hand, is a potent oxidizing agent (Cotton and

Wilkinson 1966), and is readily reduced to the trivalent form *in vivo* (Feldman 1968; Mertz 1969).

The trivalent and hexavalent forms are very different in their observed biological activities (WHO 1988; Grant and Mushak 1989). Hexavalent chromium compounds are corrosive oxidizing agents which cause local irritation and systemic nephrotoxicity (Gad 1989). In contrast, trivalent chromium is an essential nutrient (AMA 1979), required for the maintenance of normal glucose metabolism (Hopkins et al. 1968), and is essentially nontoxic (NAS 1974). Recently, NTP evaluated the toxicity and carcinogenicity of chromium picolinate (CP) in a two year feeding study (Stout et al., 2009). CP, which is a human nutritional supplement and designed to increase absorption of Cr3+, was administered in the feed of both mice and rats. No toxicity or carcinogenicity was observed in this study.

Chromium compounds are generally mutagenic, whereas the evidence for the mutagenicity of trivalent compounds is equivocal (DeFlora et al. 1990). Hexavalent chromium compounds have been associated with the production of lung cancer from inhalation in both animals (Langard 1988) and humans (Langard 1990). The equivocal epidemiological evidence from primarily trivalent chromium exposures in the ferrochromium industry, as contrasted with the clear evidence of carcinogenicity from primarily hexavalent exposures in the chromate production industry, suggests that hexavalent chromium, rather than trivalent, is responsible for the observed induction of lung cancer (Langard et al. 1990).

However, the World Health Organization (WHO), in an attempt to determine if there was sufficient data to determine the relationship between the risk of cancer and exposures to the trivalent or hexavalent forms of chromium compounds, reported conflicting conclusions from epidemiological studies regarding exposures to trivalent chromium and cancer risk (WHO 1988). In their review, WHO noted that in most of the available epidemiological studies, exposures were poorly characterized (i.e., it was difficult to determine if workers had been exposed to trivalent chromium, hexavalent chromium or both). The authors of some epidemiological studies have concluded that exposures to trivalent chromium compounds were not associated with an

increased risk of lung cancer (Korallus et al. 1974a,b,c; Axelsson et al. 1980; Langard et al. 1980; Norseth 1980). However, other authors have not reached the same conclusions (Essing et al. 1971; Mancuso 1975; Zober 1979). Based on a review of epidemiological data, including case reports, collected from studies of the chromate-producing, chromium-plating, chromate-pigment and ferrochromium industries, IARC has concluded that there is sufficient evidence of cancer of the respiratory tract in workers occupationally exposed to chromium in the chromate plating industry; however, the data are insufficient to draw conclusions regarding lung cancer risk in other occupations with potential exposures to chromium (WHO 1988). IARC has also concluded that the data are inadequate to determine the relative contributions of metallic chromium, trivalent chromium, hexavalent chromium, soluble chromium and insoluble chromium to cancer risk (WHO 1988).

WHO (1988) also reviewed the inhalation carcinogenicity studies conducted in animals. Nettesheim et al. (1971) exposed 136 mice to13 mg calcium chromate/m^3, 5 hours/day, 5 days/week for lifetime. There were 14/136 lung adenomas reported in the treated group, compared to 5/136 in the controls. There were no carcinomas reported. In a study where rats, mice and guinea pigs (number of animals/group not specified) were exposed to mixed chromate dust, 3-4 mg $Cr0_3/m^3$, 4-5 hours/day, 4 days/week for lifetime or 50 weeks, respectively, via inhalation, only three alveologenic adenomas were identified in 50 exposed guinea pigs (Steffee and Baetjer 1965). In rats exposed to 2 mg calcium chromate/m^3, for 589 exposures over 891 days, one lung squamous cell carcinoma, one squamous cell carcinoma of the larynx, and one peritruncal tumor were reported (Laskin et al. 1970; Laskin 1972). In hamsters exposed using the same protocol as for the rats, one papilloma and one squamous cell carcinoma of the larynx were reported. The number of animals/group was not specified for either study.

Mechanistically, the difference in the effects of the two valence states can be understood as resulting from two factors: cellular transport and oxidation potential. Although trivalent chromium has been shown to react with DNA in solution, it is to a large extent inactive with intact cells and tissues (DeFlora et al. 1990). The relative *in vivo* inactivity of trivalent chromium appears to result from the fact that it does not readily cross the cell membrane, in

contrast with hexavalent chromium, which readily crosses the cell membrane (Levis et al. 1978). It has been suggested that the rapid cellular uptake of hexavalent chromium is mediated by the sulfate transport system and results from the similarity of the chromate ion to sulfate ion (Wetterhahn 1981). At any rate, once hexavalent chromate reaches the interior of the cell, it is reduced to the trivalent form, which is then trapped inside the cell (Grogan 1958; Mertz 1969). Alternative theories for the carcinogenic effects of hexavalent chromium are based on (1) the intracellular production of trivalent chromium, which reacts directly with DNA or inhibits DNA repair enzymes (Tamino et al. 1981), or (2) the formation of reactive intermediates (e.g., pentavalent chromium) produced in the intracellular reduction of hexavalent chromium (Wetterhahn 1981; Wetterhahn and Hamilton 1989), as will be discussed later.

Epidemiological studies were also reviewed to determine if data regarding the carcinogenicity of specific chromium compounds were presented (Alexander et al. 1996; Aw 1997; Dalager et al. 1980; Davies 1984; Davies et al. 1991; Franchini et al. 1983; Hayes 1988; Langard 1990, 1993; Langard and Norseth 1975; Lees 1991; Mancuso 1997; Moulin 1997; Rafnsson et al. 1997). Excess lung cancer risk was reported in several of the studies reviewed (Aw 1997; Dalager et al. 1980; Davies 1984; Davies et al. 1991; Franchini et al. 1983; Langard and Norseth 1975; Mancuso 1997; Moulin 1997; Rafnsson et al. 1997). Alexander et al. (1996) reported there was no clear association between chromium exposures and lung cancer risk in workers in the aerospace industry exposed to various chromium pigments that include zinc, strontium and lead chromate or to chromium trioxide. In the epidemiological studies reviewed, exposures were poorly characterized and exposures to specific chromium compounds were determined based on the various materials used and processes performed at the plants. It should be noted that none of these studies evaluated a cohort where exposures were exclusively to a specific chromium compound, i.e., the workers in these study cohorts were exposed to more than one chromium compound. In addition, other confounding factors, such as smoking habits and exposures to other chemicals, were not evaluated in all of the studies. Therefore, from the epidemiological data reviewed, the potential carcinogenicity of a specific chromium compound cannot be stated with certainty, although Langard (1993) noted that based on a review of the epidemiological data, zinc and calcium chromate appeared to be more potent than lead chromate. However, in a

comprehensive review of the epidemiological studies of workers in the various chromium industries, Lees (1991) concluded that due to inadequate worker exposure data, the risks associated with exposures to a particular chromium compound could not be determined.

Additionally, a change in the refining process of chromite ore may have resulted in a decreased risk of lung cancer in workers employed after this change (Aw 1997; Davies et al. 1991). The previous "high lime" method involved the addition of calcium carbonate or calcium magnesium carbonate to chromite ore resulting in the formation of calcium chromate, which was reported to be carcinogenic following implantation into the lungs of rats (Laskin et al. 1970; Levy and Vennitt 1975; Levy and Martin 1983). In the current "low lime" methods, these calcium-containing materials are not used. Therefore, workers were not exposed to calcium chromate (Aw 1997; Davies et al. 1991).

Differences in the solubilities of inhaled hexavalent chromate compounds have also been found to affect their carcinogenic potency (Langard 1990). Evidence from epidemiological studies and animal studies support the generalization that the less soluble chromate salts (e.g., Zn, Ca, and Sr chromate) are the most potent respiratory carcinogens, while the highly soluble salts (e.g., Na, K, and ammonium chromate) are less active (Gibb and Chen 1989; Hathaway 1989). Presumably, the less soluble salts serve as a persistent source of locally available chromium. For example, following the implantation of cholesterol pellets containing different chromium compounds into the bronchi of rats, bronchogenic carcinomas were produced in rats that received implants containing calcium or zinc chromate; however, bronchogenic carcinomas were not observed in rats that received soluble chromates or trivalent chromium chemicals (Laskin et al. 1970; Levy and Vennitt 1975). Levy and Martin (1983) reported that sparingly soluble chromates, including strontium and calcium chromate and to a lesser extent some forms of zinc chromate, were carcinogenic in rats following implantation as described above. In contrast, a much weaker response was observed in rats that received barium or lead chromate, when compared with the response observed in rats that received calcium or strontium chromate. However, based on reviews of the epidemiologic data, Mancuso (1997) and Langard (1993) noted that there was some evidence that exposures to soluble chromium may result in lung cancer.

Extracellular Reduction of Chromium VI

Following exposure to chromium, several mechanisms exist for extracellular reduction of Cr6+ to Cr3+. Much of Cr6+ ingested or inhaled is reduced to poorly absorbed Cr3+ before the Cr6+ reaches membranes through which it might be absorbed. When ingested, Cr6+ is rapidly reduced by saliva and gastric juices. When inhaled, Cr6+ is reduced by interaction with fluids and cells of the lung (DeFlora and Wetterhahn 1989; Snow 1992; Jones 1990; Petrilli et al. 1986). The reduction of Cr6+ to Cr3+ is an important defense mechanism, since Cr3+ readily complexes with other extracellular components and does not permeate the cell membrane (Bianchi and Levis 1985; Petrilli et al. 1986; Suzuki 1988; Korallus et al. 1984). Studies have shown that the reduction of Cr6+ to Cr3+ is through saturable kinetic processes, when tested at physiological pH (Connett and Wetterhahn 1985; Snow 1992; Petrilli et al. 1986; Standeven and Wetterhahn 1989). Therefore, if these processes were to be saturated, a greater proportion of Cr6+ would be available to cross the cell membrane and enter the cell (Snow 1992; Jones 1990; Petrilli et al. 1986). However, it is likely that relatively high doses of Cr6+ (dose levels well above those typically encountered in the environment) would have to be ingested or inhaled to saturate these defense mechanisms. These extracellular reduction mechanisms that are operative following ingestion or inhalation of Cr6+ are discussed below.

Inhalation

The fate of chromium in the lung is important since the lung is the only proven target of chromium-induced cancer in humans (DeFlora and Wetterhahn 1989). When Cr6+ enters the body via inhalation, the first extracellular mechanism to reduce Cr6+ to Cr3+ is contact with the epithelial lining fluid of the lung which contains ascorbic acid and glutathione (GSH). DeFlora et al. (1997) reported that the acute capacity for Cr6+ reduction by the epithelial lining fluid (ELF) of the lung ranged from 0.9 to 1.8 mg Cr6+.

Ascorbic acid is recognized as an extremely important chromium-reducing agent and is found in the surfactant layers of the lung (Snow 1992; Suzuki 1988; Korallus et al. 1984; Jones 1990). Suzuki (1988) reported that ascorbic acid was an important reducing agent in rat lung lavage fluids. In these fluids, the mean molar ratio of oxidized ascorbic acid and reduced chromium (VI) was 3:2.3. Based on this ratio, the amount of Cr6+ reducible by ascorbic acid was 8.4 μg/g tissue. On this basis, it has been suggested that a 10-hour inhalation exposure to 1 mg Cr6+/m^3 could occur before an accumulation of Cr6+ would take place in the lining of the lungs and absorbed into the cell (Suzuki 1988). Similarly, the alveolar region of the lung contains high levels of GSH (Jones 1990), an extracellular reducing agent of Cr6+ (Snow 1992; Jones 1990; Shi and Dalal 1988). When chromium particles less than 0.5 μm are inhaled, they can reach the alveolar region of the lung. However, GSH has the ability to reduce much of the Cr6+ to the trivalent form before absorption into the cell can occur (Jones 1990).

A secondary reducing mechanism in the alveolar region of the lungs of humans and animals is via pulmonary alveolar macrophages (PAMs). PAMs rapidly phagocytize hexavalent particles and through enzymatic process, reduce them to Cr3+ within cytoplasmic phagosomes (Jones 1990; Petrilli et al. 1986). This reduction process is considered irreversible due to the long life span of these cells, the efficient removal by the mucociliary elimination process, and the inability of cells to oxidize Cr3+ back to Cr6+. DeFlora et al. (1997) reported that the acute capacity for reduction of Cr6+ by PAMs was 136 mg/day/individual, based on the results of studies conducted with PAMs collected from volunteer smokers and nonsmokers. However, Cr6+ that bypasses extracellular reduction is absorbed into the vasculature where GSH in erythrocytes and protein complexes in plasma have the opportunity to reduce Cr6+ to Cr3+ (Jones 1990). Also within the lung are the peripheral parenchymal cells that have the capacity to reduce as much as 260 mg Cr6+ entering the lung per individual (DeFlora et al. 1997). Because Cr3+ is largely impermeable to the cell membrane, it binds to other components and is then excreted in the urine (Korallus et al. 1984). However, Cr6+ which escapes extracellular reduction is available to penetrate the cell membrane and enter the cell. Although the studies just described only estimate capacities for extracellular reduction of Cr6+, the extracellular reduction and cellular uptake of Cr6+ are parallel, competing processes. Evaluation of the dose-response for the cellular uptake

of Cr6+ would also require information on the relative kinetics of extracellular reduction and cellular uptake.

Ingestion

When chromium ingestion occurs, saliva, gastric juice, and intestinal bacteria act to reduce Cr6+ to Cr3+ (Jones 1990; Snow 1992; DeFlora et al. 1985, 1997; Petrilli et al. 1986; Tandon 1985; IARC 1980). Reduction by gastric juices also reduces Cr6+ following reflux from the lung. Kerger et al. (1996) reported that more than 80 mg Cr6+/day may be reduced to Cr3+ by gastric juice of the stomach. DeFlora et al. (1997) reported that 8.3- 12.5 mg Cr6+/day/individual could be reduced by gastric juices during interdigestive periods and 25.1 mg Cr6+/individual may be reduced following ingestion of a meal. DeFlora et al. (1997) also reported that between 0.7 and 2.1 mg Cr6+/day/individual may be reduced by saliva. This capacity for Cr6+ reduction by saliva has been reported to be sufficient for detoxifying Cr6+ found in drinking water at the recommended standards (0.05 - 0.1 mg/L) of several countries.

Intestinal bacteria are also known to contain high levels of GSH. DeFlora et al. (1997) reported that a range of 1 to 24 mg Cr6+/individual may be reduced by intestinal bacteria and eliminated daily with feces. The Cr6+ which escapes reduction by saliva, gastric juices, or intestinal bacteria and is absorbed into the portal blood stream may reach the liver. However, the liver has been reported to have the capability of reducing 3300 mg Cr6+/individual (DeFlora et al. 1997).

Systemic

Cr6+ that crosses the vasculature into the blood is reduced by red blood cells to Cr3+. Inhalation of higher doses results in excess hexavalent chrome in the plasma. The capacity of the human plasma to reduce Cr6+ has been confirmed by monitoring workers at manufacturing plants of various chromium compounds (Korallus 1986). Cr6+ reaching the systemic circulation reacts with GSH found in the erythrocytes and plasma (Jones 1990; DeFlora et al. 1997). Cr6+ is then reduced to Cr3+ by GSH, leaving the Cr3+ to bind to hemoglobin and serum proteins (Tandon

1985; Jones 1990). The overall capacity of whole human blood to reduce Cr6+ has been reported to be 234 mg/individual for males and 187 mg/individual for females. The overall reduction of Cr6+ by red blood cells was reported to be 128 mg/individual for males and 93 mg/individual for females (DeFlora et al. 1997).
Duringthe reduction of Cr6+ within the blood stream, Cr5+ intermediates may also form and complex with the GSH to form GSH-Cr5+ species (Goodgame and Joy 1986; Jones 1990). However, like Cr3+ species, Cr5+ is also impermeable to biological membranes (Arslan et al. 1987).

Intracellular Reduction of Chromium VI

Solubility is an important issue in considering the bioavailability of chromium to target tissues (DeFlora and Wetterhahn 1989). It has been reported that chromium compounds with lower solubilities are less easily transported into the cell (Jones 1990). Once Cr6+ reaches the cell membrane, the transport of Cr6+ into the cell is believed to mimic the sulfate and phosphate anion transport systems (Standeven and Wetterhahn 1989; Arslan et al. 1987; Snow 1992). This assumption is based on the fact that Cr6+ is mainly found in the tetrahedral form as chromate (CrO_4^{2-}). Therefore, since sulfate and phosphate anions are also in tetrahedral form, it is assumed that Cr6+ is transported in the same manner (Standeven and Wetterhahn 1989). Trivalent chromium is found exclusively as octahedral complexes. This form does not have a distinct cellular uptake mechanism and therefore, makes Cr3+ unable to penetrate the cell membrane under normal physiological conditions (Cohen and Costa 1992).

Once Cr6+ crosses the cell membrane, a rapid reduction takes place (Snow 1992). This rapid intracellular reduction of Cr6+ to Cr3+ helps maintain a concentration gradient and allows for a steady-state influx of Cr6+. A number of intracellular reducing factors act on Cr6+ to reduce it to Cr5+ and Cr4+, which are relatively unstable species, and then to Cr3+, a stable form (Snow 1992). Thus, Cr6+ is short-lived inside the cell, due to the intracellular reducing factors within the cytosol, endoplasmic reticulum, and mitochondria (Snow 1992; Standeven and Wetterhahn 1989; Connett and Wetterhahn 1983; Mikalsen et al. 1989, 1991). The major intracellular

reductants include NAD(P)H, cytochrome P-450, ascorbate, and thiols (i.e., GSH, cysteine, and penicillamine), with ascorbate and GSH being the most significant reductants (Connett and Wetterhahn 1985; Snow 1992, DeFlora et al. 1988, 1985; Shi and Dalal 1990; Cupo and Wetterhahn 1985). The following is an overview of the reduction of Cr6+ to Cr3+ once Cr6+ reaches the cytoplasm, mitochondria and endoplasmic reticulum.

Cytoplasm

Upon entering the cytoplasm, ascorbate, DT-diaphorase, and GSH are the major contributors to the reduction of Cr6+ to Cr3+. Connett and Wetterhahn (1983) were the first to note that the intracellular metabolism of chromate is under kinetic rather than thermodynamic control. This means that the most plentiful and kinetically active electron donor will be of primary importance in the reduction of chromate, rather than the one producing the most stable product. Enzymatic reduction of Cr6+ by microsomal enzymes or the mitochondrial electron transport system is slow and therefore of less overall importance than reduction by various small compounds, such as GSH and ascorbic acid, which can be present in millimolar concentration.

GSH plays a significant role in the reduction of Cr6+ in the cytoplasm. GSH is the most abundant thiol found within the cell and takes part in a two-phase reduction of Cr6+ to Cr3+ as discussed below (Connett and Wetterhahn 1985; Shi and Dalal 1988; Suzuki and Fukuda 1990). In the presence of GSH, a Cr6+-thioester intermediate is formed as an initial reducing step. A two-phase intracellular reduction then follows. The first phase, in which the Cr6+-thioester reduces to form Cr5+ intermediates, is very rapid (Connett and Wetterhahn 1985; Snow 1992; Shi and Dalal 1988; Rossi et al. 1988; Suzuki and Fukuda 1990). During this step of reduction, a glutathionyl radical (GS·) also forms (Shi and Dalal 1988; Cupo and Wetterhahn 1985). At this point, if sufficient GSH is present, a second reduction phase occurs, reducing Cr5+ to Cr4+ and then to Cr3+ (Snow 1992; Connett and Wetterhahn 1985). However, the second step in the reduction process is much slower. The Cr3+ may then bind to other components, such as protein complexes or possibly with DNA. If there is not enough GSH present to further reduce the Cr5+ to Cr3+, Cr5+-thioester intermediates may form or Cr5+ may possibly interact with DNA

(Connett and Wetterhahn 1985; Snow 1992; Shi and Dalal 1988). An *in vitro* study conducted by Suzuki (1990), supports the two-phase reduction of Cr6+ by GSH. Suzuki (1990) reported that during the first phase of the reduction, the half-life of Cr6+ was 9.2 minutes with only a 7% decrease in Cr6+ concentration, when compared to the initial Cr6+ concentration. It was also reported that the second phase of the reduction was the main process and followed pseudo-first-order kinetics.

Ascorbate is found in high concentrations within the cell, and is one of the most important intracellular reducing agents (Snow 1992; Suzuki 1988). Extracellular ascrobic acid serves to detoxify Cr6+ by decreasing cellular uptake. On the other hand, the reduction of chromate by intracellular ascorbic acid and the resultant formation of intracellular active oxygen species increases Cr6+ toxicity. Suzuki (1990) reported that ascorbic acid, when tested *in vitro* at high concentrations, followed pseudo-first-order redox processes in a single phase, with respect to Cr6+. When tested at lower concentrations, ascorbic acid followed pseudo-first-order redox processes for only a short duration. In the presence of ascorbate, Cr6+ is more commonly reduced to Cr3+ than Cr5+. However, upon reduction of Cr6+ to Cr3+ within the presence of ascorbate, reactive oxygen species (e.g., HO, singlet oxygen, and superoxide anion [O_2A-]) may also form (Cohen et al. 1993; Snow 1992). Ascorbic acid and GSH have also been shown to work in combination with a synergistic effect on the reduction of Cr6+. Suzuki (1990) compared the effect of GSH and ascorbic acid on the reduction of Cr6+ and found that the reducing ability of ascorbic acid is much higher than that of GSH. However, when tested *in vitro* with mixed solutions of GSH and ascorbic acid at physiological pH, Cr6+ reduction was markedly accelerated.

DT-diaphorase, an intracellular enzyme, also participates in the reduction of Cr6+ to Cr3+ within the cytoplasm by catalyzing the NADPH and NADH-dependent reduction of Cr6+. However, due to the limited availability of NADPH and NADH in the cytoplasm, the DT-diaphorase mediated reduction of Cr6+ is not as significant as GSH reduction.

Mitochondria

Within the mitochondria, amino acids, such as succinate and glutamate, as well as DT-diaphorase, participate in the reduction of Cr6+ to Cr3+. Succinate and glutamate activate the production of NADPH by contributing electrons from attached sulfhydryl groups (Petrilli and De Flora 1988). DT-diaphorase again acts as a mediator of this reduction by assisting the NADPH in donating electrons to the Cr6+. This process is similar to the reduction of Cr6+ activated by GSH within the cytosol. A two-phase process takes place, with an initial rapid phase followed by a slower reduction phase (Ryberg and Alexander 1984). However, the reduction of Cr6+ activated by succinate works via a different mechanism than the reduction activated by glutamate (Arillo et al. 1987). Succinate is more active in the reduction of Cr6+ when in the presence of ADP or an uncoupler. Glutamate only contributes to the reduction of Cr6+ in the presence of respiratory-chain inhibitors (Arillo et al. 1987).

Endoplasmic Reticulum

The endoplasmic reticulum also plays a role as an intracellular site for Cr6+ reduction through an NADPH-dependent cytochrome P-450 system (DeFlora et al. 1985). Studies indicate that in the presence of NADPH, the microsomal cytochrome P-450 contributes to the reduction of Cr6+ to Cr3+. However, the contribution of cytochrome P-450 is very small and is inhibited by the presence of oxygen (Standeven and Wetterhahn 1989; 1991). Studies also indicate that cytochrome P-450 in the presence of NADPH may reduce Cr6+ to form Cr5+ complexes. These Cr5+ complexes may then interact with H_2O_2 to form OH- radicals (Shi and Dalal 1990).

These intracellular sites contribute to the overall reduction of Cr6+ to Cr3+. The specific reductants may be found in one or more of the intracellular compartments as seen with DT-diaphorase assisting in Cr6+ reduction in both the cytoplasm and within the mitochondria. However, the cytosolic fractions containing GSH have been shown to have the most significant rate of Cr6+ reduction (Connett and Wetterhahn 1985; De Flora et al. 1985). A

Genotoxicity/Mutagenicity

The mutagenicity of chromium in mammalian and bacterial species has been widely documented. Results differ for Cr+3 and Cr+6 tested with intact cells compared to tests with cells in which the cell membrane has been disrupted (i.e., "simplified systems"), due to the ability of Cr+6 to cross cell membranes. Overall, Cr+6 compounds are positive in cellular (intact) systems, whereas Cr+3 compounds have been shown to be inactive unless a direct interaction with DNA is permitted in the course of the test, as in simplified systems.

Studies of Cr6+ have shown that when tested in intact bacterial and mammalian cell cultures, results were positive for mutagenic activity. In bacterial systems, Cr6+ produced base-pair substitutions (mutations favoring A-T sequences rather than G-C), frameshift mutations, and mutations related to error-prone DNA-repair pathways (Cohen et al. 1993; Bianchi and Levis 1985; Cupo and Wetterhahn 1985; Becking 1981; Snow 1992; Mikalsen et al. 1991). Bianchi et al. (1983) reported that Cr+6 was mutagenic, based on the induction of base substitutions and frame-shift mutations, in *Salmonella typhimurium* strains when tested without metabolic activation; however, the addition of rat microsomes suppressed Cr+6 mutagenicity.

In mammalian (intact) test systems, Cr+6 produced a variety of genetic effects including mitotic cycle alterations, nucleotide pool imbalance, and sister chromatid exchange (Bianchi et al. 1983; Bianchi and Lewis 1985; DeFlora et al. 1990). Cr+6 has also been reported to induce morphological cell transformation in mouse and hamster cells (Tsuda and Kato 1977; Bianchi et al. 1983). Cr+6 has been reported to significantly increase the frequency of sister chromatid exchanges in four rodent cell lines (Bianchi et al. 1983). The frequency of chromosomal aberrations, consisting primarily of single chromatid breaks and chromatid exchanges, was significantly increased in hamster embryo cells incubated with Cr+6 compounds ($K_2Cr_2O_7$ and CrO_3); however, when Cr+6 was tested in isolated nuclei or purified DNA, it was found to be inactive (Bianchi and Levis 1985). When tested in cultured hamster cells, Cr+6 induced gene mutations indicated by 6TG resistance (Bianchi et al. 1983). An increase in nuclear protein/DNA crosslinks was reported in Novikoff ascites hepatoma cells incubated with K_2CrO_4 (Wedrychowski et al. 1985). However, the authors concluded that after the hexavalent

chromium entered the cell, it was reduced in the cytoplasm to trivalent chromium that subsequently induced the DNA crosslinks.

Bianchi et al. (1983) reported that when Cr+6 was tested in intact mammalian cells, DNA repair synthesis was not induced. When tested *in vitro* using highly purified DNA, Cr+6 was reported to inhibit DNA replication; however direct DNA damage was not observed (Bianchi et al. 1983). The authors noted that Cr+3 is capable of complexing with nucleotide precursors, polynucleotides and proteins at concentrations much lower than Cr+6 is active, and concluded that the inhibition of DNA replication by chromium compounds was attributed to Cr+3. Cr+6 was also positive for genotoxicity when tested *in vivo*, producing DNA-repair inhibition and various indicators of DNA damage (DeFlora et al. 1990).

Recent *in vitro* studies have evaluated the potential of induction and modulation of genotoxicity by hexavalent chromium and the role of apoptosis in chromium-induced carcinogenesis (Manning et al. 1994; Xu et al. 1996; Blankenship et al. 1997). Internucleosomal DNA fragmentation, typical of cells undergoing apoptosis, inhibition of cell growth and delay in the progression through the S-phase of the cell cycle were observed in intact mammalian cells exposed to hexavalent chromium as Na_2CrO_4 (Manning et al. 1994; Xu et al. 1996; Blankenship et al. 1997). Evidence of direct effects on DNA included single strand breaks, DNA adducts and interstrand crosslinks. The DNA adducts were associated with the suppression of RNA and mRNA synthesis and suppression of the expression of the GRP78 gene (Manning et al. 1994). In cells exposed to Cr+6 *in vitro* guanine-guanine interstrand DNA crosslinks, inhibition of DNA repair and suppression of thymidine incorporation into DNA, indicating an arrest in DNA replication, were reported (Xu et al. 1996). Pretreatment with vitamin C or vitamin E reduced the clastogenic effects produced by Cr+6 in cell cultures (Blankenship et al. 1997). In addition, pretreatment with vitamin C protected cells from chromium-induced toxicity and apoptosis; however, this effect was not observed in cells pretreated with vitamin E. The authors concluded that apoptosis, likely initiated by a guanine-specific termination of DNA replication that is sensitive to the effects of vitamin C but not vitamin E, is the mechanism responsible for chromium cytotoxicity. Cells that escape apoptosis may contain genes damaged by chromium, and replication of these cells could subsequently result in carcinogenesis.

An intermediate product of Cr+6 reduction, Cr+5, is capable of producing biological effects via direct interaction with DNA or enhanced reduction to Cr+3, when complexed with GSH (Goodgame and Joy 1986; Jones 1990; Stearns et al. 1995). The interaction of Cr+6 with GSH has been shown to produce both the long-lived Cr+5 intermediate and the reactive glutathionyl radical (GS·) (Shi and Dalal 1988). Reaction of Cr+6 with GSH has also been shown to result in the formation of the Cr+4-GSH intermediate and hydroxyl radicals (Liu et al. 1997). When Cr+6 was reduced with varying concentrations of ascorbate, Cr+5, Cr+4 and carbon free radicals were formed, with Cr+3 the final product (Stearns and Wetterhahn 1994; Stearns et al. 1995). Cr+5 was associated with Cr/DNA adducts and carbon radicals were associated with DNA single strand breaks. Cr+5 may also be reduced to Cr+4, which causes DNA damage and generate hydroxyl radicals (Luo et al. 1996; Liu et al. 1997).

When tested for mutagenic or genotoxic effects in intact bacterial and mammalian cell systems, Cr3+ was found to be inactive due to its impermeability to the cell membrane. For example, in strains of *S. typhimurium*, Cr+3 was nonmutagenic with and without microsomal activation (Bianchi et al. 1983). There were no increases in the frequency of chromosomal aberrations in hamster embryo cells incubated with trivalent chromium salts [$CrCl_3$ and $Cr_2(SO_4)_3$] (Tsuda and Kato 1977). DNA repair synthesis was not induced by Cr+3, and the frequency of sister chromatid exchanges was not increased when tested in intact mammalian cells (Bianchi et al. 1983). However, when Cr3+ was tested in isolated nuclei or purified DNA, it was found to produce DNA-protein cross-links, sister chromatid exchanges, chromosomal aberrations, and interruptions in DNA replication (Bianchi et al. 1983; Bianchi and Levis 1985; Cohen et al. 1993). Among the various valence states of chromium, only Cr3+ has been shown to complex directly with DNA (Jones 1990), although it is hypothesized that other chromium species and complexes may be able to interact with DNA (DeFlora and Wetterhahn 1989). Cr3+ will form chromium-DNA adducts and can produce DNA strand breaks, interference with DNA restriction enzymes, and other genotoxic effects (DeFlora and Wetterhahn 1989; Snow 1992).

Studies have also evaluated the potential for chromium to generate free radicals and for these free radicals to interact with DNA as a possible mode of carcinogenesis. As discussed above, it has been demonstrated that Cr+6 may react with reduced GSH forming the reactive intermediates, Cr+5 and Cr+4, and a glutathionyl radical (Shi and Dalal 1988; Shi et al. 1992). It

has been demonstrated that Cr+6 may be reduced to Cr+5 *in vivo* (Liu et al. 1994, 1996), with an NADPH/flavoenzyme complex the major reductant (Liu et al. 1996). The Cr+5 intermediate may interact directly with DNA (Shi et al. 1992). However, it has also been shown that reactive free oxygen species, such as the hydroxyl radical, may be formed from hydrogen peroxide or lipid hydroperoxides when Cr+6 is reduced to Cr+5 (Shi et al. 1992; Shi and Dalal 1994; Shi et al. 1994a,b; Ye et al. 1995; Luo et al. 1996; Liu et al. 1997; Shi et al. 1997; Chen et al. 1997), likely via a Fenton-type reaction (Shi and Dalal 1994; Shi et al. 1994a,b). The reaction of hydrogen peroxide with Cr+5 bound to DNA may result in the generation of hydroxyl radicals within close proximity to the DNA increasing the possibility of damage to a specific DNA site (Shi et al. 1992).

Hydroxyl radicals that could damage DNA at specific sites may also be produced by the reduction of Cr+5 to Cr+4 and Cr+3 in Fenton-like reactions (Shi et al. 1993; Shi et al. 1994a; Luo et al. 1996; Liu et al. 1996). Cr+3 may also form hydroxyl radicals via the Haber-Weiss cycle (Shi et al. 1997). As discussed above, Cr+3 is capable of binding with DNA. Therefore, it is possible that the formation of these hydroxyl radicals in close proximity to DNA could result in DNA damage. Free radicals may also be formed when chromium is reduced by intracellular thiols, such as cysteine (Shi et al. 1994b) or α-lipoic acid (Chen et al. 1997). The incubation of Cr+6 with cysteine or penicillamine resulted in the formation of thyil radicals and hydroxyl free radicals, via the Fenton reaction. The authors concluded that these data provided evidence that sulfhydryl groups present on thiols are an important functional group in the reduction of Cr+6.

Chromium may induce carcinogenesis by a mechanism other than direct interaction with DNA or by free radical generation. The reduction of Cr+6 to Cr+4 and the free radical generation associated with this reaction have been shown to activate nuclear factor κB (NF-κB) (Ye et al. 1995; Chen et al. 1997), a transcription factor that induces the overexpression of the c-*myc* gene, which in turn has been associated with the formation of Burkitt's lymphoma (Ji et al. 1994). Therefore, the activation of NF-κB by the reduction of chromium may be involved in chromium-induced carcinogenesis (Ye et al. 1995).

Mode of Action for Carcinogenicity

Even if it is accepted that the carcinogenicity of chromium is via a genotoxic mechanism, two issues concerning this mechanism remain unresolved. These are: 1) the form(s) of chromium responsible for interaction with DNA leading to genotoxic effects and ultimately to carcinogenic effects; and 2) the location where, in the intracellular environment, the active moiety is formed.

Despite the extensive study of chromium and its genetic activity, very little can be said concerning the ultimate genotoxic form. Several authors concede, however, that there may be several genetically reactive moieties (DeFlora and Wetterhahn 1989; Snow 1992). The various active forms are due to differences in a target cell's metabolic capacity within the cytoplasm and compartmentalized cell structures. Putative DNA-damaging species include: Cr5+, Cr4+ and Cr3+; active oxygen species ($HO\cdot$, $\Delta_g 0_2$, 0_2^-); and reactive radicals including $RS\cdot$ and $R\cdot$ (DeFlora and Wetterhahn 1989). All of the above, with the exception of Cr3+, are intermediate or other highly reactive species and are thought to be genetically active only when in close proximity to the nuclear envelope/material. However, a notable exception is demonstrated by binding of Cr5+ to ligands, increasing its stability and lifetime in the cell. The final stable form is Cr3+ which may form chromium-DNA adducts, and mediate cross-linking of DNA strands and DNA to protein.

Issues on intracellular sites of metabolism can be further explored by two proposed theories, as defined by DeFlora and Wetterhahn (1989), of chromium-induced carcinogenesis. The first theory is called the uptake-reduction or uptake-activation mechanism. It involves movement of Cr6+ across the target cell membrane after which it is reduced in cytoplasmic structures to the ultimate genotoxic species. The active genotoxic form(s) would then migrate into the nucleus and cause DNA damage and initiation of cancer (DeFlora and Wetterhahn 1989). This theory infers that Cr6+ is not the genetically active species, but other reduced intermediate species, including the ultimate reduced form, Cr3+, could be the genotoxic agents.

The other theory is the uptake-detoxification mechanism. This theory holds that genotoxic effects would result only when Cr6+ taken into the cell exceeds the reducing mechanisms of the cytoplasm thereby escaping detoxification via reduction. As Cr6+ approaches the nucleus, it, or a reduced form, could interact with DNA.

The authors note that "...a crucial point is the site of the cytoplasm where reduction is achieved. An activating effect is more likely to ensue when reduction occurs in proximity of the nuclear envelope...or even inside the nucleus," whereas production of reduced forms is favored when reduction takes place in organelles or in cytoplasmic sites at distance from the nucleus (DeFlora and Wetterhahn 1989). Both theories may be valid; however, both leave unresolved the issue of the ultimate species which reacts with DNA material to cause genotoxicity and potential carcinogenicity.

REFERENCES

Agency for Toxic Substances and Disease Registry (ATSDR). 1989. Toxicological Profile for Chromium. ATSDR/TP-88/10. ATSDR, Atlanta, GA.

Albert RE, Lippmann M, Brisco W. 1969. The characteristics of bronchial clearance in humans and the effects of cigarette smoking. Arch Environ Health 18:738-755.

Albert RE, Lippmann M, Peterson HT, Jr. 1971. The effects of cigarette smoking on the kinetics of bronchial clearance in humans and donkeys. In: Walton WH, ed. Inhaled Particles III. Unwin Bros. Ltd., The Gresham Press, England. pp. 165-182.

Alexander BH, Checkoway H, Wechsler L, Heyer NJ, Muhm JM, O'Keeffe TP. 1996. Lung cancer in chromate-exposed aerospace workers. J Occup Environ Med 38:1253-1258.

American Conference of Governmental Industrial Hygienists, Inc. (ACGIH). 1997. Documentation of the Threshold Limit Values and Biological Exposure Indices. Chromium.

American Medical Association (AMA). 1979. Guidelines for essential trace element preparations for parenteral use. J Am Med Assoc 241:2051-2054.

Arillo A, Melodia F, Frache R. 1987. Reduction of hexavalent chromium by mitochondria: methodological implications and possible mechanisms. Ecotoxicol Environ Saf 14:164-177.

Arslan P, Beltrame M, Tomasi A. 1987. Intracellular chromium reduction. Biochim Biophys Acta 931:10-15.

Axelson G, Rylander R, Schmidt A. 1980. Mortality and incidence of tumours among ferrochromium workers. Br J Ind Med 37:121-127 (As cited in WHO 1988).

Aw T-C. 1997. Clinical and epidemiological data on lung cancer at a chromate plant. Reg Toxicol Pharmacol 26:S8-S12.

Ballew MA, Kriebel D, Smith TJ. 1995. Epidemiologic application of a dosimetric model of dust overload. Am J Epidemiol 141:690-696.

Becking GC. 1981. Recent advances in the toxicity of health metals—an overview. Fundam Appl Toxicol 1:348-352.

Bianchi B, Levis AG. 1985. Mechanisms of chromium genotoxicity. In: Merian E, Fre RW, Hardi W, Schlatter C, eds. Carcinogenic and Mutagenic Metal Compounds, Environmental and Analytical Chemistry and Biological Effects. Gordon and Breach Science Publishers, London. pp. 269-294.

Bianchi V, Dal Toso R, Debetto P, Levis AG, Luciani S, Majone F, Tamino G. 1980. Mechanisms of chromium toxicity in mammalian cell cultures. Toxicology 17:219-224.

Bianchi V, Celotti L, Lanfranchi G, Majone F, Marin G, Montaldi A, Sponza G, Tamino G, Venier P, Zantedeschi A, Levis AG. 1983. Genetic effects of chromium compounds. Mutat Res 117:279-300.

Black A, Evans JC, Hadfield EH, Macbeth RG, Morgan A, Walsh M. 1974. Impairment of nasal mucociliary clearance in woodworkers in the furniture industry. Br J Ind Med 31:10-17.

Blankenship LJ, Carlisle DL, Wise JP, Orenstein JM, Dye LE, Patierno SR. 1997. Induction of apoptotic cell death by particulate lead chromate: differential effects of vitamins C and E on genotoxicity and survival. Toxicol Appl Pharmacol 146:270-280.

Bourne HG Jr, Yee HT. 1950. Occupational cancer in a chromate plant. An environmental appraisal. Ind Med Surg 19:563-567.

Chan TL, Lippmann M. 1980. Experimental measurements and empirical modelling of the regional deposition of inhaled particles in humans. Am Ind Hyg Assoc J. Jun;41(6):399-409.

Chen F, Ye J, Zhang X, Rojanasakul Y, Shi X. 1997. One-electron reduction of chromium(VI) by α-lipoic acid and related hydroxyl radical generation, dG hydroxylation and nuclear transcription factor-κB activation. Arch Biochem Biophys 338:165-172.

Cohen MD, Costa M. 1992. Chromium compounds. In: Rom WN. Environmental and Occupational Medicine. 2nd ed. Little, Brown and Company, Boston. Pp 799-805.

Cohen MD, Kargacin B, Klein CB, Costa M. 1993. Mechanisms of chromium carcinogenicity and toxicity. Crit Rev Toxicol 23:255-281.

Connett PH, Wetterhahn KE. 1983. Metabolism of the carcinogen chromate by cellular constituents. Struct Bond 54:93-124.

Connett PH, Wetterhahn KE. 1985. In vitro reaction of the carcinogen chromate with cellular thios and carboxylic acids. J Am Chem Soc 107:4282-4288.

Cotton AF, Wilkinson G. 1966. Advanced Inorganic Chemistry. Interscience Publishers, New York.

Cupo DY, Wetterhahn KE. 1985. Modification of chromium(VI)-induced DNA damage by glutathione and cytochromes P-450 in chicken embryo hepatocytes. Proc Natl Acad Sci 82:6755-6759.

Dalager NA, Mason TJ, Fraumeni JF, Hoover R, Payne WW. 1980. Cancer mortality among workers exposed to zinc chromate paints. J Occup Med 22:25-29.

Davies JM. 1984. Lung cancer mortality among workers making lead chromate and zinc chromate pigments at three English factories. Br J Ind Med 41:158-169.

Davies JM, Easton FD, Bidstrup PI. 1991. Mortality from respiratory cancer and other causes in United Kingdom chromate production workers. Br J Ind Med 48:299-313.

DeFlora S, Wetterhahn KE. 1989. Mechanisms of chromium metabolism and genotoxicity. Life Chem Rept 7:169-244.

DeFlora S, Camoirano A, Bagnasco M, Bennicelli C, Corbett GE, Kerger BD. 1997. Estimates of the chromium(VI) reducing capacity in human body compartments as a mechanism for attenuating its potential toxicity and carcinogenicity. Carcinogenesis 18:531-537.

DeFlora S, Morelli A, Basso C, Romano M, Serra D, DeFlora A. 1985. Prominent role of DT-diaphorase as a cellular mechanism reducing chromium(VI) and reverting its mutagenicity. Cancer Res 45:3188-3196.

DeFlora S, Bagnasco M, Serra D, Zanacchi P. 1990. Genotoxicity of chromium compounds. A review. Mutat Res 238:99-174.

DeFlora S, Bennicelli C, Camoirano A, Serra D, Hochstein P. 1988. Influence of DT diaphorase on the mutagenicity of organic and inorganic compounds. Carcinogenesis 9:611-617.

Essing HG, Szadkowski D, Valentin H. 1971. [Significance of the valence gradations of chromium compounds in occupational medicine examinations.] Med Sachverstand 67:35-39 (German) (As cited in WHO 1988).

Fan AM, Harding-Barlow I. 1987. Chromium. In: Fishbein L, Furst A, Mehlman MA, eds. Advances in Modern Environmental Toxicology, Genotoxic and Carcinogenic Metals: Environmental and Occupational Occurrence and Exposure. Vol. XI. Princeton Scientific, Princeton, NJ. pp. 87-125.

Feldman F. 1968. The state of chromium in biological materials. Fed Proc 27:482.

Franchini I, Magnani F, Mutti A. 1983. Mortality experience among chrome plating workers. Scand J Work Environ Health 9:247-252.
Gad SC. 1989. Acute and chronic systemic chromium toxicity. Sci Total Environ 86:149-157.

Gibb J, Chen C. 1989. Evaluation of issues relating to the carcinogen risk assessment of chromium. Sci Total Environ 86:181-186.

Glaser U, Hochrainer D, Kloppel H, Kuhnen H. 1985. Low-level chromium VI inhalation effects on alveolar macrophages and immune functions in Wistar rats. Arch Toxicol 57:250-256.

Goodgame DML, Joy AM. 1986. Relatively long-lived chromium(V) species are produced by the action of glutathione on carcinogenic chromium(VI). J Inorg Biochem 26:219-224.

Goyer RA. 1986. Toxic effects of metals. In: Klaassen CD, Amdur MO, Doull J, eds. Casarett and Doull's Toxicology. 3rd ed. Macmillan Publishing Company, New York. pp. 582-635.

Grant LD, Mushak P. 1989. Specification of metals and metal compounds: implications for biological monitoring and development of regulatory approaches. Toxicol Ind Health 5:891-908.

Grogan CH. 1958. Experimental studies in metal carcinogenesis. XI. On the penetration of chromium into the cell nucleus. Cancer 11:1195-1203.

Hathaway JA. 1989. Role of epidemiologic studies in evaluating the carcinogenicity of chromium compounds. Sci Total Environ 86:169-179.

Hayes RB. 1988. Review of occupational epidemiology of chromium chemicals and respiratory cancer. Sci Total Environ 71:331-339.

Hopkins LL, Jr, Ransome-Kuti O, Majaj AS. 1968. Improvement of impaired carbohydrate metabolism by chromium(III) in malnourished infants. Am J Clin Nutr 21:203-211.

International Agency for Research on Cancer (IARC). 1980. IARC Monographs on the Evaluation of the Carcinogenic Risk of Chemicals to Humans. Some Metals and Metallic Compounds. Vol. 23. World Health Organization, Lyon.

ICRP. 1966. Deposition and retention models for internal dosimetry of the human respiratory tract. Health Phys 12:173-207.

International Life Sciences Institute (ILSI). 1990. Present Knowledge in Nutrition. 6th ed. ILSI, Nutrition Foundation, Washington, DC. p. 290.

Ji L, Arcinas M, Boxer LM. 1994. NF-κB sites function as positive regulators of expression of the translocated c-*myc* allele in Burkitt's lymphoma. Mol Cell Biol 14:7967-7974.

Jones RE. 1990. Hexavalent chrome: threshold concept for carcinogenicity. Biomed Environ Sci 3:20-34.

Kerger BD, Paustenbach DJ, Corbett GE, Finley BL. 1996. Absorption and elimination of trivalent and hexavalent chromium in humans following ingestion of a bolus dose in drinking water. Toxicol Appl Pharmacol 141:145-158.

Korallus U. 1986. Biological activity of chromium (VI) against chromium (III) compounds: New aspects of biological monitoring. In: Serrone DM, ed. Proceedings, Chromium Symposium 1986: An Update. Industrial Health Foundation, Pittsburgh. pp.210-230.

Korallus U, Ehrlicher H, Wuestefeld E. 1974a. [Trivalent chromium compounds. Results of a study in occupational medicine. I. General; technology; preliminary study.] Arbeitsmed Sozialmed Praventivmed 9:51-54 (German) (As cited in WHO 1988).

Korallus U, Ehrlicher H, Wuestefeld E. 1974b. [Trivalent chromium compounds: results of a study in occupational medicine. II. Disease status analysis.] Arbeitsmed Sozialmed Praventivmed 9:76-79 (German) (As cited in WHO 1988).

Korallus U, Ehrlicher H, Wuestefeld E. 1974c. [Trivalent chromium compounds: results of a study in occupational medicine. III. Clinical studies.] Arbeitsmed Sozialmed Praventivmed 9:248-252 (German) (As cited in WHO 1988).

Korallus U, Harzdorf C, Lewalter J. 1984. Experimental bases for ascorbic and acid therapy of poisoning by hexavalent chromium compounds. Int Arch Occup Environ Health 53:247-256.

Langard S. 1988. Chromium carcinogenicity: a review of experimental animal data. Sci Total Environ 71:341-350.

Langard S. 1993. Role of chemical species and exposure characteristics in cancer among persons occupationally exposed to chromium compounds. Scand J Work Environ Health 19(Suppl 1):81-89.

Langard S. 1990. One hundred years of chromium and cancer: a review of epidemiological evidence and selected case reports. Am J Ind Med 17:189-215.

Langard S, Norseth T. 1975. A cohort of bronchial carcinomas in workers producing chromate pigments. Br J Ind Med 32:62-65.

Langard S, Andersen A, Gylseth B. 1980. Incidence of cancer among ferrosilicon workers. Br J Ind Med 37:114-120 (As cited in WHO 1988).

Langard S, Andersen A, Ravnestad J. 1990. Incidence of cancer among ferrochromium and ferrosilicon workers: an extended observation period. Br J Ind Med 47:14-19.

Laskin S. 1972. Research in Environmental Sciences. Institute of Environmental Medicine, Washington, DC. pp. 92-97 (As cited in WHO 1988).

Laskin S, Kuschner M, Drew RT. 1970. Studies in pulmonary carcinogenesis. In: Hanna MG, Nettesheim P, Gilbert JR, eds. Inhalation Carcinogenesis. Division of Technical Information Extension, U.S. Atomic Energy Commission, Oak Ridge, Tennessee. U.S. Atomic Energy Commission Symposium Series No. 18. pp. 321-351 (As cited in WHO 1988).

Lees PSJ. 1991. Chromium and disease: review of epidemiologic studies with particular reference to etiologic information provided by measures of exposure. Environ Health Perspect 92:93-104.

Levis AG, Bianchi V, Tamino G, Pegoraro B. 1978. Cytotoxic effects of hexavalent and trivalent chromium on mammalian cells *in vitro*. Br J Cancer 37:386-396.

Levy LS, Martin PA. 1983. The effects of a range of chromium-containing materials on rat lung. Department of Environmental and Occupational Health, University of Aston, Birmingham. p. 224 and suppl (Prepared for Dry Color Manufacturers Association, Alexandria, Virginia) (As cited in WHO 1988).

Levy LS, Venitt S. 1975. Carcinogenic and mutagenic activity of chromium-containing materials. Br J Cancer 32:254-255 (As cited in WHO 1988).

Liu K, Jiang J, Swartz HM, Shi X. 1994. Low-frequency EPR detection of chromium(V) formation by chromium(VI) reduction in whole life mice. Arch Biochem Biophy 313:248-252.

Liu K, Shi X, Jiang J, Goda F, Dalal N, Swartz HM. 1996. Low frequency electron paramagnetic resonance investigation on metabolism of chromium(VI) by whole live mice. Ann Clin Lab Sci 26:176-184.

Liu K, Shi X, Dalal NS. 1997. Synthesis of Cr(VI)-SGH, its identification and its free hydroxyl radical generation: a model compound for Cr(VI) carcinogenicity. Biochem Biophys Res Commun 235:54-58.

Lourenco RV, Klimek MF, Borowski CJ. 1971. Deposition and clearance of 2 μ particles in the tracheobronchial tree of normal subjects — smokers and nonsmokers. J Clin Invest 50:1411-1420.

Luo H, Lu Y, Shi X, Mao Y, Dalal NS. 1996. Chromium(IV)-mediated Fenton-like reaction causes DNA damage: implication to genotoxicity of chromate. Ann Clin Lab Sci 26:185-191.
Mancuso TF. 1997. Chromium as an industrial carcinogen: Part 1. Am J Ind Med 31:129-139.

Mancuso TF. 1975. Consideration of chromium as an industrial carcinogen. Presented at the International Conference on Health Metals in the Environment, Toronto, Ontario. October 27-31, 1975.

Mancuso TF, Hueper WC. 1951. Occupational cancer and other health hazards in a chromate plant: A medical appraisal. I. Lung cancers in chromate workers. Ind Med Surg 20:358-363.

Manning FCR, Blankenship LJ, Wise JP, Xu J, Bridgewater LC, Patierno SR. 1994. Induction of internucleosomal DNA fragmentation by carcinogenic chromate: relationship to DNA damage, genotoxicity, and inhibition of macromolecular synthesis. Environ Health Perspect 102(Suppl 3):159-167.

Mauderly JL. 1994. Noncancer pulmonary effects of chronic inhalation exposure of animals to solid particles. In: Mohr U, Dungworth D, Mauderly J, Oberdorster G, eds. Toxic and Carcinogenic Effects of Solid Particles in the Respiratory Tract. ILSI Press, Washington, DC. pp. 43-55.

Mertz W. 1969. Chromium occurrence and function in biological systems. Physiol Rev 49:165-239 (as cited in Steven et al. 1976).

Mikalsen A, Alexander J, Andersen RA, Daae H-L. 1989. Reduction of hexavalent chromium in a reconstituted system of cytochrome P-450 and cytochrome b_5. Chem-Biol Interact 71:213-221.

Mikalsen A, Alexander J, Wallin H, Ingelman-Sundberg M, Andersen RA. 1991. Reductive metabolism and protein binding of chromium(VI) by P450 protein enzymes. Carcinogenesis 12:825-831.

Morrow P. 1988. Possible mechanisms to explain dust overloading of the lungs. Fundam Appl Toxicol 10:369-384.

Moulin JJ. 1997. A meta-analysis of epidemiologic studies of lung cancer in welders. Scand J Work Environ Health 23:104-113.

National Academy of Sciences (NAS). 1974. Medical and Biological Effects of Environmental Pollutants: Chromium. National Academy Press, Washington, DC.

National Toxicology Program (NTP). (2008). Toxicology and carcinogenesis studies of sodium dichromate dehydrate (CAS No. 7789-12-0) in F344/N rats and B6C3F1mice (drinking water studies). Technical Report 546. Research Triangle Park, NC: National Toxicology Program.

Nettesheim P, Hanna MG, Doherty DG, Newell RF, Hellman A. 1971. Effect of calcium chromate dust, influenza virus, and 100% whole-body X-radiation on lung tumour incidence in mice. J Natl Cancer Inst 47:1129-1144.

Norseth T. 1980. Cancer hazards caused by nickel and chromium exposure. J Toxicol Environ Health 6:1218-1227 (As cited in WHO 1988).

O'Flaherty EJ. 1993. A pharmacokinetic model for chromium. Toxicol Lett 68:145-158.

O'Flaherty EJ, Radike MJ. 1991. Pharmacokinetic Modeling of Trivalent and Hexavalent Chromium Based on Ingestion and Inhalation of Soluble Chromium Compounds. AL-TR-1991-0162. Air Force Systems Command, Wright Patterson Air Force Base, OH.

Patierno S. 1996. Presentation at the Industrial Health Foundation Chromium Conference, Crystal City, Virginia. April 23-24, 1996.

Petrilli FL, DeFlora S. 1988. Metabolic reduction of chromium as a threshold mechanism limiting its *in vivo* activity. Sci Total Environ 71:357-364.

Petrilli FL, Rossi GA, Camoirano A, Romano M, Serra D, Bennicelli C, DeFlora A, DeFlora S. 1986. Metabolism reduction of chromium by alveolar macrophages and its relationships to cigarette smoke. J Clin Invest 77:1917-1924.

Rafnsson V, Gunnarsdottir H, Kiilunen M. 1997. Risk of lung cancer among masons in Ireland. Occup Environ Med 54:184-188.

Roschina TA. 1964. [A comparative evaluation of the effects of carbide dust and chromium boride on the organism.] Gig I Sanit 8:25-28 (Russian).

Rossi SC, Gorman N, Wetterhahn KE. 1988. Mitochondrial reduction of the carcinogen chromate: formation of chromium(V). Chem Res Toxicol 1:101-107.

Ryberg D, Alexander J. 1984. Inhibitory action of hexavalent chromium (Cr(VI)) on the mitochondrial respiration and a possible coupling to the reduction of Cr(VI). Biochem Pharmacol 33:2461-2466.

Sanchis J, Dolovich M, Chalmers R, Newhouse MT. 1970. Regional distribution and lung clearance mechanisms in smokers and non-smokers. Inhaled Part. 1:183-91.

Scheuch G, Kohlhaufl M, Sommerer K, Lichte H, Hess W, Schulz H, Haussinger K, Heyder J. 1999. Diagnostic pneumology using model aerosols. Pneumologie. Jul;53(7):329-36.

Schlesinger RB, Lippmann M. 1972. Particle deposition in a hollow cast of the human tracheobronchial tree. J Aerosol Sci 8:429-445.

Schlesinger RB, Lippmann M. 1978. Selective particle deposition and bronchogenic carcinoma. Environ Res 15:424-431.

Shi X, Dalal NS. 1988. On the mechanism of the chromate reduction by glutathione: SER evidence for the glutathionyl radical and an isolable Cr(V) intermediate. Biochem Biophys Res Commun 156:137-142.

Shi X, Dalal NS. 1990. On the hydroxyl radical formation in the reaction between hydrogen peroxide and biologically generated chromium(V) species. Arch Biochem Biophys 277:342-350.

Shi X, Dalal NS. 1994. Generation of hydroxyl radical by chromate in biologically relevant systems: role of Cr(V) complexes versus tetraperoxochromate(V). Environ Health Perspect 102(Suppl 3):231-236.

Shi X, Dalal NS, Kasprzak KS. 1993. Generation of free radicals from hydrogen peroxide and lipid hydroperoxides in the presence of Cr(III). Arch Biochem Biophys 302:294-299.

Shi X, Sun X, Gannette PM, Dalal NS. 1992. Deferoxamine inhibition of Cr(V)-mediated radical generation and deoxyguanine hydroxylation: ESR and HPLC evidence. Arch Biochem Biophys 293:281-286.

Shi X, Mao Y, Knapton AD, Ding M, Rojanasakul Y, Gannette PM, Dalal N, Liu K. 1994a. Reaction of Cr(VI) with ascorbate and hydrogen peroxide generates hydroxyl radicals and causes DNA damage: role of a Cr(IV)-mediated Fenton-like reaction. Carcinogenesis 15:2475-2478.

Shi X, Dong Z, Dalal NS, Gannette PM. 1994b. Chromate-mediated free radical generation from cysteine; penicillamine, hydrogen peroxide, and lipid hydroperoxides. Biochim Biophys Acta 1226:65-72.

Shi X, Leonard SS, Zang L, Gannett P, Rojanasakul Y, Castranova V, Vallyathan V. 1997. Cr(III)-mediated hydroxyl radical generation via Haber-Weiss cycle. J Inorg Biochem (to appear).

Smith TJ. 1985. Development and application of a model for estimating alveolar and interstitial dust levels. Ann Occup Hyg 29:495-516.

Snipes MB. 1989. Long-term retention and clearance of particles inhaled by mammalian species. Crit Rev Toxicol 20:175-211.

Snow ET. 1992. Metal carcinogenesis: mechanistic implications. Pharmacol Ther 53:31-65.

Snow ET, Xu L-S. 1991. Chromium(III) bound to DNA templates promotes increased polymerase processivity and decreased fidelity during replication *in vitro*. Biochemistry 30:11238-11245.

Standeven A, Wetterhahn K. 1991. Is there a role for reactive oxygen species in the mechanism of chromium(VI) carcinogenesis? Chem Res Toxicol 4:616-625.

Standeven A, Wetterhahn K. 1989. Chromium(VI) toxicity: uptake, reduction, and DNA damage. J Am Coll Toxicol 8:1275-1283.

Stearns DM, Wetterhahn KE. 1994. Reaction of chromium(IV) with ascorbate products chromium(VI, chromium(IV), and carbon-based radicals. Chem Res Toxicol 7:219-230.

Stearns DM, Kennedy LJ, Courtney KD, Giangrande PH, Phieffer LS, Wetterhahn KE. 1995. Reduction of chromium(VI) by ascorbate leads to chromium--DNA binding and DNA strand breaks in vitro. Biochemistry 34:910-929.

Steffee CH, Baetjer AM. 1965. Histopathologic effects of chromate chemicals. Report of studies in rabbits, guinea-pigs, rats, and mice. Arch Environ Health 11:66-75 (As cited in WHO 1988).

Steven JD, Davies LJ, Stanley EK, et al. 1976. National Research Council of Canada Associate Committee on Scientific Criteria for Environmental Quality: Effects of Chromium in the Canadian Environment. Publ. No. 15017.

Stober W, Einbrodt HJ, Klosterkotter W. 1967. Quantitative studies of dust retention in animal and human lungs after chronic inhalation. In: Davies CN, ed. Inhaled Particles and Vapours II. Pergamon Press, New York. pp. 409-418.

Stout, M.D., Herbert, R.A., Kissling, G.E., Collins, B.J., Travlos, G.S., Witt, K.L., Melnick, R.L., Abdo, K.M., Marlarkey, D.E., and Hooth, M.J. (2008). Hexavalent chromium is carcinogenic to F344/N rats and B6C3F1 mice following chronic oral exposure. Environ. Health Perspectives. doi: 10.1289/ehp.0800208 (http://dx.doi.org/) Online 31 December 2008.

Stout, M. D., A. Nyska, B. J. Collins, K. L. Witt, G. E. Kissling, D. E. Malarkey and M. J. Hooth (2009). Chronic toxicity and carcinogenicity studies of chromium picolinate monohydrate administered in feed to F344/N rats and B6C3F1 mice for 2 years. Food Chem Toxicol 47(4): 729-33.

Suzuki Y. 1988. Reduction of hexavalent chromium by ascorbic acid in rat lung lavage fluid. Arch Toxicol 62:116-122.

Suzuki Y. 1990. Synergism of ascorbic acid and glutathione in the reduction of hexavalent chromium *in vitro*. Ind Health 28:9-19.

Suzuki Y, Fukuda K. 1990. Reduction of hexavalent chromium by ascorbic acid and glutathione with special reference to the rat lung. Arch Toxicol 64:169-176.

Tamino G, Peretta L, Levis A. 1981. Effects of trivalent and hexavalent chromium on the physicochemical properties of mammalian cell nucleic acids and synthetic polynucleotides. Chem-Biol Interact 37:309-319.

Tandon SK. 1985. Essential metal co-ordination in biochemistry. Arh Hig Rada Toksikol 36:307-323.

Tsuda H, Kato K. 1977. Chromosomal aberrations and morphological transformation in hamster embryonic cells treated with potassium dichromate in vitro. Mutat Res 46:87-94.

Wedrychowski A, Ward WS, Schmidt WN, Hnilica LS. 1985. Chromium-induced cross-linking of nuclear proteins and DNA. J Biol Chem 260:7150-7155.

Wetterhahn J. 1981. Role of metals in carcinogenesis: biochemistry and metabolism. Environ Health Perspect 40:233-252.

Wetterhahn K, Hamilton J. 1989. Molecular basis of hexavalent chromium carcinogenicity: effect on gene expression. Sci Total Environ 86:113-129.

Wolff RK, Griffith WC, Cuddihy RG, Snipes MB, Henderson RF, Mauderly JL, McClellan RO. 1989. Modeling accumulations of particles in lung during chronic inhalation exposures that lead to impaired clearance. Health Phys 57(Suppl 1):61-68.

Wolff RK, Henderson RF, Snipes MB, Griffith WC, Mauderly JL, Cuddihy RG, McClellan RO. 1987. Alterations in particle accumulation and clearance in lung of rats chronically exposed to diesel exhaust. Fundam Appl Toxicol 9:154-166.

World Health Organization (WHO). 1988. Chromium. Environmental Health Criteria 61. World Health Organization, Geneva.

Xu J, Bubley GJ, Detrick B, Blankenship LJ, Patierno SR. 1996. Chromium(VI) treatment of normal human lung cells results in guanine-specific DNA polymerase arrest, DNA-DNA cross-links and S-phase blockage of cell cycle. Carcinogenesis 17:1511-1517.

Ye J, Zhang X, Young HA, Mao Y, Shi X. 1995. Chromium(VI)-induced nuclear factor-κB activation in intact cells via free radical reactions. Carcinogenesis 16:2401-2405.

Yu CP, Morrow PE, Chan TL, Strom KA, Yoon KJ. 1988. A nonlinear model of alveolar clearance of insoluble particles from the lung. Inhal Toxicol 1:97-107.

Zober A. 1979. [On the problems of evaluating bronchial carcinoma after exposition to chromium compounds.] Int Arch Occup Environ Health 43:107-121 (German) (As cited in WHO 1988).

ATTACHMENT 2

Final Report

Chromium Pilot Study
Work Order No. 1
Tasks 1 through 4

Final Report

Chromium Pilot Study

Work Order No. 1

Tasks 1 through 4

March 30, 2009

Prepared for:

Tierra Solutions, Inc.
Two Tower Center Blvd.
East Brunswick, NJ 08816

Submitted by:

The Hamner Institutes for Health Sciences
P.O. Box 12137
Research Triangle Park, NC 27709

Table of Contents

Preface

The Hamner Institutes for Health Sciences (The Hamner) submitted to Tierra Solutions, Inc. (TSI), a Chromium Pilot Study proposal on January 30, 2008. There were six tasks identified in the proposal. Goals, rationale, description, references, deliverables, and a cost estimate were provided for each task in the proposal. On February 28, 2008, TSI's Work Order No. 1 approved funds for the following Tasks: 1-part a, 2, 3, and 4. On May 16, 2008, TSI approved funds for Task 1-part b. Funds for Tasks 5 and 6 were withdrawn, but additional funds for Task 3 were approved on September 15, 2008, via a variance to Work Order No. 1. An additional task (Task 7 – Pre-study planning, protocol development, and costing of Phase 1) was proposed on April 24, 2008, and funds to conduct this task were also approved on September 15, 2008.

This report is a final report for Tasks 1 through 4. Progress status reports were submitted previously on May 1, 2008, June 5, 2008, July 11, 2008, August 27, 2008, and October 15, 2008. A final deliverable for Task 7 has been submitted as a separate document.

Executive Summary

This report documents the results of several pilot studies that were performed as part of the preparations for a comprehensive experimental evaluation of the mode of action for the oral carcinogenicity of hexavalent chromium. These pilot studies were designed to answer questions regarding the feasibility of a number of experimental approaches that were being considered for the comprehensive studies.

Task 1 involved the reconstruction of a previously published physiologically based pharmacokinetic (PBPK) model for chromium (Cr) in rats (O'Flaherty, 1996), its adaptation to provide a physiological description for the mouse, and the addition of the target tissues for Cr carcinogenicity: rat buccal cavity and mouse small intestine. The published rat model was successfully reconstructed, scaled to the mouse, and modified to include compartments for the buccal cavity tissue and intestinal tissue. The resulting model was able to provide a consistent description of the kidney concentration of Cr from the NTP drinking water studies for both rats and mice, and accurately predicted the percent Cr in kidney and liver from a published study not used in the development of the model. This model will serve as the framework for the continued incorporation of Cr kinetic data as it becomes available from the planned studies.

Task 2 consisted of an examination of tissues from a previous 90-Day NTP rat study to determine if there was evidence of pre-neoplastic lesions in the rat oral cavity where tumors were observed in the 2-year bioassay. The NTP agreed to conduct this examination themselves. The NTP report has been completed and will be released shortly. In informal discussions between the NTP and The Hamner, the NTP stated that the examination was essentially negative. That is, there was no evidence of pre-neoplastic lesions in the 90-day study.

Task 3 was an evaluation of the feasibility of using magnetic resonance imaging (MRI) to measure trivalent Cr (III) in vivo to monitor the reduction of hexavalent Cr(VI) to Cr(III). Although improvements, including animal preparations, imaging protocols, and image analysis will be needed to provide quantitative measurements of Cr(III) concentrations in vivo, qualitative assessment of the MRI results suggests that the use of MRI to provide both in vitro and in vivo measurement of Cr(III) is highly feasible.

Task 4 was an evaluation of the feasibility of buccal and duodenal cell collection to support assays of the genotoxicity of Cr(VI) using micronucleus (MN) induction assays. It was determined that there is a sufficient number of cells in the buccal cavity of the rat to evaluate MN induction by conventional slide scoring, but not by flow cytometry. In the mouse duodenum it was determined that there is a sufficient number of cells for either method.

The results of these pilot studies have been taken into consideration during the development of the proposal for the comprehensive mode of action studies for Cr(VI) carcinogenicity.

Attachment 1

Task 1. Reconstruction and Refinement of a Physiologically Based Pharmacokinetic (PBPK) Model

Principal Investigator: Harvey J. Clewell III, PhD, The Hamner Institutes

The goal of Task 1 was to reconstruct a previously published chromium PBPK model for rats (O'Flaherty, 1996), to develop a physiological description of the mouse, and to add a description of the target tissues for carcinogenicity: rat buccal cavity and mouse small intestine (NTP, 2007). The development of PBPK models which can integrate knowledge of the rate of reduction of Cr (VI) at specific target tissues will allow for improved estimates of dose. These models can also be used to identify data gaps that can be filled in subsequent studies conducted as a part of Phase 1. Gathering such information will serve not only to assist in model verification but also to test hypotheses regarding the proposed key events by which Cr (VI) causes site and species specific tumors.

A PBPK model that links external Cr (VI) exposure concentration to internal dose of total Cr has been previously reported in rats (O'Flaherty, 1996) and humans (O'Flaherty et al., 2001). The rat model describes oral exposure to Cr (VI) but does not have compartments described for the sites where tumors develop (i.e., oral mucosa in rats) following chronic exposure to Cr (VI) in drinking water (NTP, 2007) and there was no description for the mouse.

The first step was to update the O'Flaherty rat model and verify the model against the published description. Initially, the model was translated to acslX from ACSL 11.8. In order for the model to be suited to describe the rat and mouse, there were several modeling issues that had to be resolved. First the model rate constants were not scaled to body weight. Second, the model was designed to run on a per day time scale. Consequently, it was necessary to change the rate constants, ventilation rate and cardiac output to per-hour and scale to body weight in order to allow allometric scaling to the mouse description. Compartments were added for the buccal cavity and the intestine in order to assess target tissue dosimetry (Figures 1 and 2). Due to a lack of pharmacokinetic data in the mouse, a single model combing the tissues necessary for the rat and mouse target tissue assessment were put into a single model code. Thus, the mouse model will represent a scaled version of the rat model. Parameter values are given in Table 1.

The original model of O'Flaherty et al. (1997) seriously overpredicted the internal exposure to chromium at the high concentrations used in the NTP (2007) study. To improve the model fit to the measured concentrations from the NTP (2007) study, we have assessed the influence of the absorption rate in the intestine on the measured concentration of chromium in the kidney (Figure 4). After review, it was determined that nonlinear Michaelis Menten (M-M) kinetics (Eq. 1) was the most prudent approach to describe the transporter mediated absorption process in the intestine. This finding is similar to observations for both iron and manganese intestinal absorption. The kidney concentrations reported in the NTP study and the tissue time course data reported by Weber et al. (1983) were used in the fitting of the M-M parameters. The 1st order (h^{-1}) description of uptake from the GI lumen in the O'Flaherty model was converted to a clearance (L/h) description. The M-M description results in a lower uptake of CrVI with increasing intestinal concentration.

Eq 1.
$$KGIi = KGIiI * \frac{KMOGIi}{KMOGIi + CGIi}$$

where: KGIi (L/h) is the clearance for Cr from the GI tract, KGIiI (L/h) is the maximal clearance for GI uptake of Cr, KMOGIi (mg/L) is the transporter affinity and CGIi is the concentration of Cr in the GI tract.

Incorporation of M-M kinetics to the oral absorption of Cr (III and VI) provided a consistent description of the kidney concentration of chromium from the NTP drinking water studies for both rats and mice (Figure 5). The M-M absorption model also adequately predicted the percent Cr in kidney and liver from the Weber (1983) study (Figure 6).

The model was used to estimate the concentration of Cr (VI and total) in the buccal cavity tissue of rats (Figure 7) and the intestinal tissue of mice (Figure 8). As we were not yet able to obtain MRI measurements of the *in vivo* conversion of Cr (VI) to Cr (III), the rate of reduction in the model is an estimate based on the previous work in the O'Flaherty model. The rate constants for the buccal cavity tissue and intestine were set to give values similar to that seen in the slowly perfused tissue that would include the major epithelial tissues of the body such as skin.

Overall, the preliminary model for rats was successful in allometrically scaling to the mouse. The incorporation of a compartment for the buccal cavity tissue and intestinal tissue had little impact on the overall absorption and distribution of Cr (III and VI). This model will serve as the basis for the continued incorporation of chemical specific data as it becomes available from the planned experiments.

Table 1. Chromium III and VI model parameters for rats and mice.

	Mouse	Rat	
Physiological Parameters			
QCC	16.5	15.0	Cardiac output (L/h/kg)
Fraction of Cardiac Output			
QLC	0.02	0.25	Liver
QKC	0.17	0.17	Kidney
QIC	0.141	0.17	GI Tract
QBC	0.03	0.03	Bone
QOCC	0.01	0.01	Oral Cavity
Oral Cavity			
SAOC	2.5	5	Surface Areas (cm2)
VLOC	1.2	2.4	Volumes (mL)
WLO	0.006	0.006	Lumen Thickness (cm)
WTO	0.01	0.01	Tissue Thickness (cm)
WXO	0.02	0.02	Sumucosal Thickness (cm)
FRACS	0.43	0.43	Saliva flow rate as fraction of ingestion rate
Tissue volume (fraction of BW)			
VLC	0.055	0.04	Liver

VKC	0.0167	0.01	Kidney
VIC	0.0422	0.03	GI Tract
VRBCC	0.03	0.03	RBC
VWC	0.2	0.2	Well perfused (less liver, kidney and GI)
VPC	0.7	0.7	Slowly perfused (less bone)
Chemical Specific Parameters			
Chromium kinetics			
KREDC	0.0311	0.0311	Rate for reduction of Cr(VI) to Cr(III) in all tissues/fluid except GI (1/h)
KREDGIC	0.311	0.311	Rate for reduction of Cr(VI) to Cr(III) in GI (1/h)
KREDLUC	0.0155	0.0155	Rate for reduction of Cr(VI) to Cr(III) in lung (1/h)
KREDRCC	0.0207	0.0207	Rate for reduction of Cr(VI) to Cr(III) in red blood cells (1/h)
KREDKC	0.0309	0.0309	Reduction rate of Cr(VI) to Cr(III) in Kidney
KREDOCC	0.0037	0.0037	Reduction rate of Cr(VI) to Cr(III) in Oral Cavity
KREDETC	0.0311	0.0311	Reduction rate of Cr(VI) to Cr(III) in Oral Cavity Tissue
KIN3C	3.08E-05	3.08E-05	Clearance of Cr(III) from arterial plasma into red cells (L/h)
KIN6C	0.1542	0.1542	Clearance of Cr(VI) from arterial plasma into red cells (L/h)
KOUT3C	3.08E-05	3.08E-05	Clearance of Cr(III) from red cells to arterial plasma (L/h)
KOUT6C	1.036	1.036	Clearance of CR(VI) from red cells to arterial plasma (L/h)
QEC3	0.0027	0.0027	Total elimination clearance of Cr(III) from blood (L/h/kg)
QEC6	0.0027	0.0027	Total elimination clearance of Cr(VI) from blood (L/h/kg)
CR3	5	5	Fractional deposition of Cr(III) from blood to forming bones
CR6	15	15	Fractional deposition of Cr(VI) from blood to forming bones
Urinary values			
FU3	0.8	0.8	Fraction of body burden excreted in urine
FU6	0.8	0.8	Fraction of body burden secreted in urine
FR	0.7	0.7	Fraction to retained urine
Rate retained urine excreted (mg/hr)			
KHOLD3C	0.00284	0.034	
KHOLD6C	0.00284	0.034	
Tissue specific clearance values (L/h)			
LDIN3C	1.03E-05	1.03E-05	Clearance of Cr(III) plasma to liver
LDOUT3C	3.08E-05	3.08E-05	Clearance of Cr(III) liver to plasma
LDIN6C	0.1542	0.09542	Clearance of Cr(VI) plasma to liver
LDOUT6C	1.029	1.029	Clearance of Cr(VI) liver to plasma
KDIN3C	0.00072	0.0009	Clearance of Cr(III) plasma to kidney
KDOUT3C	0.000103	0.000015	Clearance of Cr(III) kidney to plasma
KDIN6C	0.1542	0.032	Clearance of Cr(VI) plasma to kidney
KDOUT6C	1.029	0.0708	Clearance of Cr(VI) kidney to plasma
WDIN3C	1.03E-05	1.03E-05	Clearance Cr(III) plasma to intestine
WDOUT3C	0.0010	0.0010	Clearance Cr(III) intestine to plasma

WDIN6C	0.15	0.15	Clearance Cr(VI) plasma to intestine
WDOUT6C	1.029	1.029	Clearance Cr(VI) intestine to plasma
PDIN3C	1.03E-05	1.03E-05	Clearance Cr(III) plasma to poorly-perfused tissues
PDOUT3C	0.000308	0.000308	Clearance Cr(III) poorly-perfused tissues to plasma
PDIN6C	0.01029	0.01029	Clearance Cr(VI) plasma to poorly-perfused tissues
PDOUT6C	1.029	1.029	Clearance Cr(VI) poorly-perfused tissues to plasma
BDIN3C	1.03E-05	1.03E-05	Clearance Cr(III) plasma to surface bone
BDOUT3C	0.000308	0.000308	Clearance Cr(III) surface bone to plasma
BDIN6C	0.0103	0.0103	Clearance Cr(VI) plasma to surface bone
BDOUT6C	1.029	1.029	Clearance Cr(VI) surface bone to plasma
KABSC	0.077	0.077	IV absorption rate (per hr)
KFXC	0.6	0.0463	Passage of chromium out of the intestine and into feces (1/h)
Buccal Cavity Absoprtion Parameters			
Maximum Clearance (mg/kg/h)			
KGI6IC	0.00045	0.00025	
KGI3IC	0.00023	1.03E-05	
Affinity for transporter (mg/L)			
KMOGI6	5.6	9.5	
KMOGI3	12.5	10.5	
Buccal Cavity Absorption Rates (L/h/kg)			
Lumen to GI			
KGIOC6C	0.703	0.703	
KGIOC3C	0.703	0.703	
Lumen to Tissue			
KLTOC6C	4.07E-05	4.07E-05	
KTXOC6C	2.16E-05	2.16E-05	
Tissue to Submucossal Tissue			
KLTOC3C	4.07E-06	4.07E-06	
KTXOC3C	2.16E-06	2.16E-06	

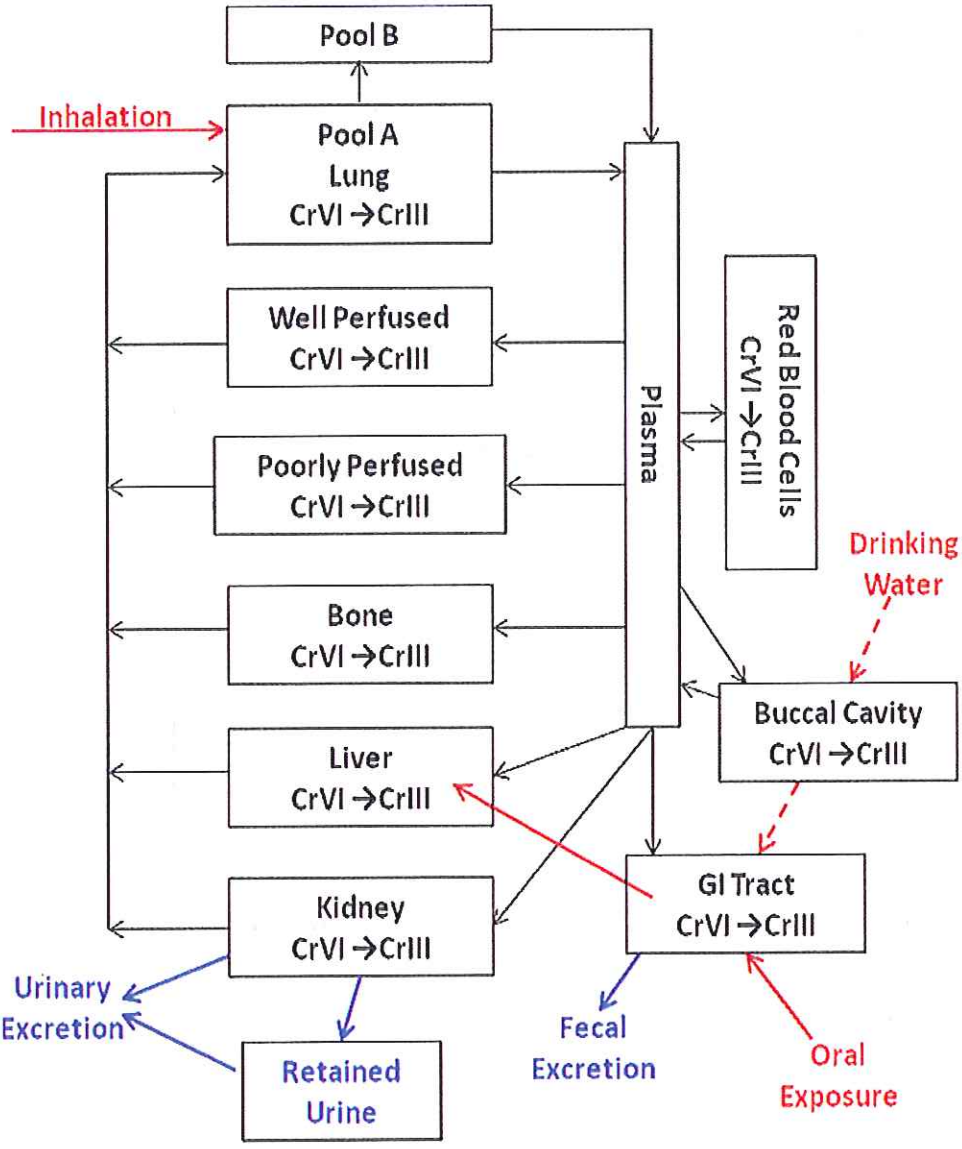

Figure 1. Chromium PBPK model structure for rat and mouse. Red arrows describe dose routes and blue arrows describe routes of excretion.

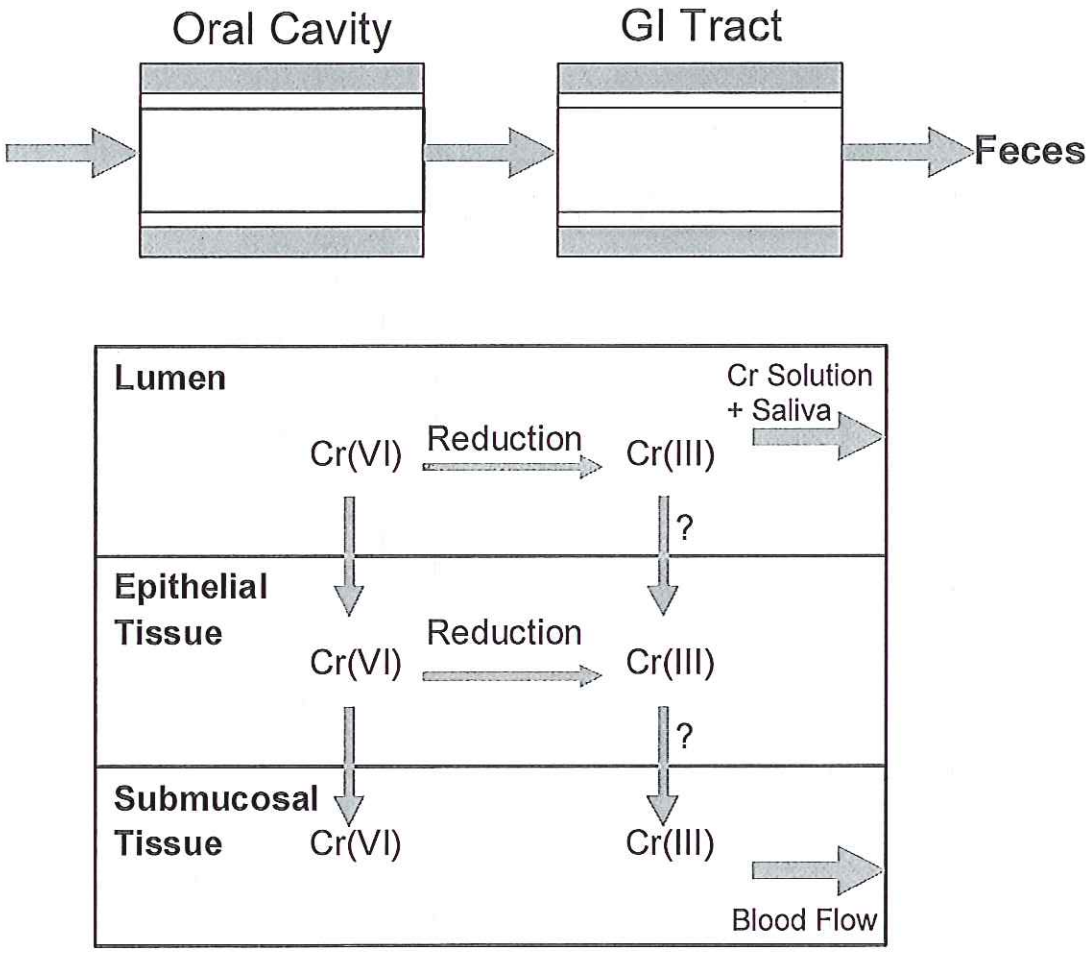

Figure 2. Detail of the PBPK model structure for the GI tract in the rat and mouse.

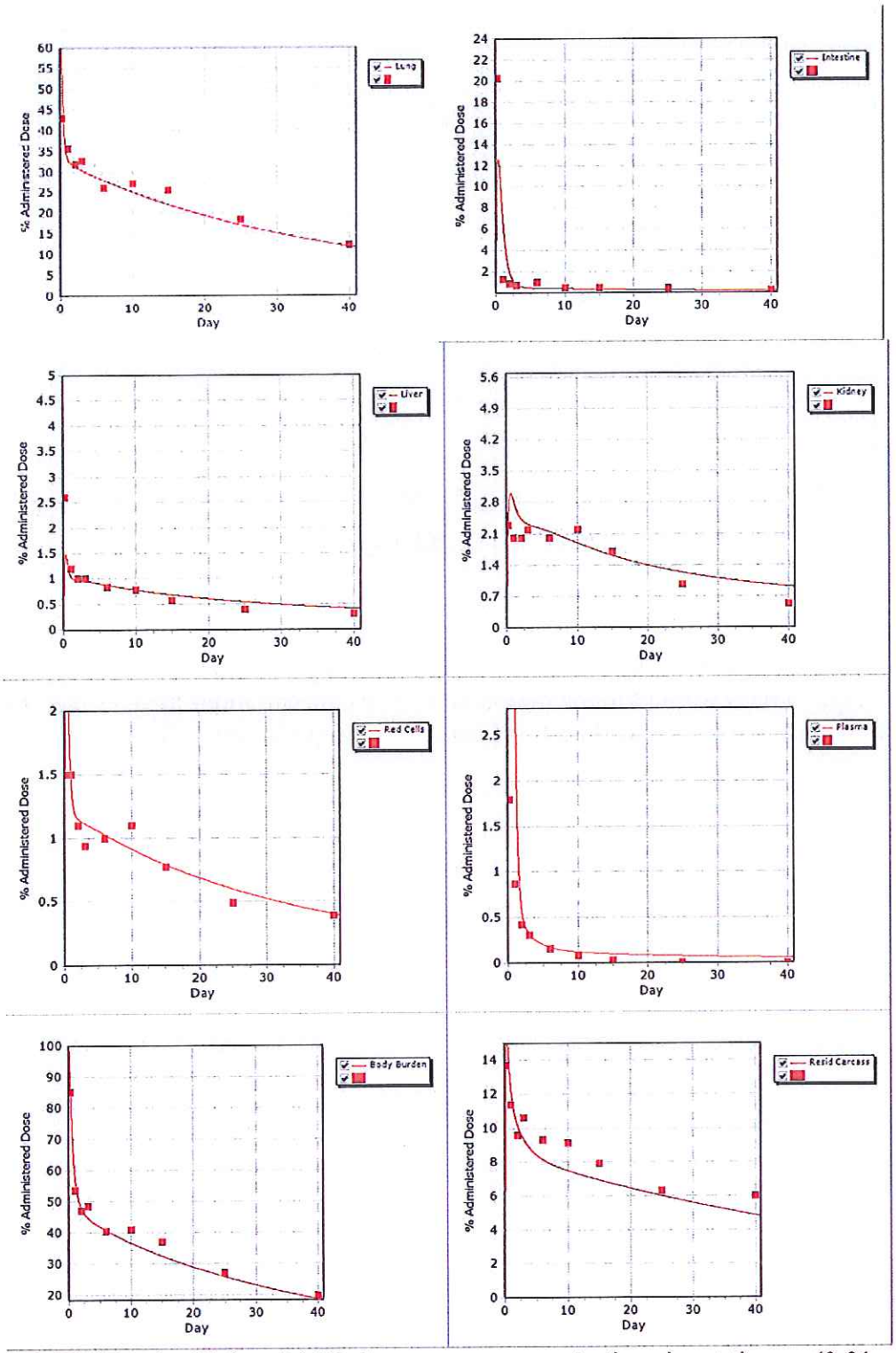

Figure 3. Model fit to the Weber (1983) time course concentrations in rat tissues (0.01 mg/kg intratracheal dose of sodium dichromate) after scaling of rate constants and incorporation of buccal cavity description.

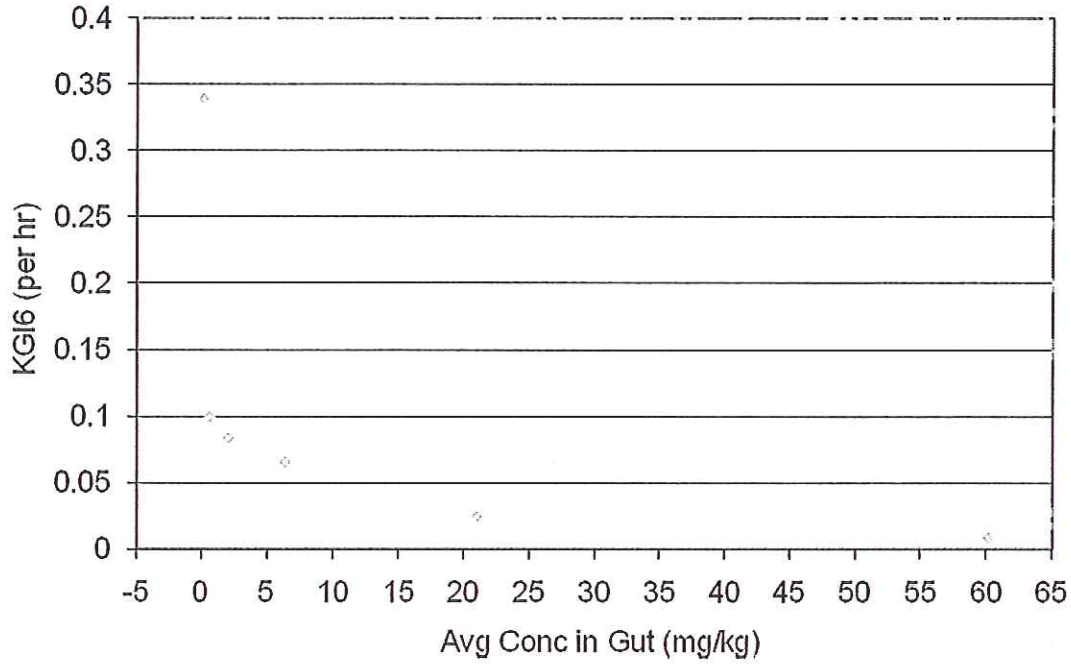

Figure 4. The rate of oral absorption plotted against the average chromium concentration in the gut. Oral absorption rates were fit to the measured kidney concentrations after 21 days exposure to Cr(VI) in drinking water at 1, 3, 10, 30, 100 and 300 ppm (Data from NTP study).

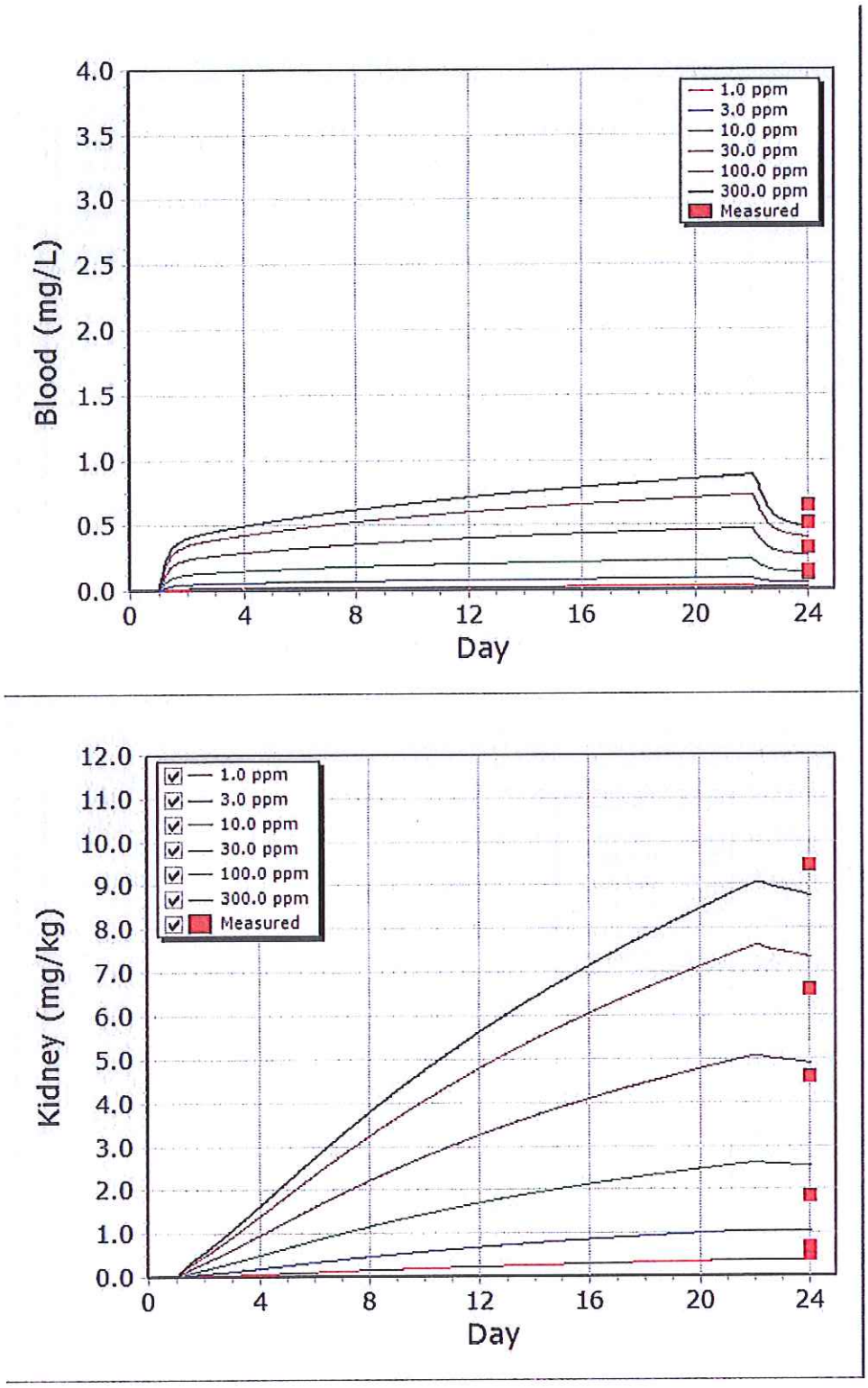

Figure 5. Total chromium in blood (top panel) and liver (bottom panel) of rats following the NTP study protocol of 21 days on drinking water containing sodium dichromate and two days post dosing (data are 48 hours following 21 days on study).

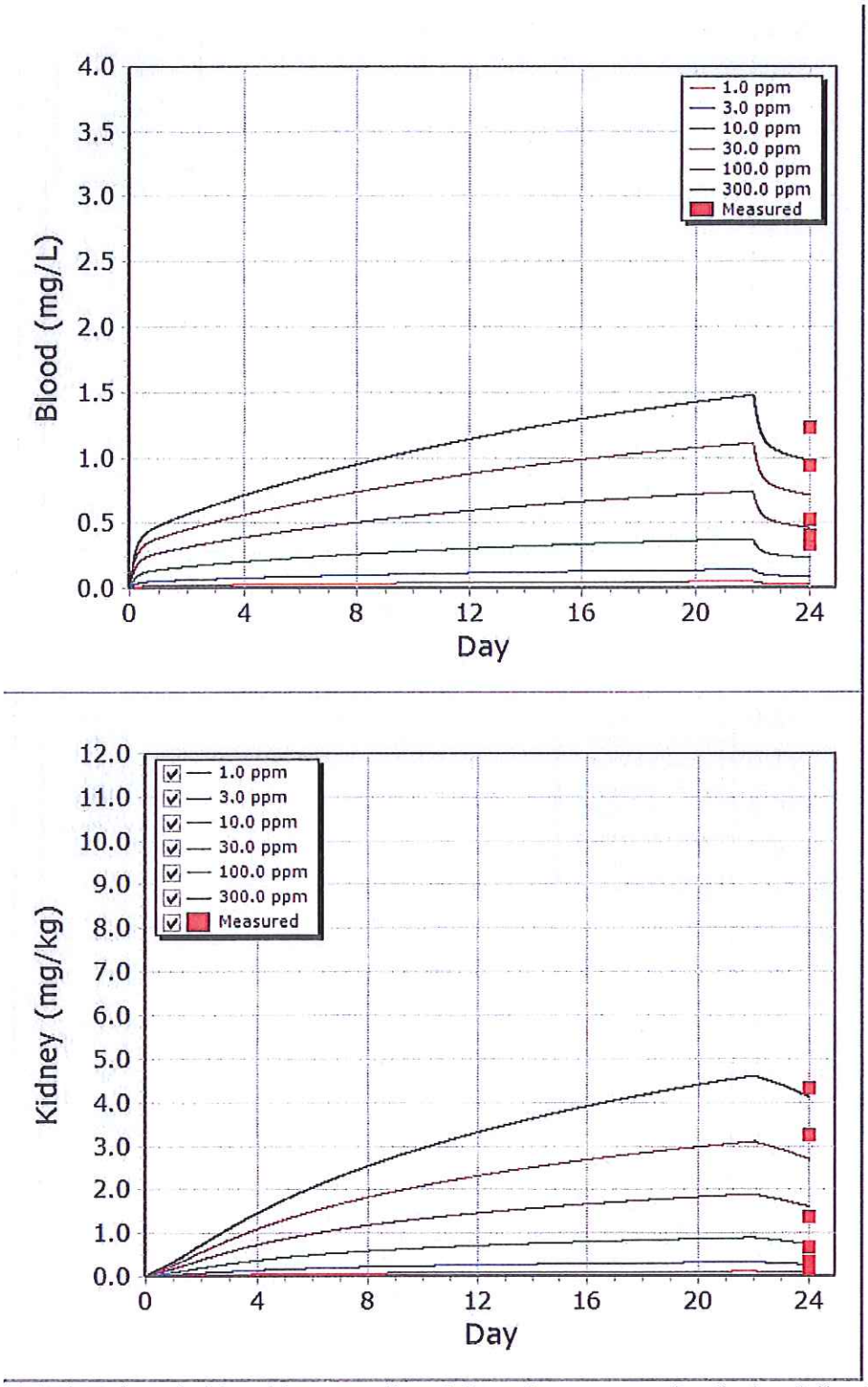

Figure 6. Total chromium in blood (top panel) and liver (bottom panel) of mice following the NTP study protocol of 21 days on drinking water containing sodium dichromate and two days post dosing (data are 48 hours following 21 days on study).

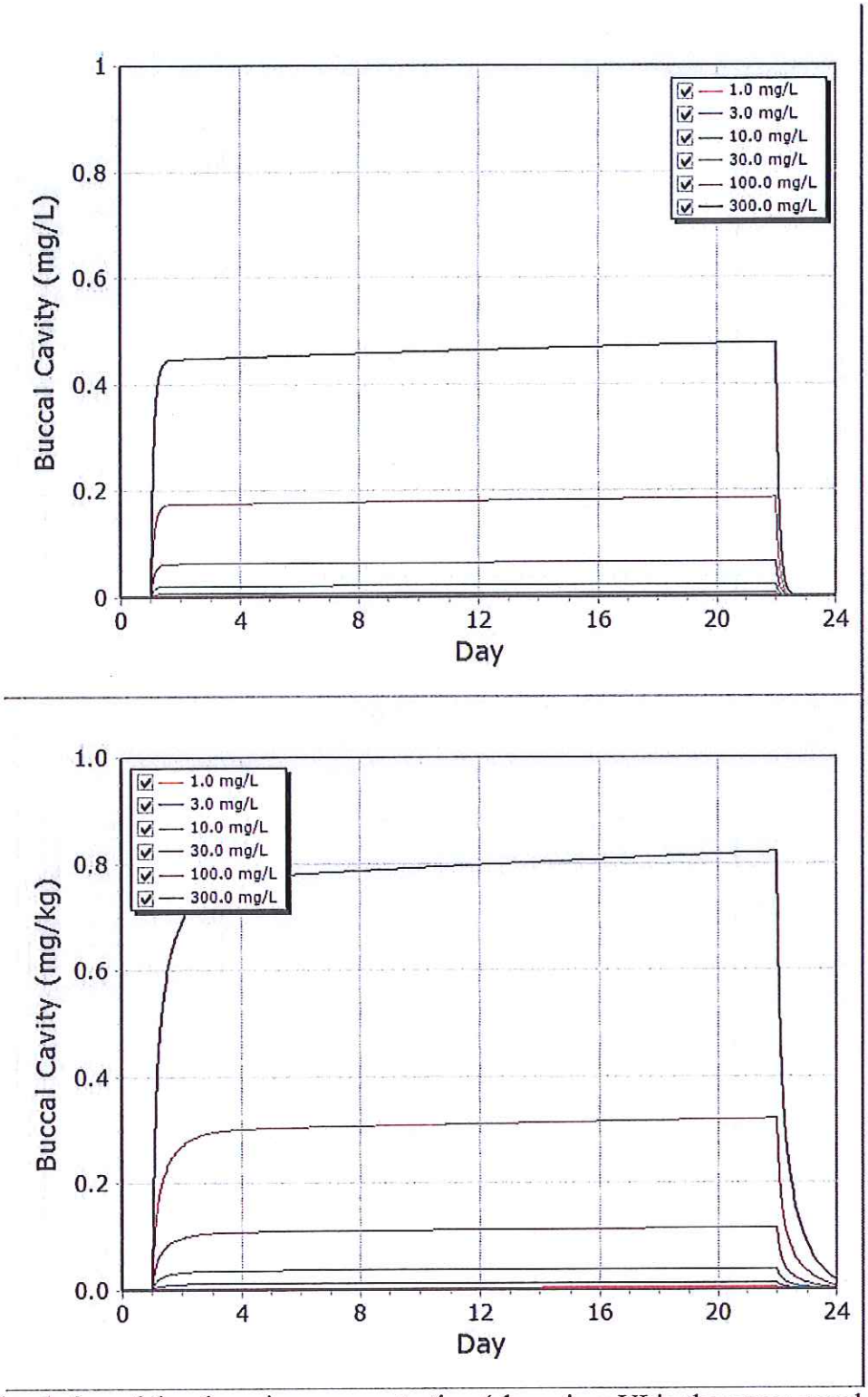

Figure 7. Simulation of the chromium concentration (chromium VI in the upper panel and total chromium in lower panel) in the buccal cavity tissue of rats exposed to sodium dichromate in drinking water for 21 days (based on the NTP study protocol for kinetic data collection).

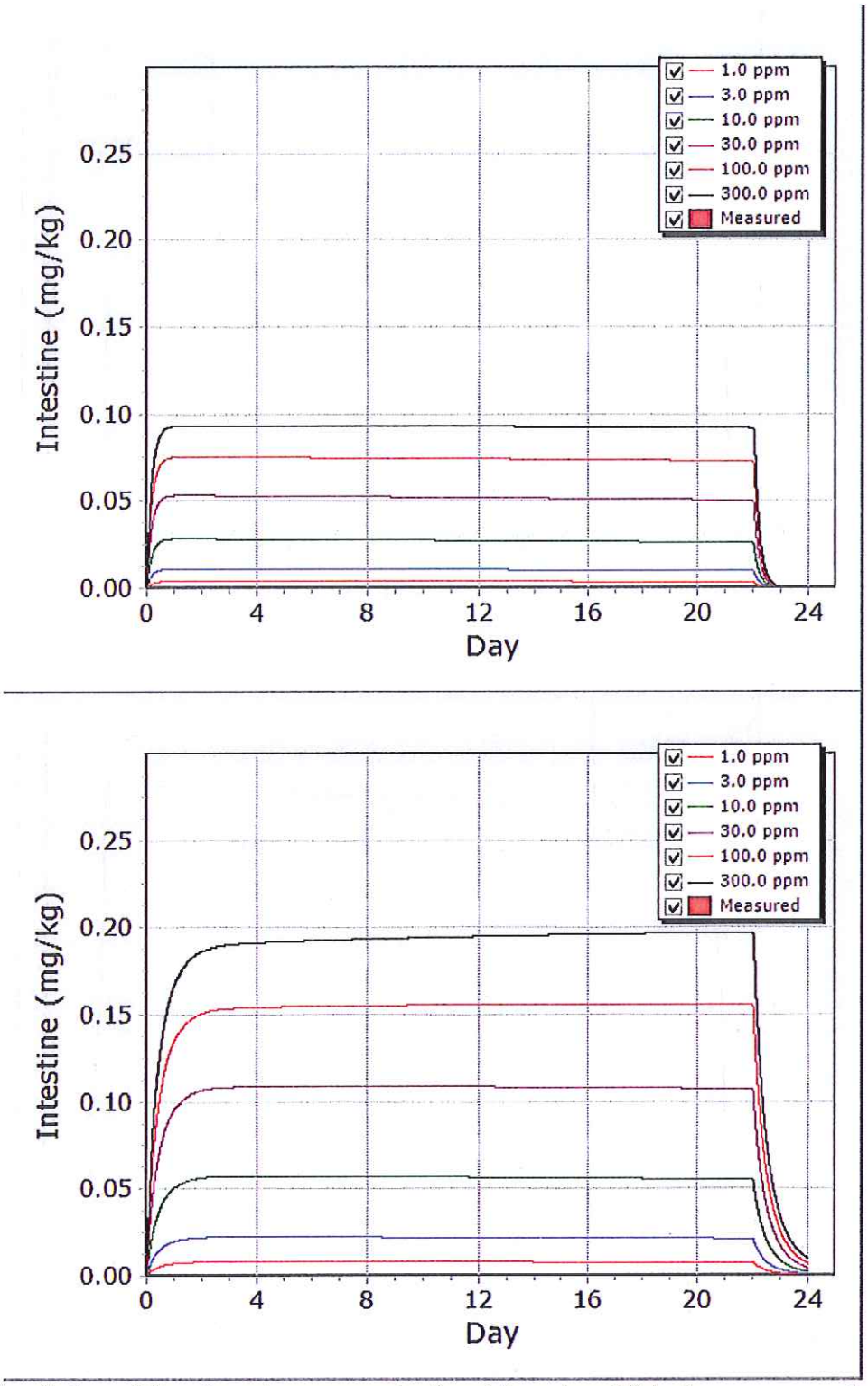

Figure 8. Simulation of the chromium concentration (chromium VI in the upper panel and total chromium in lower panel) in the intestinal tissue of mice exposed to sodium dichromate in drinking water for 21 days (based on the NTP study protocol for kinetic data collection).

Attachment 2

Task 2. Examine Tissues from the Previous 90-Day NTP Rat Study To Determine If There Is Evidence of Pre-Neoplastic Lesions in the Rat Oral Cavity

Principal Investigator: Darol Dodd

Background. In the NTP sodium dichromate dehydrate toxicity study male and female rats were exposed to various concentrations for up to 13 weeks (NTP, 2007). Although the tongue and oral cavity were examined and fixed, they were not processed and examined histologically (per the study protocol) because gross lesions were not observed. This is the same strategy that was used for the 2 year study. However, since gross lesions were observed at these sites in the 2-year study, the NTP decided retrospectively to go back and examine these tissues histologically once they'd received the wet tissues from their contractor following completion of the 2 year study.

Results. After considerable efforts to obtain a response from the NTP, Dr. Ronald A. Herbert of the NTP responded on June 27, 2008. The NTP made a decision to perform the retrospective histopathology evaluation of select target tissues from the 13-week NTP study. The histopathology report was completed on August 28, 2008. A second report of pathology peer review was completed on January 13, 2009. The general public will be notified of the availability of the histopathology and pathology peer-review reports. No timeline was provided when this information would be available. In informal discussions between the NTP and The Hamner, the NTP stated that the examination was essentially negative. That is, there was no evidence of pre-neoplastic lesions in the 90-day study.

NTP Technical Report (2007). Toxicity of Sodium Dichromate Dihydrate (CAS No. 7789-12-0). Administered in Drinking Water to Male and Female F344/N Rats and B6C3F1 Mice and Male NBALB/c and am3-C57BL/6 Mice. NTP TR 72

Attachment 3

Task 3. Magnetic Resonance Imaging (MRI) as a Tool to Investigate the Reduction Rate of Cr(VI).

Principal Investigator: Weili Lin, PhD, UNC-Chapel Hill

Summary. Cr(III) has been suggested to be paramagnetic while Cr(VI) is diamagnetic. Therefore, the presence of Cr(III) is likely to induce magnetic resonance (MR) signal changes while Cr(VI) should have minimal effects on MR signal. While some evidence has demonstrated that the presence of Cr(III) leads to T1 shortening or signal enhancement in T1-weighted images, detailed *in vitro* and *in vivo* characterizations have been lacking. Therefore, experiments were designed to carefully assess the feasibility of whether or not MR is capable of monitoring the reduction of Cr(VI) to Cr(III) *in vivo*. To achieve this goal, both *in vitro* and *in vivo* experiments were conducted in the Biomedical Research Imaging Center at UNC – Chapel Hill. Specifically, the *in vitro* studies were further sub-divided into two parts, including the determination of MR signal change as a function of the concentration of Cr(III) and the measurement of Cr(VI) reduction rate *in vitro*. The former experiments revealed a highly linear relation between R1 (=1/T1) and the concentration of Cr(III). The latter experiment demonstrated that MR imaging approaches are capable of delineating the temporal characteristics of the reduction of Cr(VI) to Cr(III). Finally, preliminary *in vivo* studies were conducted to evaluate whether or not MR is capable of revealing signal changes in the presence of Cr(III). With oral gavage of Cr(III), MR reliably demonstrates signal enhancement in the stomach. More importantly, with oral gavage of Cr(VI), MR also exhibited positive signal changes in the stomach, implying the direct visualization of the reduction of Cr(VI) to Cr(III). Overall, the goals set forward for this feasibility study have been completed and promising results obtained, demonstrating that MR could be employed to reliably monitor the reduction of Cr(VI) to Cr(III) *in vivo*, a stepping stone for the future larger studies.

Introduction. Determining the rate of reduction of Cr(VI) at tumor sites is a proposed key event in Cr(VI) carcinogenic mode of action. However, standard analytical procedures cannot differentiate between the oxidation states of Cr in biological tissues. A direct approach to monitor the reduction of Cr(VI) and its distribution is possible through the use of magnetic resonance imaging (MRI). MRI relies on the fact that paramagnetic materials have magnetic moments/spins that can be measured. This provides an opportunity to evaluate in "real time" the site-specific reduction of Cr(VI) *in vivo* by tracking the distribution of its paramagnetic forms (e.g. Cr(III)). MRI has been used to monitor paramagnetic Cr as a biomarker of effective dose (Cr VI) *in vitro* and in rat lung demonstrating the reductive conversion of Cr(VI) (Shayer *et al.*, 2004). MRI imaging has also been used successfully to monitor the distribution of manganese in different regions of the brain in exposed primates (Dorman *et al.*, 2006).

This pilot study was conducted to assess the feasibility of MRI as a tool to investigate the reduction rate of Cr(VI). To achieve this goal, three sets of experiments were conducted. Experiment 1 was conducted to determine the feasibility of using MR to detect Cr(III) in solution and to determine the dynamic concentration range that can be monitored by MRI. Experiment 2 was conducted to determine whether MR can be used to depict the *in vitro* reduction of Cr(VI) to Cr(III). Lastly, experiment 3 was conducted to assess the feasibility of detecting *in vivo* Cr(VI) conversion to MRI. Experimental details, results and conclusions are provided below.

Experiment 1. Determining the feasibility of using MR to detect the presence of Cr(III)

Objectives: The main objectives of this set of experiments were to determine 1) whether or not Cr(III) will induce MR signal changes as one would expect and 2) if so, what the signal characteristics are regarding Cr(III)induced MR signal changes in relation to Cr(III) concentration.

Methods and results: Several different chromium solutions were prepared and T1 relaxation times were measured using a 9.4T MR scanner. Several sets of experiments were conducted. Detailed experimental information as well as results are provided below.

Experiment 1A included Cr(III) solutions that were created from Cr(VI) by incubating different concentrations of sodium dichromate dihydrate ($Na_2Cr_2O_7 \cdot 2H_2O$, Sigma, #483060) with 1mM ascorbate for at least 2 hours, allowing Cr(VI) to reduce to Cr(III). Figure 1A shows a typical MR image consisting of 6 samples with different concentrations of Cr(VI). Measured T1 relaxation times are listed in Table 1 and the relationship between Cr(III) concentrations and relaxation rate (inverse of T1) is provided in Figure 1B. It is evident that a highly linear relation is observed between the concentration of Cr(III) and R1, allowing an estimate of the relaxivity of Cr(III). These results are of critical importance for the following reasons. First, these results demonstrate that indeed the presence of Cr(III) will result in a shortening of T1 and thus an increased MR signal intensity in T1-weighted images. Second, the measurements of T1 relaxivity for Cr(III) will directly facilitate the design of *in vivo* experiments by providing guidance on Cr(III) concentrations that yield detectable MR signals. For the *in vitro* study, the lowest Cr(III) concentration detected by MR –was 0.0075 mM.

We have further determined the reproducibility of the relationship between R1 and Cr(III) concentration by repeating the same experiments on different days. With Cr(III) concentrations ranging from 0.0075 mM to 0.25 mM, the results from the two measurements on two different days are provided in Figure 1C. A highly consistent result is observed, demonstrating the consistency of the MRI approaches.

Table1. T1 relaxation time constant measured for different concentrations of Cr(III) solution created from Cr(VI).

Concentration(mM)*	T1 (ms)	STD (ms)
0.5	959.322	5.134
0.25	1363.88	58.073
0.125	1889.11	46.463
0.0625	2197.41	74.5
0.03125	2449.54	114.624
0.015	2486.11	262.822
0.0075	2775.28	116.303
0.00375	2737.44	151.43
0.001875	2612	297.215

* Assuming all the Cr(VI) is reduced to Cr(III), the Cr(III) concentration is then equal to the initial Cr(VI) concentration.

A

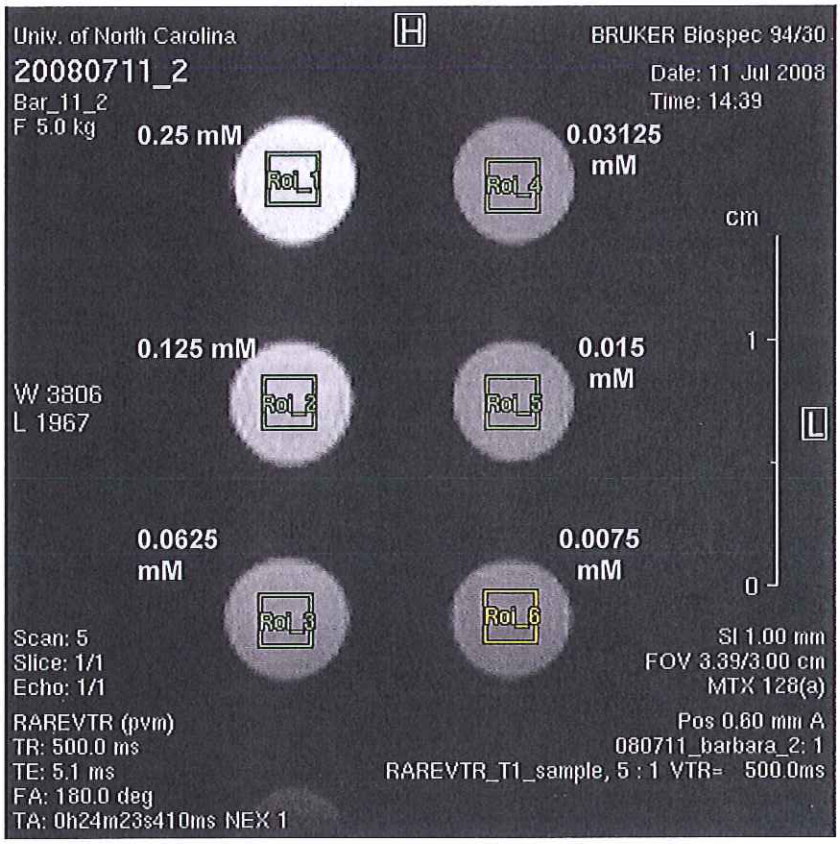

B

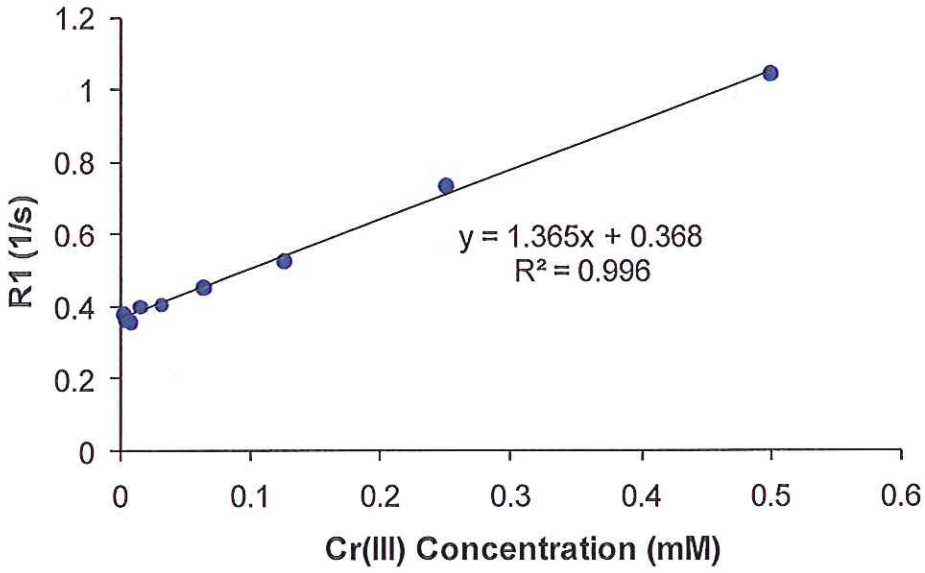

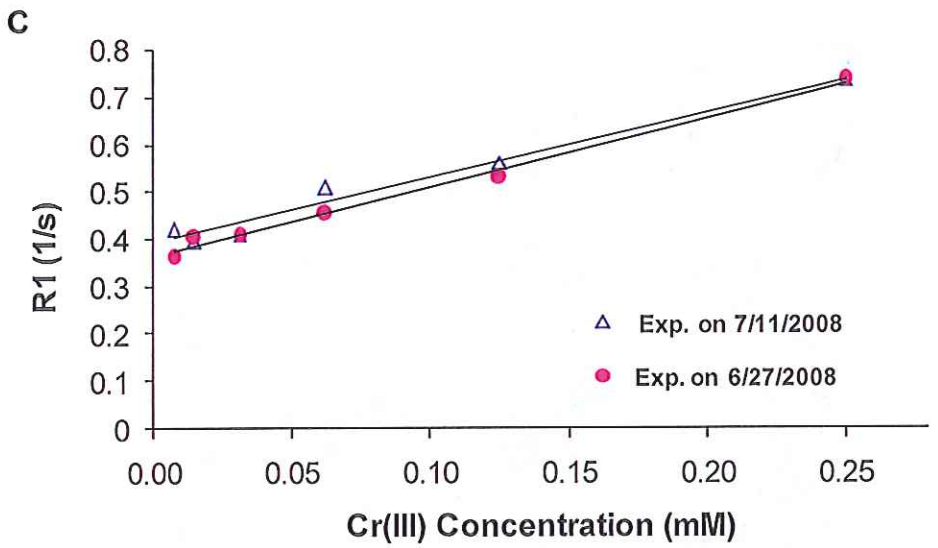

Figure 1. (A) Representative examples of the MR images for the measurements of T1 on different concentrations of Cr(III) created from Cr(VI). (B) The relation between R1 and Cr(III) concentration and (C) results from the reproducibility studies, demonstrating the consistency of the MR approaches.

Experiment 1B employed Cr(III) solutions that were prepared from chromium oxide (Cr_2O_3, Sigma Cat# 203068). This set of experiments was intended to determine whether or not Cr_2O_3 could provide measurable signal from a Cr(III) solution of known concentration. Such a measurable signal could then be used to determine the true Cr(III) concentration in the solutions used in Experiment A. Experimental protocols identical to those in Experiment A were employed. Interestingly, unlike Experiment A, there is little enhancement from these solutions, and no concentration dependency was found (see Figure 2 and Table 2). Analysis of the samples after MR revealed that the Cr_2O_3 had fallen out of solution over time. This insolubility likely contributed to the lack of enhancement: since there was no interaction between Cr molecules and water, there were no T1 effects in MR imaging.

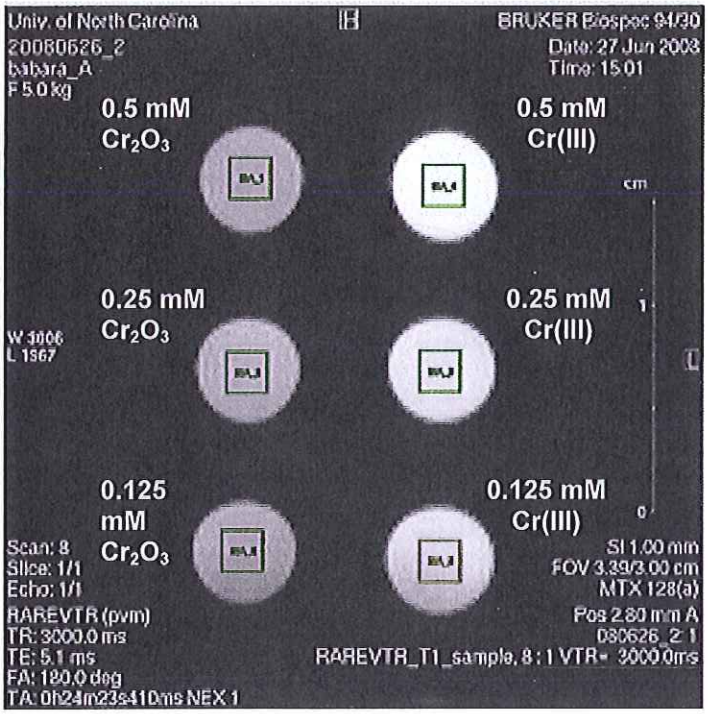

Figure 2. T1 measurement on different concentrations of Cr(III) that were made from Cr_2O_3 (on the left side) or created from Cr(VI) (on the right side).

Table-2: T1 relaxation time measurement for Cr(III) solution made from Chromium oxide.

Cr(III) Concentration in Cr_2O_3 (mM)	T1 (ms)	STD (ms)
0.5	2951.73	112.644
0.25	2917.73	276.591
0.125	2963.48	133.504

Continuing the same rationale as that in Experiment 1B, Experiment 1C employed standard Cr(III) solution directly provided by Sigma (#356166) in 10 mg/ml concentration. The identical experimental protocols as those in Experiment A were employed for this set of experiments. Similar to that observed in Experiment B, the MR signal is relatively lower, suggesting a lack of effect on MR signal. However, unlike Cr_2O_3 which is water insoluble, the Cr(III) solutions employed in this set of experiments should have no difficulties interacting with water. One potential alternative explanation is that the concentrations used in this set of experiments were too high leading to T2/T2* shortening. To test if T2 effects account for the observed low signal in T1-weighted images, T2-weighted images were acquired. Low signal intensity in T2-weighted images was observed, suggesting that indeed T2 may be shortened with the presence of a high concentration of Cr(III). Since the main focus of this pilot study was not to determine the effects of T1 and T2 together, further investigations were not followed.

Experiment 1D was a control study, where Cr(VI) solutions, liver homogenate, and GSH solutions were assessed using the identical imaging protocols as described above. The results show the expected low MR signal with a much longer T1 for all the negative control solutions.

Finally, in Experiment 1E, we compared two Cr(III) solutions that were created from 0.125 mM Cr(VI) in sodium dichromate dihydrate ascorbate incubation with or without liver homogenate, respectively. The results show a higher T1 relaxation rate for Cr(III) made with liver homogenate incubation (0.78 s^{-1}) than that without liver homogenate (0.58 s^{-1}), suggesting that more Cr(VI) was reduced to Cr(III) in liver homogenate mixture when compared to that with only the ascorbate mixture.

Experiment 2. Depicting Cr(VI) reduction to Cr(III) *in vitro* using MRI

Objective: To determine whether MR can be used to depict the reduction of Cr(VI) to Cr(III) *in vitro*.

Methods and Results: For the second step of this pilot study, we focused on how MRI can be used to discern the temporal reduction of Cr(VI) to Cr(III) in biological tissues and fluids *in vitro*. Several compounds, including liver homogenate and GSH, were used as reducing compounds which were added to Cr(VI) solutions right before MR imaging sessions. The solution was then placed in the 9.4T MR scanner and continuous T1-weighted imaging was performed to monitor the reduction reaction. Based on the dynamic MR signal changes, we also explored the ability of MR in estimating the reduction rate of Cr(VI) to Cr(III).

The temporal characteristics of MR signal of Cr(VI) with liver homogenate or GSH were examined. A pure Cr(VI) solution was also measured and served as the baseline signal. The MR signal obtained after adding liver homogenate or GSH was then corrected by the background signal level and plotted against time (Figure 3). Due to the preparation time for MR scanning, the signal characteristics immediately after mixing were not available. Evidently, the reaction curves reach a plateau 10 min after addition of the liverhomogenate, while it tookapproximately 40 min to reach a similar plateau after addition of GSH. This indicates a much faster reaction rate with liver homogenate when compared to GSH mixing. However, the Cr(III) signal level is much higher when reduced by 5mM GSH than by 100 µl of liver homogenate, suggesting that the reductive capacity of the *in vitro* liver preparation was exhausted before complete reduction of Cr(VI) to Cr(III) occurred. To test this hypothesis, an additional experiment was conducted in which the amount of liver homogenate was almost doubled (190 µl added).. The result is shown in Figure 4. This increase in the amount of liver homogenate led to an increase in the Cr(VI) reduction to Cr(III) and a concomitant increase in signal intensity, which exceeded those observed in the GSH-containing samples.

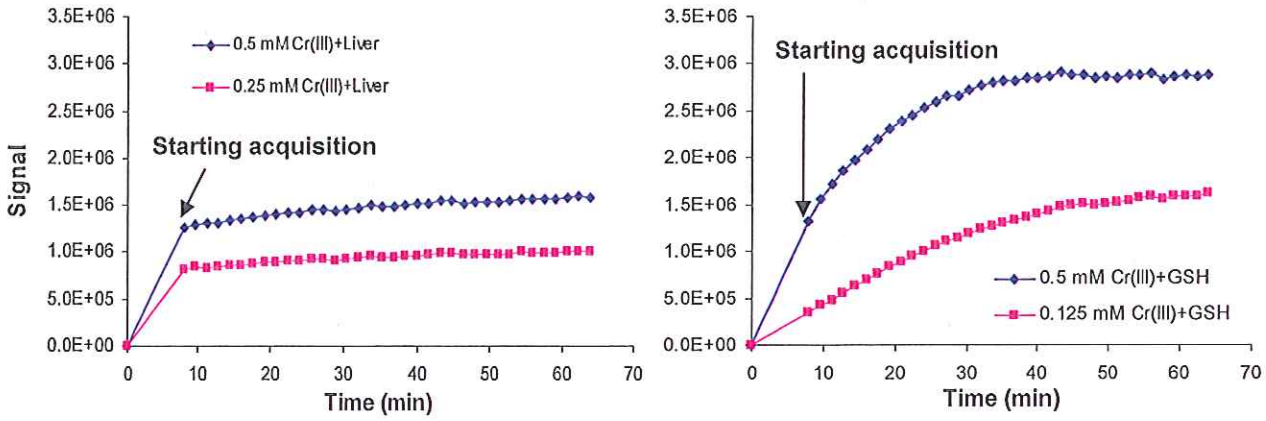

Figure 3. MR signal-time curves for reduction reaction between Cr(VI) and 100 µl liver homogenate or 5 mM GSH. Signal is normalized to background level.

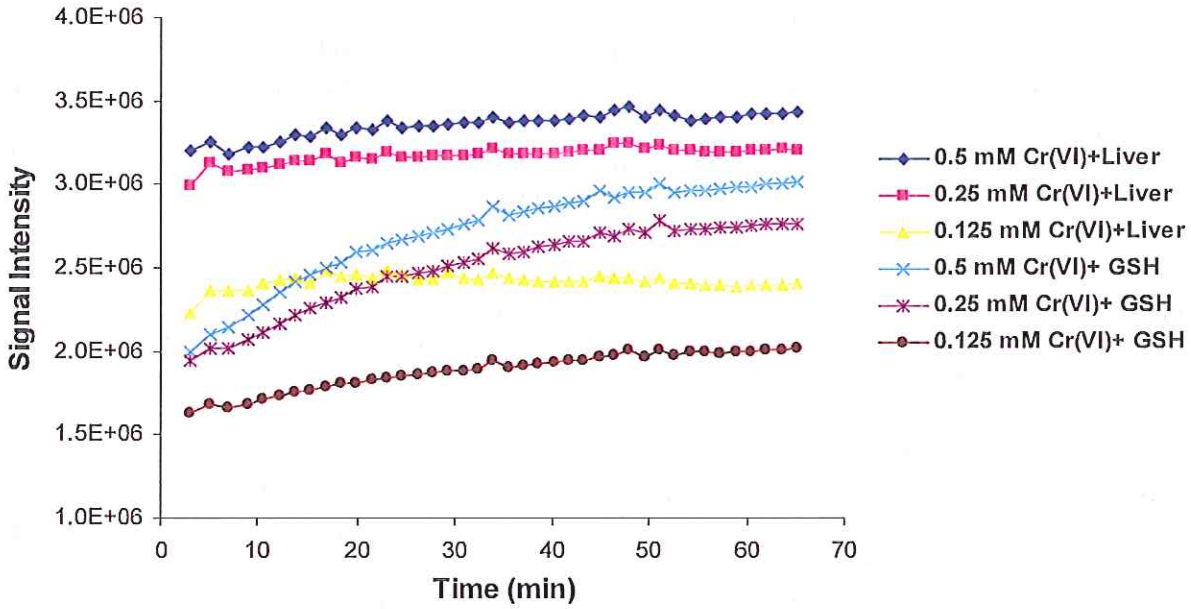

Figure 4. MR signal-time curves for Cr(VI) reduction with 190 µl liver homogenate or 5 mM GSH.

The effects of GSH concentrations on Cr(VI) reduction were also monitored using different concentrations of GSH. The results (Figure 5) demonstrate the concentration dependence of Cr(VI) reduction with GSH.

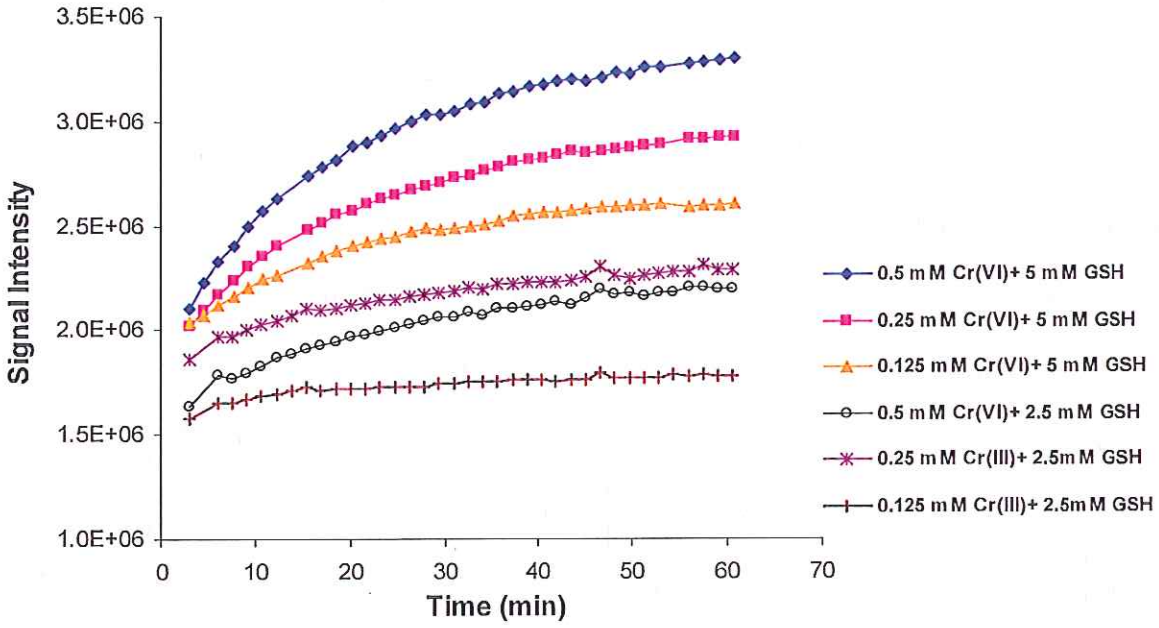

Figure 5. Effects of GSH concentration on Cr(VI) reduction.

Experiment 3. Demonstrating the feasibility of detecting *in vivo* Cr(VI) conversion using MRI

Objectives: The main objectives of this set of experiments were to determine the feasibility of MRI in detecting *in vivo* reduction of Cr(VI) to Cr(III), the sensitivity of MRI, and the anatomical locations of Cr(VI) reduction in mice.

Methods and Results: Mice were divided into two groups. Group-1 served as a positive control group which received oral gavage of Cr(III) solution and was imaged before and right after the gavage for 30 min. Group-2 was further sub-divided into different groups depending on the amount of Cr(VI) the animals received.

Group2-1: gavage 0.1 ml of 1 mM Cr(VI)
Group2-2: gavage 0.1 ml of 0.5 mM Cr(VI)
Group2-3: gavage 0.1 ml of 0.25 mM Cr(VI)

Group-2 mice were imaged at 5 time points: 1) before gavage; 2) right after gavage for 2 hour; 3) 4 hours after gavage; 4) 24 hours after gavage; and 5) 48 hours after gavage. More detailed experimental information is summarized in Table 3.

Table-3: Experiment record for *in vivo* Chromium imaging on mice

Date	Animal ID	Weight (g)	Gavage		MR Imaging				
			Dose	Time	Pre-	0 hr/ for 2 hrs	4 hrs	24 hrs	48 hrs
12/08/2008	20081208-1	28.1	1mM Cr(VI)	11:17 am	11:00	11:30	3:30	2:45pm/ 2^{nd} D	
	20081208-2	26.4	1mM Cr(III)	2:00 pm	1:45	2:10			
	20081208-3	26.1	0.5mM Cr(III)	2:50 pm	2:41	3:00			
12/09/2008	20081209-1	31.0	1mM Cr(VI)	10:15 am	10:00	10:20	3:20	9:00am/ 2^{nd} D	
	20081209-2	28.2	0.5mM Cr(VI)	12:40 pm	12:25	12:45	4:20	9:50am/ 2^{nd} D	
12/16/2008	20081216-1	29.6	1mM Cr(VI)	9:40 am	9:35	9:50	2:00	2:20pm/ 2^{nd} D	9:15am/ 3^{rd} D
	20081216-2	28.4	0.5mM Cr(VI)	12:25 pm	12:17	12:30	4:15	2:45pm/ 2^{nd} D	9:33am/ 3^{rd} D
12/17/2008	20081217-1	30.0	0.5mM Cr(VI)	9:40 am	9:30	9:45	3:10	9:52am/ 2^{nd} D	10:54am /3^{rd} D
	20081217-2	28.9	1mM Cr(VI)	12:15 pm	12:10	12:23	4:00	10:15am /2^{nd} D	11:15am 3^{rd} D
01/05/2009	20090105-1	30.4	0.25 mM Cr(VI)	10:25 am	10:00	10:30	2:55	2:30 pm/2^{nd}	1:30 pm /3^{rd} D
	20090105-2	30.2	0.25 mM Cr(VI)	1:00 pm	12:50	1:05	4:20	2:50 pm/2^{nd}	1:50 pm/3^{rd} D
01/06/2009	20090106-1	32.4	0.5 mM Cr(VI)	10:00 am	9:45	10:10	3:15	10:00am /2^{nd} D	10:00am /3^{rd} D
	20090106-2	31.1	0.25 mM Cr(VI)	12:25 am	12:10	12:30	4:15	10:30am /2^{nd} D	10:30am /3^{rd} D

For the control group, there is a significant enhancement in the stomach region (Figure 6) after Cr(III) gavage, similar to what we observed in the *in vitro* experiments. For animals administered Cr(VI) by gavage, the enhancement was also apparent though to a lesser degree than after Cr(III) administration. With 1mM Cr(VI) gavage, the enhancement can be easily detected after gavage through 24 hrs (Figure 7). Enhancement index was calculated by normalizing MR signal of the stomach to muscle at each time point in each animal and compared to its baseline signal (before gavage). The enhancement at different time points was plotted for three different gavage concentrations (Figure 8 A). Note that the image analysis was based on manual drawing of ROIs on one slice, which could be subjective and might not reflect the complete enhancement patterns. There are some inconsistencies between animals (data not shown). As a result, three animals in each group might not give a sufficient power for meaningful statistical analysis. Results shown in Figure 8A are from one animal in each group. For a more accurate analysis, more advanced image processing, such as the model-based segmentation, and volume measurement might be needed.

A dynamic curve of MR signal for the first two hours immediately after gavage is shown in Figure 8B. Although signal fluctuations were observed, comparing with the signal obtained from muscle, the signal in the stomach and liver showed some enhancement, suggesting the reduction of Cr(VI) to Cr(III) can be observed *in vivo*. The temporal resolution is probably not enough to monitor the whole reduction process. Nevertheless, modifying the imaging protocols could be easily accomplished to further improve the temporal resolution.

Summary. In summary, the main goal of this pilot study was to determine the feasibility of utilizing MR in monitoring the reduction of Cr(VI) to Cr(III). Although improvements, including animal preparations, imaging protocols, and image analysis will be needed to provide more quantitative measurements, the qualitative assessments of MR results suggest that MR is highly feasible in providing both *in vitro* and *in vivo* monitoring of the reduction processes.

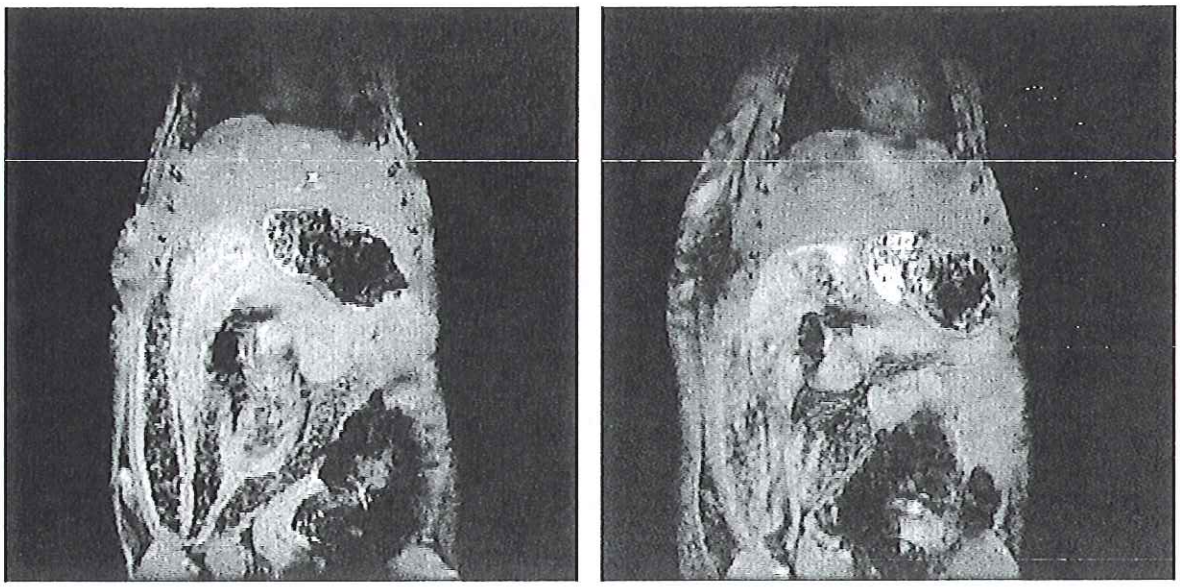

Figure 6. Images from pre-contrast (left) and 15 min post-contrast (right) of the mouse with Cr(III) gavage (0.1 ml of 1 mM Cr(III)).

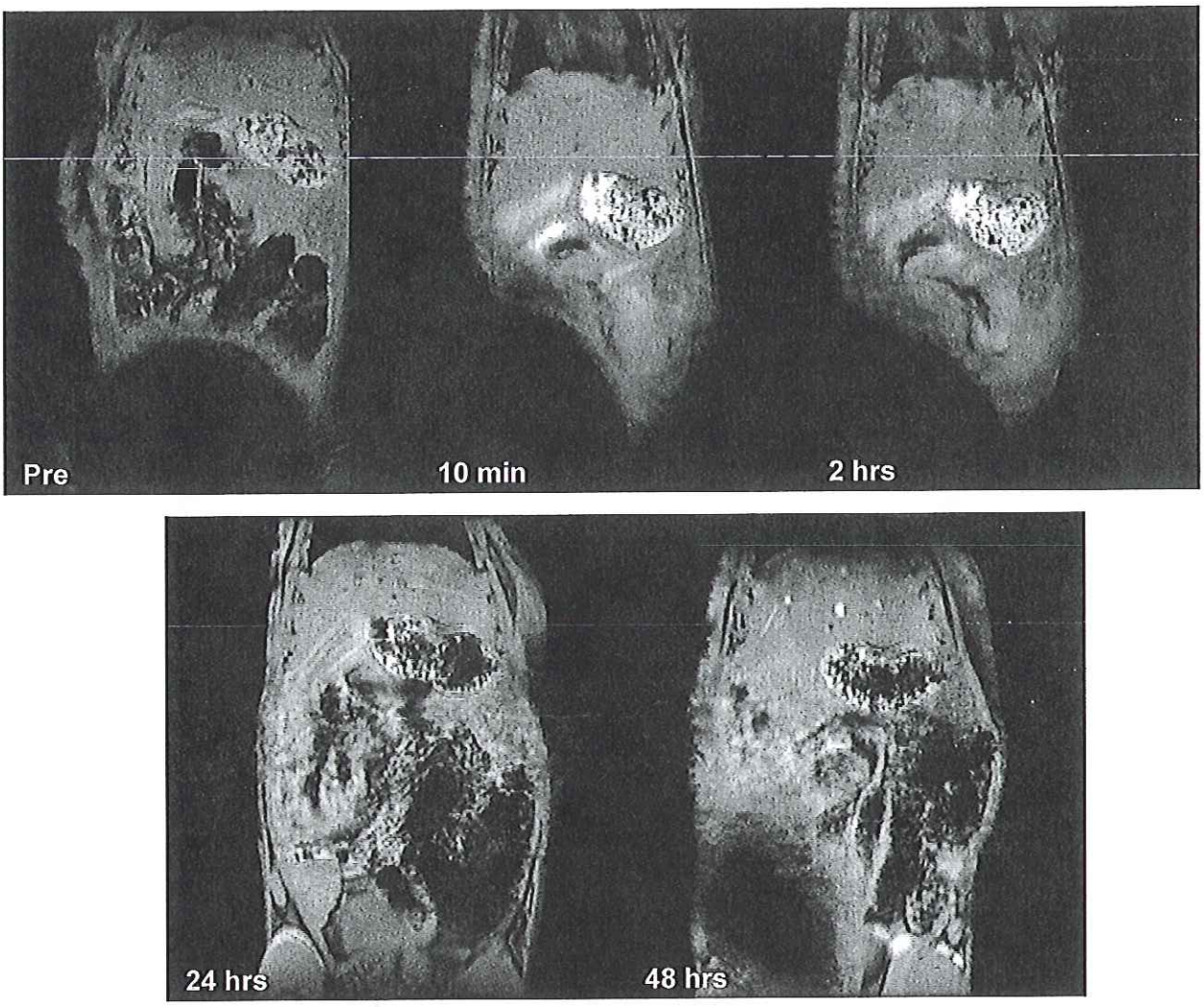

Figure 7. MR Images of a mouse at different time points after gavaging Cr(VI) (0.1 ml of 1 mM Cr(VI)).

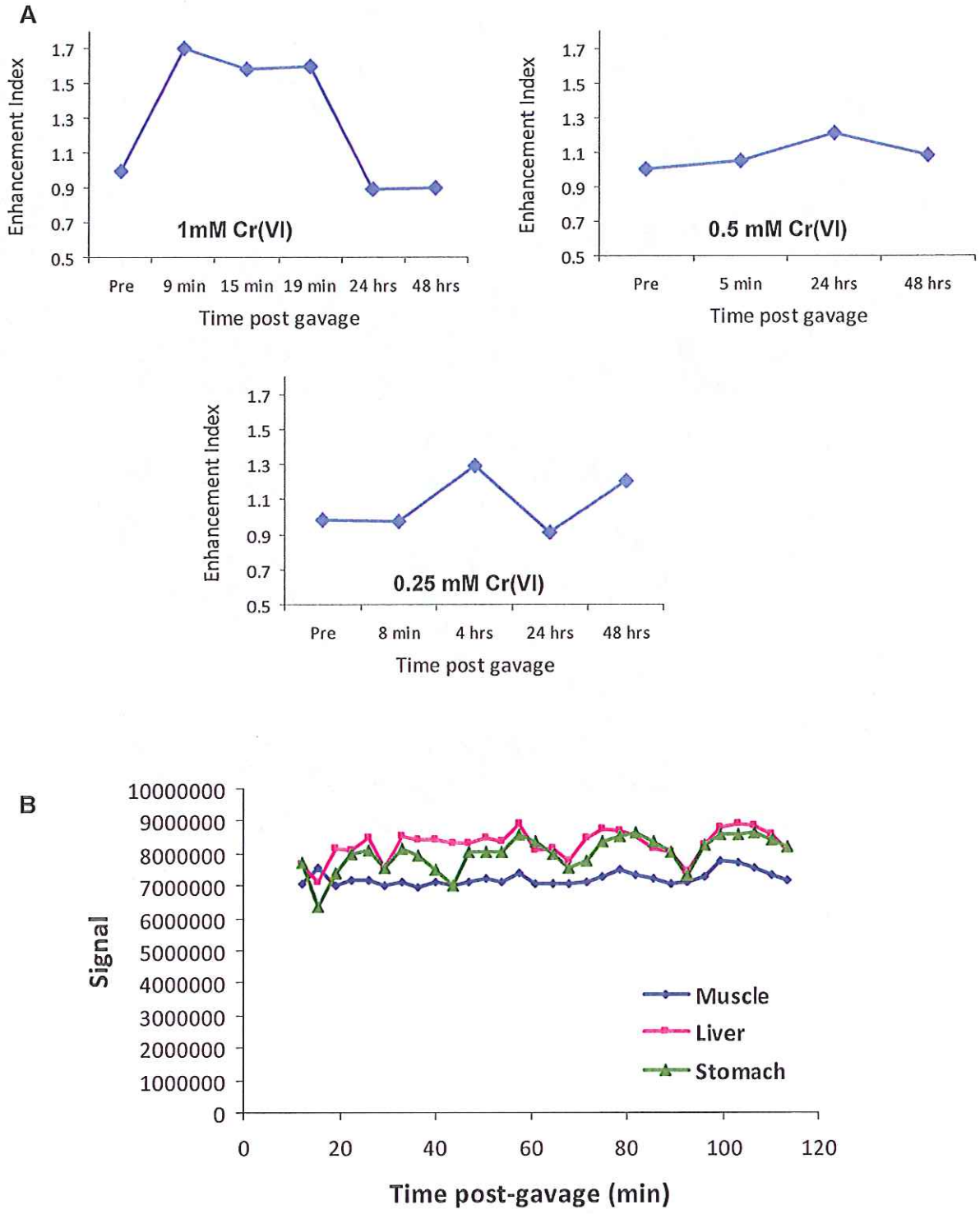

Figure 8. Signal enhancement after oral gavage of different concentrations of Cr(VI) (Panel A). Panel B shows the signal curves of the first 2 hours after gavage.

Attachment 4

Task 4. Evaluation of the Genotoxicity of Cr(VI) in the Oral Cavity and Duodenum: Feasibility of Buccal and Duodenal Cell Collection

Principal Investigator: Sheela Sharma, PhD, The Hamner Institutes

Objective 1. Determine the number of cells that can be obtained for micronucleus analysis in the oral cavity of rats.

Methods:

Six female rats (F 344) were used for cell collection. Animals were sacrificed with CO_2 inhalation and an incision was made on either side of the mouth to open the jaws wide. After rinsing the oral cavity with PBS (phosphate buffered saline), surface buccal cells were collected by repeat scraping in one direction with a wooden spatula. The scraped cells from each animal were suspended in .3 ml media of F 12 + 5% FBS (fetal bovine serum) to ensure viability, spun at 1000 rpm in a refrigerated centrifuge. The cell pellet was resuspended in 1 ml medium, and an aliquot was used for counting cells in a hemocytometer and calculated the total number of cells.

Results:

The average number of cells ranged from $5x10^4$ to $1x10^5$ /rat (see Table 1 for details).

Table 1. Total Number of Oral Epithelial Cells from Individual Rat

Animal Number	Total Cell Number/Rat
1	1×10^5
2	8×10^4
3	5×10^4
4	9×10^4
5	9×10^4
6	7×10^4

Conclusion:

It appears that there is sufficient number of cells to evaluate MN induction by conventional slide scoring. However, MN analysis by flow cytometry is not feasible as it requires a minimum of $1x10^6$ cells.

Objective 2. Determine the number of cells that can be obtained from mouse duodenum for micronucleus analysis.

Methods:

Six mice were used for cell collection. Animals were sacrificed with CO_2 inhalation, opened the abdominal cavity by making a longitudinal incision and the blood was drained by making an incision in the vena cava. After rinsing the abdominal area with PBS, the

intestine was exposed and the duodenum (~1cm) was collected by snipping with a surgical scissors. The excised tissue was placed in a 60 mm dish, cut open using a fine surgical scissors, spread flat and rinsed with PBS to clean the surface. A narrow wooden spatula was used to scrape and collect cells, which was then suspended in 1 ml media (F 12 + 5% FBS), spun at 1000 rpm for 15 min. in a refrigerated centrifuge. The cell pellet was resuspended in 1 ml medium, and an aliquot was used for counting cells in a hemocytometer and calculated the total number of cells.

Results:

The average number of cells ranged from 9.5×10^5 to 1.93×10^6 /mouse (see Table 2 for details).

Table 2. Total Number of Duodenal Epithelial Cells from Individual Mouse

Animal Number	Total Cell Number/Mouse
1	1.93×10^6
2	1.41×10^6
3	1×10^6
4	1.02×10^6
5	9.5×10^5
6	1.31×10^6

Conclusion:

The data shows that there is sufficient number of cells to evaluate MN induction by conventional slide scoring and by flow cytometry.

Future Efforts - Other Procedures for Rat Oral Epithelial Cell Isolation

Method A. Manual exfoliation plus enzyme treatment

Sacrifice rat via CO_2 and expose the oral cavity by surgical resection from the middle of the lower jaw. Dissect right and left cheek mucosa and the upper jaw (palate area), and then place dissected tissue on a clean dissecting board and spread using small pins, and wash thoroughly with PBS for 3 times. Manually exfoliate epithelial layer carefully from the surface of cheek mucosa and upper jaw by using fine forceps. Place separated epithelium into the buffer (F12 + 5% FBS), add trypsin (amount TBD) to the buffer containing epithelium and incubate for 5 min. at 37°C or until the epithelial layer becomes single cell suspension. Centrifuge cells, re-suspend and evaluate cell number from an aliquot of cell suspension using hemocytometer and a microscope.

Method B. Manual exfoliation plus immunomagnetic bead separation

Sacrifice rat via CO_2 and follow the steps as described in Method A up to the trypsin digestion and obtaining a single cell suspension. Centrifuge the cells and re-suspend. Prepare epithelial specific antibody using DSB-X Biotin Protein Labeling Kit. Incubate the DSB-X labeled antibody with the cell suspension for a few minutes. Add Flow Comp Dynabeads to the labeled cells and isolate the bead-bound cells using a magnet. Release epithelial cells that are bound to the beads by using the FlowComp Release Buffer. This procedure would yield a pure population of epithelial cells.

ATTACHMENT 3

A Method to Integrate Benchmark Dose Estimates with Genomic Data to Assess the Functional Effects of Chemical Exposure

Russell S. Thomas,*,1 Bruce C. Allen,† Andy Nong,* Longlong Yang,* Edilberto Bermudez,* Harvey J. Clewell III,* and Melvin E. Andersen*

*The Hamner Institutes for Health Sciences, Division of Computational Biology, Research Triangle Park, North Carolina 27709-2137;
†Bruce Allen Consulting, 101 Corbin Hill Circle, Chapel Hill, North Carolina 27514

Received February 9, 2007; accepted April 16, 2007

TOXICOLOGICAL SCIENCES 98(1), 240–248 (2007)
doi:10.1093/toxsci/kfm092
Advance Access publication April 21, 2007

A Method to Integrate Benchmark Dose Estimates with Genomic Data to Assess the Functional Effects of Chemical Exposure

Russell S. Thomas,*[,1] Bruce C. Allen,† Andy Nong,* Longlong Yang,* Edilberto Bermudez,* Harvey J. Clewell III,* and Melvin E. Andersen*

*The Hamner Institutes for Health Sciences, Division of Computational Biology, Research Triangle Park, North Carolina 27709-2137; †Bruce Allen Consulting, 101 Corbin Hill Circle, Chapel Hill, North Carolina 27514

Received February 9, 2007; accepted April 16, 2007

The use of genomic technology for assessing health risks associated with chemical exposure has significant potential, but its direct application has proven to be challenging for the toxicology and risk assessment communities. In this study, a method was established for analyzing dose-response microarray data using benchmark dose (BMD) calculations and gene ontology (GO) classification. Gene expression changes in the rat nasal epithelium following acute formaldehyde exposure were used as a case study. The gene expression data were first analyzed using a one-way ANOVA to identify genes that showed significant dose-response behavior. These genes were then fit to a series of four statistical models (linear, second-degree polynomial, third-degree polynomial, and power models) and the least complex model that best described the data was selected. The genes were matched to their associated GO categories, and the average BMD and benchmark dose lower confidence limit (BMDL) were calculated for each GO category. The results were used to identify doses at which individual cellular processes were altered. For the formaldehyde exposures, the BMD estimates for the GO categories related to cell proliferation and DNA damage were similar to those measured in previous studies using cell labeling indices and DNA-protein cross-links and consistent with the BMD estimated for rat nasal tumors. The method represents a significant advance in applying genomic information to risk assessment by allowing a comprehensive survey of molecular changes associated with chemical exposure and providing the capability to identify reference doses at which particular cellular processes are altered.

Key Words: bioinformatics; methods; dose-response; risk assessment; nose; respiratory toxicology; microarray; methods; regulatory/policy; risk assessment; toxicogenomics; methods.

A major objective of toxicology and chemical risk assessment is to identify permissible exposure levels based on data from human or experimental animal studies together with other relevant scientific information. In the past, the permissible exposure levels were based on doses corresponding to lowest observed adverse effect levels (LOAEL) or no observed adverse effect levels (NOAEL). The LOAEL has been traditionally defined as the first dose producing a statistically significant, adverse change in the response and the NOAEL as the dose preceding the LOAEL. The weakness of this approach is that dose spacing and the experimental sample size can have a dramatic impact on the final NOAEL and LOAEL, and the approach does not account for variability in the estimate of the dose-response or the slope of the dose-response curve. To overcome these limitations, benchmark dose (BMD) analysis was introduced (Crump, 1984). BMD analysis fits a statistical model to the dose-response data and identifies a dose that causes a defined change in the adverse response. The application of BMD analysis provides several advantages including better use of dose-response information, more appropriate reflection of experimental sample sizes, and the lack of constraint to experimental doses (Filipsson *et al.*, 2003).

The application of microarray technology in toxicology has proven to be both useful for simultaneously measuring the expression of thousands of genes and challenging with respect to interpreting what changes in these genes mean in relation to the toxic response. The transcriptional changes represent only a snapshot of the state of the cell or tissue and include a complex mix of primary and secondary responses to the chemical treatment (Page *et al.*, 2006). Previous efforts to interpret these changes have focused on applying standardized functional annotations to each gene involved in the response and identifying whether certain biological processes or molecular functions are over- or underrepresented (Beissbarth and Speed, 2004; Dennis *et al.*, 2003; Khatri *et al.*, 2004; Yu *et al.*, 2006; Zhang *et al.*, 2004). This approach has been referred to as a gene ontology (GO) enrichment analysis and allows large lists of transcriptional alterations to be distilled down into changes in cellular processes such as the immune response, DNA repair, or apoptosis.

Although GO enrichment analyses provide insights into what biological processes are altered, this type of analysis has

[1] To whom correspondence should be addressed at The Hamner Institutes for Health Sciences, Division of Computational Biology, 6 Davis Drive, PO Box 12137, Research Triangle Park, NC 27709-2137. Fax: (919) 558-1300. E-mail: rthomas@thehamner.org.

been primarily applied to studies designed to examine only a single experimental variable at a time. The informatic tools available for analyzing higher dimensional data such as dose-response and time course studies have so far been limited. Recently, Yu *et al.* (2006) introduced an approach to apply GO analysis to dose-response studies. Using this approach, the dose-response changes in the various functional categories are summarized using EC_{50} values allowing the identification of cellular processes that have different dose-response characteristics (Yu *et al.*, 2006). The approach represents a significant contribution for analyzing dose-response data within toxicology. To broadly apply genomic studies to chemical risk assessment, the functional changes must be linked to a defined increase in risk through a more rigorous statistical approach, such as BMD.

Formaldehyde is a major industrial chemical and is widely used as a raw material in the manufacture of synthetic resins, lubricants, adhesives, and fertilizers. In 1992, 8.3 billion pounds were produced within the United States and its production ranked 22nd overall (ATSDR, 1999). Among the acute effects elicited by formaldehyde, sensory irritation has been reported to occur at less than 1 ppm in humans and 2 ppm in animals (Arts *et al.*, 2006). Following longer term exposures, regenerative cell proliferation and DNA-protein cross-links have been observed together with an increased incidence of nasal squamous cell carcinomas in rodent models at doses ranging from 2 to 15 ppm (Casanova *et al.*, 1989; McGregor *et al.*, 2006; Monticello *et al.*, 1996). In these studies, the dose-dependent contribution of genotoxicity versus regenerative cell proliferation in the carcinogenic process remains controversial. The International Agency for Research on Cancer (IARC) has listed formaldehyde as a human carcinogen due to increased risk of nasopharyngeal cancer (IARC, 2006). An increased incidence of myeloid leukemia and sinonasal cancer has also been observed in epidemiologic studies, but the level of evidence has not been sufficient for causal association with formaldehyde exposure (IARC, 2006).

The objective of this study was to develop a method that integrates BMD calculations with GO classification analysis in the examination of genomic dose-response data. The combination of microarray technology with these analysis methods results in a unique risk assessment tool that provides both a comprehensive survey of molecular changes following chemical exposure and dose estimates at which different cellular processes are altered based on a defined increase in risk. A case study for application of the method is provided using gene expression changes in the rat nasal epithelium following acute formaldehyde exposure. Despite the initial focus on formaldehyde, the method should serve as a template for a broader application of genomic data to chemical risk assessment.

MATERIALS AND METHODS

Animals and treatment. Male F344/NCrl rats were obtained from Charles River Laboratories (Wilmington, MA) at 6 weeks of age. Upon receipt, the rats were randomized by weight and divided into treatment groups. Following randomization, rats were acclimated for a period of 2 weeks and exposures began at 8 weeks of age. Rats were housed in 8-m^3 stainless steel and glass inhalation chambers. Temperature was kept between 17.8 and 26.1°C, and humidity was maintained at 30–70%. Lighting was kept on a standard 12-h light/dark cycle, and all animals were given access to NIH-07 certified diet (Zeigler Brothers Corp., Gardners, PA) and water *ad libitum* except during the 6-h formaldehyde exposure when food was withheld. Animal use in this study was approved by the Institutional Animal Use and Care Committee of CIIT Centers for Health Research and was conducted in accordance with the National Institutes of Health guidelines for the care and use of laboratory animals. Animals were housed in fully accredited American Association for Accreditation of Laboratory Animal Care facilities.

Animals were exposed to target concentrations of 0.7, 2.0, 6.0, and 15.0 ppm (0.86, 2.46, 7.38, 18.5 mg/m^3) formaldehyde for a period of 6 h. Previous studies have demonstrated increased regenerative cell proliferation and DNA-protein cross-links following a 6-h exposure (Casanova *et al.*, 1989; Monticello *et al.*, 1991). Control animals were exposed to filtered air only. The exposure atmospheres were generated by thermal depolymerization of paraformaldehyde (lot#: 035K1609; Sigma-Aldrich Corp., St Louis, MO). The concentration of formaldehyde was monitored using a calibrated infrared analyzer (Miran 1A, Foxboro Instruments, Foxboro, MA). Airflow was maintained at 12–15 air changes per hour. For formaldehyde-treated groups, a total of eight animals per dose level were used for histopathology and four animals per dose level were used for microarray analysis. For air-exposed control animals, a total of 16 animals were used for histopathology and eight animals were used for microarray analysis.

Following the 6-h exposure, the rats were euthanized by exsanguination following an ip dose of sodium pentobarbital (Abbott Laboratories Corp., Chicago, IL). In animals exposed for histopathology, the nasal cavity was flushed retrograde with 10% neutral buffered formalin and fixed for 72 h. Following fixation, the noses were rinsed and decalcified (Immunocal, Decal Chemical Corp., Tallman, NY) for 3–4 days. The decalcified noses were gross trimmed, embedded in paraffin, sectioned at 5 μm, and stained with hematoxylin and eosin. Histological changes in the level II region were assessed by an accredited pathologist. In animals exposed for microarray analysis, the noses were dissected to isolate the level II region (Monticello *et al.*, 1996). The maxillo turbinate and olfactory epithelium from this region were discarded. and the lateral meatus and nasoturbinate were retained for further processing. The dissected nasal sections were then rinsed with cold phosphate-buffered saline to remove the blood. After rinsing, a 5 ml buffered mixture of proteases (collagenase, 80 U/ml, Sigma-Aldrich; pronase, 10 mg/ml, Sigma-Aldrich; HEPES, 0.1M) in Hams F12 medium (Invitrogen, Inc., Carlsbad, CA) was added to each nose and incubated at 37°C for 40 min to remove the epithelial cell layer. The epithelial cells acquired from this section of the nose consisted primarily of transitional epithelium with some respiratory epithelium. Following incubation, the mixtures were vortexed, and the resulting cell suspensions were collected in clean centrifuge tubes. The cell suspensions were centrifuged (200 × g, 10 min, 10°C), and the cell pellet was resuspended in 50 μl PBS and 200 μl RNA*later* (Ambion Corp., Austin, TX).

Gene expression microarray measurements and initial selection of responsive genes. Cell suspensions were centrifuged for 10 min (16,000 × g), and total RNA was isolated from the cell pellet using the RNeasy Micro RNA isolation kit (Qiagen Corp., Valencia, CA). The cell pellet was resuspended with 350 μl of lysis buffer containing β-mercaptoethanol. Each sample was homogenized and processed through the tissue protocol with an elution volume of 17 μl. The quantity of RNA was measured spectrophotometrically (NanoDrop ND-1000, NanoDrop Technologies, Inc., Montchanin, DE), and the integrity of the RNA was verified with the Agilent 2100 Bioanalyzer (Palo Alto, CA).

Double-stranded cDNA was synthesized from 2 μg of total RNA using the One-Cycle cDNA synthesis kit (Affymetrix Corp., Santa Clara, CA). Biotin-labeled cRNA was transcribed from the cDNA using the GeneChip IVT Labeling Kit (Affymetrix). Fifteen micrograms of labeled cRNA was

fragmented and hybridized to an Affymetrix Rat Genome 230 2.0 array for 16 h at 45°C. The hybridized array was washed using the GeneChip Fluidics Station 450 and scanned using a GeneChip 3000 scanner. The gene expression results have been deposited in the National Center for Biotechnology Information Gene Expression Omnibus (accession no.: GSE7002).

The data analysis steps associated with the method are outlined in Figure 1. Initially, microarray data were processed using robust multi-array average normalization with a $\log_2$ transformation (Irizarry *et al.*, 2003). The $\log_2$-transformed data were analyzed using a one-way ANOVA to identify probe sets on the array for which there was a difference in expression associated with treatment (dose). Probability values were adjusted for multiple comparisons using a false discovery rate of 5% (Benjamini and Hochberg, 1995). Only probe sets identified as significant based on the ANOVA were used in the subsequent BMD analysis. This initial probe set selection was necessary to reduce the computational requirements in the BMD calculations.

BMD calculations and model selection. The probe sets identified by the ANOVA were fit as continuous data to a series of four different dose-response models—linear, second-degree polynomial, third-degree polynomial, and power models. Each probe set was fit independently using the BMDExpress software program (http://sourceforge.net/projects/bmdexpress/). The parameter settings used for the software are provided as supplemental material (Supplementary Table 1). Each model was run assuming constant variance, and the benchmark response (BMR) factor was set to 1.349 multiplied by the SD in the control animals. To derive this value, a normal distribution was assumed for control animals, and it was assumed, *a priori*, that the transcriptional response could occur in either tail, with a 1% change of that occurring in the absence of exposure (0.5% in each tail). A BMR of 1.349 is the amount required to shift the mean transcriptional response of the control distribution such that the treated distribution contains 11% in a single tail, i.e., a 10% increase over the assume background rate of response (Fig. 2). Finally, each of the four models was run twice—once with the direction of the transcriptional response in the positive and once in the negative direction. The direction of the transcriptional response with the lowest BMD was selected for further analysis. The requirement to run each model twice was due to limitations in the BMDS software used to do the curve fitting. Unless stipulated, the BMDS software will automatically choose the direction of the response based on the direction observed at the highest dose. For probe sets that demonstrated nonmonotonic behavior, any significant change at the lower doses would be ignored in favor of the direction of the transcriptional response at the highest dose.

For model selection, a nested likelihood ratio test was performed on the linear, second-degree polynomial, third-degree polynomial models. If the more complex model provided a significantly improved fit ($p < 0.05$), the more complex model was selected. If the more complex model did not provide a significantly improved fit ($p \geq 0.05$), the simpler model was selected (Posada and Buckley, 2004). The Akaike information criterion (AIC) for the selected polynomial model was then compared with the AIC for the power model. The model with the lowest AIC (Akaike, 1973) was selected as the final model and was used to calculate a BMD and benchmark dose lower confidence limit (BMDL). To avoid model extrapolation, probe sets with a BMD value greater than the highest dose (i.e., 15 ppm) were removed from further analysis.

GO analysis and calculation of summary values. The gene annotations and GO classifications for all probe sets on the Affymetrix Rat Genome 230 2.0 array were downloaded from the Affymetrix Web site. Affymetrix probe sets that demonstrated significant dose-response behavior and had a BMD < 15 ppm were converted into unique genes based on their NCBI Entrez Gene ID. When two or more probe sets were associated with a single gene, the BMDs and BMDLs for the individual probe sets were averaged to obtain a single BMD and BMDL. The Entrez Gene identifiers were then matched to their corresponding

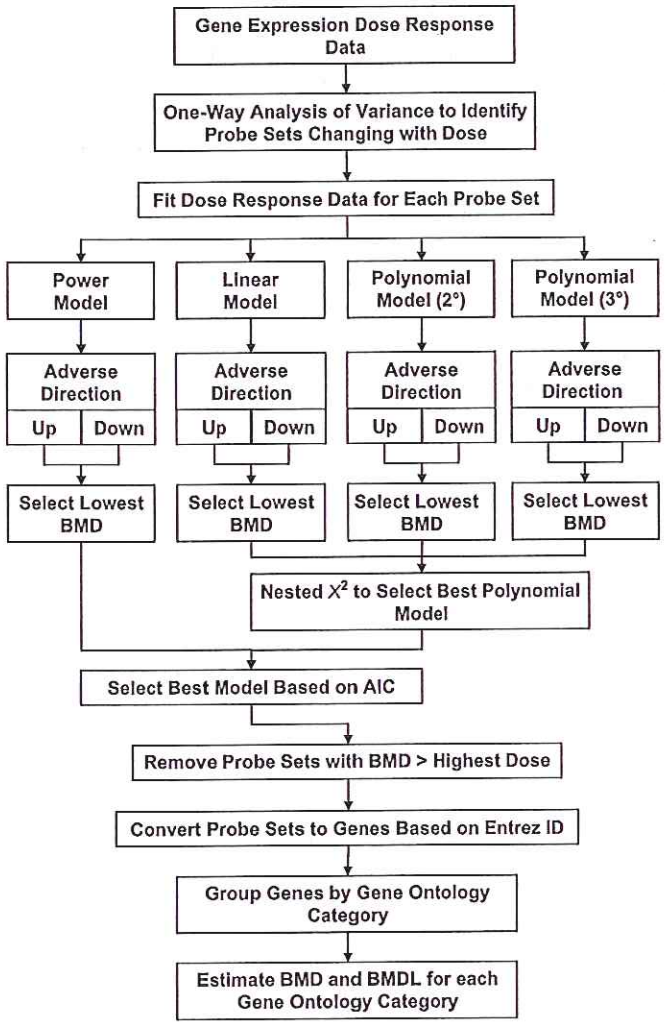

FIG. 1. A flow chart outlining the stepwise analysis of dose-response microarray data using BMD calculations and GO classification analysis. The methodology provides dose estimates at which different cellular processes are altered at a defined increase in risk based on expression levels in the untreated controls.

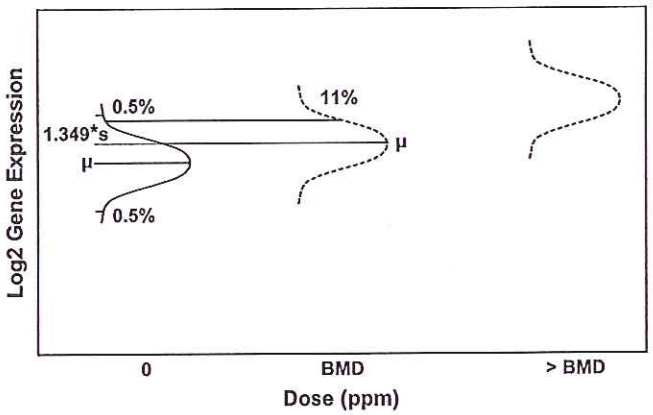

FIG. 2. An illustration of the rationale for selection of the BMR. The BMR was derived by assuming a normal distribution in control animals with 0.5% in both tails ($\alpha = 1\%$ total). A value of 1.349 multiplied by the SD in the control animals is the amount required to shift the mean response of the control distribution such that the treated distribution contains 11% in a single tail.

biological process and molecular function GO categories. GO categories with less than three genes were removed from the analysis. The three-gene cut-off was based on the minimum number required to define a mean and SD for the category.

In this study, there was no attempt to distinguish between adverse and nonadverse changes in gene expression within the various GO categories. The discrimination between adverse and nonadverse effects has been the subject of considerable debate within toxicology (Foster and McIntyre, 2002; Karbe *et al.*, 2002; Lewis *et al.*, 2002), and this discrimination can be even more difficult when analyzing gene expression changes. Therefore, all transcriptional changes that were significantly different from control animals were assumed to be adverse, and summary values for all GO categories were reported.

RESULTS

Formaldehyde Exposure and Histopathological Analysis

Rats were exposed for 6 h via whole-body inhalation to four concentrations of formaldehyde (0.7, 2.0, 6.0, and 15.0 ppm) plus an air control. The histopathological changes were relatively minor with only inflammatory infiltrate observed in seven out of eight animals at the 15.0 ppm concentration. No other histopathological changes were observed.

Dose-Response Microarray Measurements and Initial Gene Selection

Measurement of gene expression changes was performed on epithelial cell suspensions isolated from the level II region of individual rat noses. The cell suspensions contained primarily transitional epithelium with some respiratory epithelium. In addition, this section of the nose contained the regions of high formaldehyde flux (Kimbell *et al.*, 1993) and nasal tumors in chronic exposure studies (Kerns *et al.*, 1983; Monticello *et al.*, 1991, 1996; Morgan *et al.*, 1986). For the initial gene selection, a one-way ANOVA was used to identify probe sets on the array that were significantly changed with dose. A total of 4263 probe sets were identified at a false discovery rate of 5%.

BMD Calculations and Model Selection

Using the probe sets identified by the ANOVA, four different statistical models (linear, second-degree polynomial, third-degree polynomial, and power models) were fit to the data, and the model that best described the data with the least amount of complexity was selected. Following model selection, a total of 108 probe sets had a BMD greater than the highest dose (15.0 ppm) and were removed from the analysis to avoid model extrapolation. The model breakdown among the final probe sets was 38.8% linear model, 48.3% second-degree polynomial model, 12.4% third-degree polynomial model, and 0.4% power model. Based on the likelihood ratio test performed by the BMDS software, the dose-response behaviors for greater than 80% of the probe sets were adequately described by the final selected model ($p > 0.05$) (Fig. 3). An example of each model together with their goodness-of-fit p value is provided in Figure 4.

GO Analysis and Calculation of Summary Values

The final genes from the BMD analysis were assigned into groups based on their GO classifications. The genes were

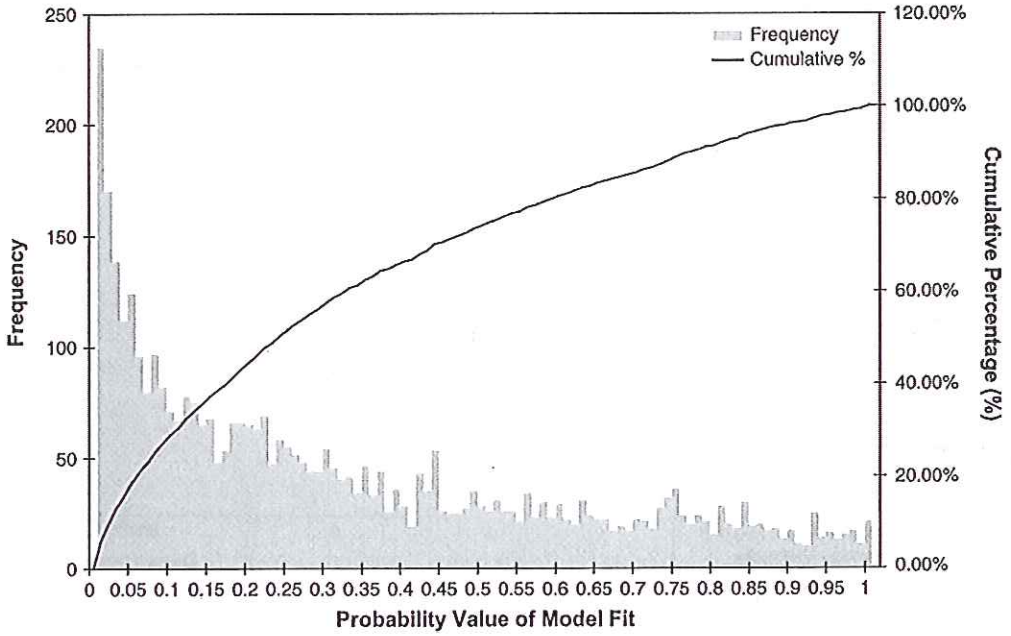

FIG. 3. A histogram showing the distribution of p values for the goodness-of-fit tests of the final models selected for the genes demonstrating significant dose-response behavior. For this test, a higher p value means a better fit between the model and the experimental data. The left y-axis and the bar chart shows the frequency at which the various p values were observed and the right y-axis shows the cumulative percentage.

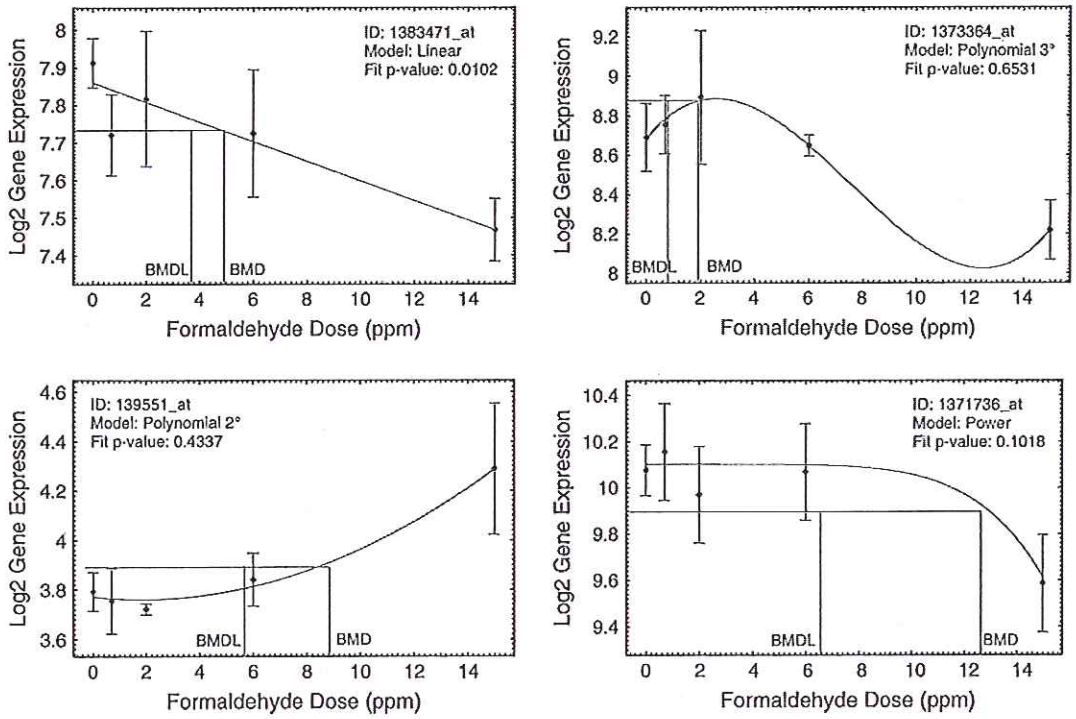

FIG. 4. Examples of the fit for each of the four statistical models (linear, second-degree polynomial, third-degree polynomial, and power models) with experimental data. The specific genes were intentionally chosen with different goodness-of-fit p values to provide examples of the relationship between the various p values and the fit of the model. For each graph, the experimental data are shown in blue (mean ± SD) with the model fit as the red line. The green lines represent the BMD and BMDL calculated based on a BMR of 1.349 × SD of the control animals.

grouped by both their biological process categories (e.g., cell division, DNA repair, cell proliferation, or apoptosis) and their molecular function categories (e.g., lipase activity, heparin binding, protein kinase activity, or cytokine activity). The GO categories with the lowest average BMD values are presented in Tables 1 and 2. For comparison, the average BMD for all genes with significant dose-response behavior was 6.42 ± 4.16 ppm (mean ± SD). Among the biological process GO categories, the microtubule polymerization category had the lowest average BMD (1.57 ± 0.66 ppm) followed by the response to xenobiotic stimulus (2.19 ± 1.29 ppm) and regulation of c-jun N-terminal kinase cascade (2.25 ± 1.48 ppm). Other GO categories associated with the presumed formaldehyde mode-of-action, such as the response to DNA damage, cell proliferation, and the inflammatory response, had higher average BMD values and were generally in the 6–7 ppm range (Table 3). Among the molecular function GO categories, the subtilase activity group had the lowest average BMD (1.85 ± 0.15 ppm) followed by calcium-transporting ATPase activity (2.16 ± 1.07 ppm) and heat shock protein binding (2.17 ± 1.60 ppm).

DISCUSSION

The general methods employed in this study are all well established within their respective fields. BMD methods are regularly employed by the U.S. EPA for estimating reference doses and setting standards for noncancer human health effects (EPA, 1995). Microarray technology has been broadly accepted as an efficient and reproducible way to simultaneously measure the expression of thousands of genes (Shi *et al.*, 2006). Finally, GO classification analysis has demonstrated broad applicability for grouping genes based on their cellular function (Beissbarth and Speed, 2004; Dennis *et al.*, 2003; Khatri *et al.*, 2004; Yu *et al.*, 2006; Zhang *et al.*, 2004). In this study, the three tools were brought together in order to advance the application of genomic technologies in chemical risk assessment.

In combining the three tools, several challenges were encountered that require additional discussion. The first challenge was related to the selection of the BMR type based on the SD of the control animals. The BMR based on the SD was chosen under the assumption that the natural variation in expression for a particular gene could be characterized based on the control population. In other words, this natural variation would need to be exceeded in order to potentially observe an adverse effect. For example, if a gene is critical to cellular function and tightly regulated within a tissue, then the SD in the control animals would be relatively small. Conversely, less tightly regulated genes would have a higher SD in the control animals. Although the logic in selecting this BMR type is consistent with the underlying biology, the broad application of the approach across multiple chemicals and testing laboratories

TABLE 1
Biological Process GO Categories with the Lowest Mean BMD

Biological process GO category[a]	Total genes in category	Genes with BMD < 15 ppm	Mean BMD (ppm)	SD BMD	Mean BMDL (ppm)	Minimum BMD (ppm)	BMD at 10th percentile (ppm)
Microtubule polymerization or depolymerization	18	3	1.57	0.66	1.06	0.81	1.35
Response to xenobiotic stimulus	26	3	2.19	1.29	1.34	0.71	2.94
Regulation of c-jun N-terminal kinase cascade	11	3	2.25	1.48	1.34	0.64	1.61
Protein targeting to endoplasmic reticulum	8	3	2.26	0.13	1.48	2.17	2.17
Epidermis morphogenesis	17	4	2.26	1.47	1.24	0.75	1.04
Female sex differentiation	29	3	2.27	2.22	1.60	0.80	3.00
Menstrual cycle process	25	3	2.27	2.22	1.60	0.80	3.00
Activation of immune response	35	4	2.32	0.86	1.36	1.54	3.06
Sodium ion transport	48	3	2.32	1.74	1.68	0.68	—
Integrin-mediated signaling pathway	25	5	2.40	1.71	1.68	0.67	1.83
Aminoglycan catabolic process	7	3	2.49	0.42	1.60	2.02	2.02
Peptide hormone secretion	19	3	2.50	0.34	1.58	2.11	2.40
Positive regulation of locomotion	20	4	2.51	2.31	1.70	0.93	1.55
Regulation of transcription factor import into nucleus	10	3	2.54	1.22	1.84	1.45	1.45
Negative regulation of cell organization and biogenesis	19	5	2.57	1.96	1.87	0.81	0.82
Translational elongation	14	3	2.57	1.49	1.69	0.93	1.93
Immune response–regulating signal transduction	15	3	2.58	0.84	1.57	1.61	2.30
T cell receptor signaling pathway	10	3	2.58	0.84	1.57	1.61	1.61
Antigen receptor–mediated signaling pathway	15	3	2.58	0.84	1.57	1.61	2.30
Regulation of GTPase activity	10	3	2.65	3.09	1.57	0.70	0.70

[a]Redundant child GO categories containing the same genes and mean BMD were removed from the list. For a complete list, see Supplementary Table 2.

poses significant challenges. In a testing environment, an increased variability in the control animals beyond that normally observed would artificially increase the BMD and BMDL estimates for the individual genes and the associated GO categories. Therefore, it could be potentially advantageous for a testing laboratory to maintain a stressed set of control animals. To overcome this limitation, the regulatory agencies would need to maintain a database of control gene expression values for the common test species and strains to ensure that the variability in expression was within normal bounds.

The second challenge posed in combining these tools was the selection of the BMR value itself. The proposed BMR was derived by assuming a normal distribution in control animals with adverse levels selected *a priori* to include 0.5% in each tail (1% total). A BMR of 1.349 times the estimated SD is the amount required to shift the mean response from that in the control distribution such that the treated distribution contains 11% in a single tail. Although other studies have also used a 10% shift in tail area (Crump, 1995; Gaylor and Slikker, 2004), the BMR in their studies was based on a shift from a 1% area in a single tail for the control distribution to an 11% area in the treated distribution. In our study, we used two tails for the control distribution since we did not assume that we knew *a priori* in which direction the gene would change and we performed the BMD analysis in both adverse directions (i.e., increased and decreased expression) while selecting the direction with the lowest BMD.

The third challenge was the selection of the primary point of comparison across the various GO categories to represent the dose at which the specific cellular functions were altered. Three different values were considered—the minimum BMD, the BMD at the 10th percentile among all genes in the category, and the average BMD. The use of the minimum BMD as the point of comparison may hold certain appeal since it provides the most conservative estimate for selecting a reference dose. A fundamental biological question is whether the minimum BMD from the effect on a single gene really reflects the dose that can elicit a complex, adverse response such as cell proliferation or apoptosis. Several biological reasons argue against using the minimum BMD as the point of comparison. First, external stressors or perturbations cause changes in the expression of large batteries of genes, many within the same functional class, suggesting that complex biological process are altered through coordinate changes in the expression of families of genes (Currie *et al.*, 2005; Hughes *et al.*, 2000; Murray *et al.*, 2004). Second, complex biological systems are inherently robust against small perturbations (Kitano, 2004; Kitano and Oda, 2006). Biological processes have evolved compensatory mechanisms that limit the effect of changes in a single gene. For example, the altered expression of an important gene such as a growth factor by a hypothetical toxicant would also elicit a feedback response within the pathway. A new steady state would be reached between the effects of the toxicant and the feedback mechanisms. The functional outcome for this

TABLE 2
Molecular Function GO Categories with the Lowest Mean BMD

Molecular function GO category[a]	Total genes in category	Genes with BMD < 15 ppm	Mean BMD (ppm)	SD BMD	Mean BMDL (ppm)	Minimum BMD (ppm)	BMD at 10th percentile (ppm)
Subtilase activity	9	3	1.85	0.15	1.28	1.69	1.69
Calcium-transporting ATPase activity	8	3	2.16	1.07	1.34	0.95	0.95
Heat shock protein binding	11	3	2.17	1.60	1.59	0.65	1.33
Calcium ion transporter activity	13	4	2.36	0.96	1.46	0.95	1.75
RNA methyltransferase activity	7	3	2.50	3.48	2.08	0.46	0.46
Signal sequence binding	17	8	2.57	1.96	1.77	0.47	0.60
Icosanoid receptor activity	9	3	2.89	3.08	1.96	0.81	0.81
Transferase activity, transferring nitrogenous groups	17	4	2.96	1.54	1.61	1.00	1.73
Receptor signaling protein tyrosine kinase activity	10	4	2.97	3.57	2.01	0.51	0.51
3′-5′ exonuclease activity	13	3	3.09	1.71	2.30	1.96	2.11
Microtubule motor activity	26	4	3.17	1.90	1.69	0.81	3.20
Metalloendopeptidase activity	40	5	3.27	3.69	2.18	0.50	2.06
Oxidoreductase activity, acting on sulfur group of donors, NAD or NADP as acceptor	7	3	3.35	3.42	2.42	0.86	0.86
Lysine N-acetyltransferase activity	10	3	3.39	3.55	2.35	0.77	0.77
Phorbol ester receptor activity	12	3	3.54	3.21	2.42	1.00	1.74
Cation-transporting ATPase activity	21	4	3.57	2.95	2.36	0.95	2.76
G-protein–coupled receptor binding	60	9	3.65	2.51	2.50	0.65	4.49
SNARE binding	26	5	3.68	2.27	2.60	2.01	2.15
Phosphoric diester hydrolase activity	53	7	3.71	2.46	2.49	0.92	4.99
Ligase activity, forming carbon-sulfur bonds	18	5	3.72	2.01	2.62	1.92	2.02

[a]Redundant child GO categories containing the same genes and mean BMD were removed from the list. For a complete list, see Supplementary Table 3.

perturbation would be reflected in the downstream effects of the growth factor on genes for cell proliferation, developmental patterning, and others. From this perspective, basing decisions on expression changes in a single gene would not accurately reflect the aggregate behavior of the biological system or the functional effects of chemical exposure.

The use of a percentile-based summary value is similar to the logic that underlies the benchmark methodology. In essence, the BMD at the 10th percentile for all genes in a GO category suggests that altering 10% of the genes is the threshold for producing the associated biological response. This may be a reasonable estimate for a GO category that represents a relatively detailed biological process, but as one proceeds through the GO hierarchy toward more general biological descriptions, a change in 10% of the genes would become increasing diluted through the addition of unaffected genes (e.g., MAPKKK cascade → protein kinase cascade → intracellular signaling cascade → signal transduction → cell communication → cellular process). One solution to this problem would be to vary the percentile depending on the level of the GO category within the hierarchy. However, this approach requires a relatively uniform amount of biological detail at each hierarchical level. Currently, the relative amount of detail is variable within the GO hierarchy, which makes

TABLE 3
BMD Values for Selected Biological Process GO Categories Relevant to Traditional Thinking on Formaldehyde Mode-of-Action

Biological process GO category	Total genes in category	Genes with BMD < 15 ppm	Mean BMD (ppm)	SD BMD	Mean BMDL (ppm)	Minimum BMD (ppm)	BMD at 10th percentile (ppm)
Positive regulation of cell proliferation	182	49	5.68	4.00	4.15	0.51	3.16
Response to DNA damage stimulus	142	45	6.31	4.01	4.69	0.53	3.22
Response to unfolded protein	28	11	6.32	3.93	4.61	1.22	2.66
Regulation of apoptosis	384	98	6.61	4.13	4.77	0.64	4.38
DNA repair	104	28	6.76	4.19	5.05	0.53	4.33
Inflammatory response	187	29	7.11	4.12	5.15	1.11	7.95

the percentile-based BMD less appealing as the point of comparison.

In the development of this method, the mean BMD was selected as the primary point of comparison based on its ability to reflect the aggregate behavior of genes within a GO category. For formaldehyde exposure, the mean BMD within several GO categories was closely associated with the phenotypic effects. A previous study has reported NOAEL and LOAEL values for epithelial hyperplasia of 2 and 6 ppm, respectively, for a 6-h exposure (Monticello *et al.*, 1991). The $BMD_{10\%}$ for the cell labeling index based on multiple time points has been calculated at 4.91 ppm (Schlosser *et al.*, 2003). By comparison, the mean BMD value in our study for the positive regulation of cell proliferation was 5.68 ppm (Table 3). For the DNA damage response, the use of DNA-protein cross-links by formaldehyde has been proposed as a surrogate for mutagenicity (Conolly *et al.*, 2003). In a study by Casanova *et al.* (1994), the DNA-protein cross-links in the rat nose was significantly increased beginning at 6 ppm following a 3-h exposure. In our study, the BMD value for the DNA damage response was 6.31 ppm (Table 1). Overall, mean BMD values for the gene expression changes related to cell proliferation and the DNA damage response were both near 6 ppm and were comparable to the $BMD_{10\%}$ estimated for tumor formation of 6.40 ppm (Schlosser *et al.*, 2003). The general concordance of these numbers suggests that the mean BMD provides the most appropriate summary value for the biological effects in this study. Moreover, in the absence of traditional histopathological and biochemical measurements, similar conclusions concerning the dose-dependent effects may be reached using only the gene expression information. However, transcriptional changes do not necessarily equate with functional changes, and the results should be interpreted with an appropriate amount of caution.

Apart from the changes in cell proliferation and DNA damage, the gene expression studies also showed changes in microtubule-related processes between 1 and 2 ppm (Table 1). These changes are consistent with the ability of formaldehyde to cross-link macromolecules (Swenberg *et al.*, 1983). One possibility is that microtubule-related processes may be responding to cytoskeletal cross-links formed at the cell surface. Another possibility is that this category may be transcriptionally more active than other categories in response to multiple pathologies. Additional studies would have to be performed in order to directly link these effects to formaldehyde cross-links.

In conclusion, the development and broad availability of genomic tools continues to hold significant promise for the toxicology and risk assessment communities (Thomas *et al.*, 2002; Travis *et al.*, 2003). The technology has the potential to transform chemical risk assessments through its ability to rapidly identify chemical hazards, reveal the underlying mechanism-of-action, and provide a better understanding of the dose-response behavior. However, despite the initial enthusiasm surrounding the technology, the risk assessment community has struggled to directly integrate them into the risk assessment process. The results from this study represents a significant step forward in applying genomic information to assessing health risks by both allowing a comprehensive survey of molecular and cellular changes associated with chemical exposure and providing the capability to identify reference doses at which cellular processes are altered.

SUPPLEMENTARY DATA

Supporting material is provided online and includes (1) model parameter values for the BMDS software that was run in batch mode to calculate BMD and BMDL values for each gene with significant dose-response behavior (Supplementary Table 1); (2) a complete list of BMD and BMDL summary values for all the biological process GO categories (Supplementary Table 2); (3) a complete list of BMD and BMDL summary values for all the molecular function GO categories (Supplementary Table 3); (4) Detailed results from the fitting and selection of the four statistical models to each of the Affymetrix probe sets that passed the one-way ANOVA analysis (Supplementary Table 4); (5) Variability in gene expression values among control animals in the Level II region of the rat nose (Supplementary Table 5); and (6) a histogram of BMD values for all responsive probe sets (Supplementary Figure 1). Supplementary data are available online at http://toxsci.oxfordjournals.org/.

ACKNOWLEDGMENTS

The research in this study was supported by the American Chemistry Council's Long Range Research Initiative and a contract from the Formaldehyde Council, Inc.

REFERENCES

Akaike, H. (1973). Information theory and an extension of the maximum likelihood principle. In *Second International Symposium on Information Theory* (B. N. Petrov and F. Csaki, Eds.), Budapest: Academiai kiado, 267–281.

Arts, J. H., Rennen, M. A., and de Heer, C. (2006). Inhaled formaldehyde: Evaluation of sensory irritation in relation to carcinogenicity. *Regul. Toxicol. Pharmacol.* **44,** 144–160.

ATSDR. (1999). *Toxicological Profile for Formaldehyde.* U.S. Department of Health and Human Services, Washington, DC.

Beissbarth, T., and Speed, T. P. (2004). GOstat: Find statistically over-represented gene ontologies within a group of genes. *Bioinformatics* **20,** 1464–1465.

Benjamini, Y., and Hochberg, Y. (1995). Controlling the false discovery rate: A practical and powerful approach to multiple testing. *J. R. Stat. Soc. Ser B* **57,** 289–300.

Casanova, M., Deyo, D. F., and Heck, H. D. (1989). Covalent binding of inhaled formaldehyde to DNA in the nasal mucosa of Fischer 344 rats: Analysis of formaldehyde and DNA by high-performance liquid chromatography and provisional pharmacokinetic interpretation. *Fundam. Appl. Toxicol.* **12,** 397–417.

Casanova, M., Morgan, K. T., Gross, E. A., Moss, O. R., and Heck, H. A. (1994). DNA-protein cross-links and cell replication at specific sites in the nose of F344 rats exposed subchronically to formaldehyde. *Fundam. Appl. Toxicol.* **23,** 525–536.

Conolly, R. B., Kimbell, J. S., Janszen, D., Schlosser, P. M., Kalisak, D., Preston, J., and Miller, F. J. (2003). Biologically motivated computational modeling of formaldehyde carcinogenicity in the F344 rat. *Toxicol. Sci.* **75,** 432–447.

Crump, K. S. (1984). A new method for determining allowable daily intakes. *Fundam. Appl. Toxicol.* **4,** 854–871.

Crump, K. S. (1995). Calculation of benchmark dose from continuous data. *Risk Anal.* **15,** 79–89.

Currie, R. A., Orphanides, G., and Moggs, J. G. (2005). Mapping molecular responses to xenoestrogens through gene ontology and pathway analysis of toxicogenomic data. *Reprod. Toxicol.* **20,** 433–440.

Dennis, G., Jr, Sherman, B. T., Hosack, D. A., Yang, J., Gao, W., Lane, H. C., and Lempicki, R. A. (2003). DAVID: Database for annotation, visualization, and integrated discovery. *Genome. Biol.* **4,** P3.

EPA. (1995). *The Use of the Benchmark Dose Approach in Health Risk Assessment.* Office of Research and Development, U.S. Environmental Protection Agency, Washington, DC.

Filipsson, A. F., Sand, S., Nilsson, J., and Victorin, K. (2003). The benchmark dose method—review of available models, and recommendations for application in health risk assessment. *Crit. Rev. Toxicol.* **33,** 505–542.

Foster, P. M., and McIntyre, B. S. (2002). Endocrine active agents: Implications of adverse and non-adverse changes. *Toxicol. Pathol.* **30,** 59–65.

Gaylor, D. W., and Slikker, W., Jr. (2004). Role of the standard deviation in the estimation of benchmark doses with continuous data. *Risk. Anal.* **24,** 1683–1687.

Hughes, T. R., Marton, M. J., Jones, A. R., Roberts, C. J., Stoughton, R., Armour, C. D., Bennett, H. A., Coffey, E., Dai, H., He, Y. D., *et al.* (2000). Functional discovery via a compendium of expression profiles. *Cell.* **102,** 109–126.

IARC. (2006). *IARC Monographs on the Evaluation of Carcinogenic Risks to Humans: Formaldehyde, 2-Butoxyethanol and 1-tert-Butoxypropan-2-ol.* International Agency for Research on Cancer, Lyon, France.

Irizarry, R. A., Bolstad, B. M., Collin, F., Cope, L. M., Hobbs, B., and Speed, T. P. (2003). Summaries of Affymetrix GeneChip probe level data. *Nucleic. Acids. Res.* **31,** e15.

Karbe, E., Williams, G. M., Lewis, R. W., Kimber, I., and Foster, P. M. (2002). Distinguishing between adverse and non-adverse effects. Session summary. *Exp. Toxicol. Pathol.* **54,** 51–55.

Kerns, W. D., Pavkov, K. L., Donofrio, D. J., Gralla, E. J., and Swenberg, J. A. (1983). Carcinogenicity of formaldehyde in rats and mice after long-term inhalation exposure. *Cancer. Res.* **43,** 4382–4392.

Khatri, P., Bhavsar, P., Bawa, G., and Draghici, S. (2004). Onto-Tools: An ensemble of web-accessible, ontology-based tools for the functional design and interpretation of high-throughput gene expression experiments. *Nucleic. Acids. Res.* **32,** W449–W456.

Kimbell, J. S., Gross, E. A., Joyner, D. R., Godo, M. N., and Morgan, K. T. (1993). Application of computational fluid dynamics to regional dosimetry of inhaled chemicals in the upper respiratory tract of the rat. *Toxicol. Appl. Pharmacol.* **121,** 253–263.

Kitano, H. (2004). Biological robustness. *Nat. Rev. Genet.* **5,** 826–837.

Kitano, H., and Oda, K. (2006). Robustness trade-offs and host-microbial symbiosis in the immune system. *Mol. Syst. Biol.* **2:** 22.

Lewis, R. W., Billington, R., Debryune, E., Gamer, A., Lang, B., and Carpanini, F. (2002). Recognition of adverse and nonadverse effects in toxicity studies. *Toxicol. Pathol.* **30,** 66–74.

McGregor, D., Bolt, H., Cogliano, V., and Richter-Reichhelm, H. B. (2006). Formaldehyde and glutaraldehyde and nasal cytotoxicity: Case study within the context of the 2006 IPCS human framework for the analysis of a cancer mode of action for humans. *Crit. Rev. Toxicol.* **36,** 821–835.

Monticello, T. M., Miller, F. J., and Morgan, K. T. (1991). Regional increases in rat nasal epithelial cell proliferation following acute and subchronic inhalation of formaldehyde. *Toxicol. Appl. Pharmacol.* **111,** 409–421.

Monticello, T. M., Swenberg, J. A., Gross, E. A., Leininger, J. R., Kimbell, J. S., Seilkop, S., Starr, T. B., Gibson, J. E., and Morgan, K. T. (1996). Correlation of regional and nonlinear formaldehyde-induced nasal cancer with proliferating populations of cells. *Cancer Res.* **56,** 1012–1022.

Morgan, K. T., Jiang, X. Z., Starr, T. B., and Kerns, W. D. (1986). More precise localization of nasal tumors associated with chronic exposure of F-344 rats to formaldehyde gas. *Toxicol. Appl. Pharmacol.* **82,** 264–271.

Murray, J. I., Whitfield, M. L., Trinklein, N. D., Myers, R. M., Brown, P. O., and Botstein, D. (2004). Diverse and specific gene expression responses to stresses in cultured human cells. *Mol. Biol. Cell.* **15,** 2361–2374.

Page, T. J., Sikder, D., Yang, L., Pluta, L., Wolfinger, R. D., Kodadek, T., and Thomas, R. S. (2006). Genome-wide analysis of human HSF1 signaling reveals a transcriptional program linked to cellular adaptation and survival. *Mol. Biosyst.* **2,** 627–639.

Posada, D., and Buckley, T. R. (2004). Model selection and model averaging in phylogenetics: Advantages of akaike information criterion and bayesian approaches over likelihood ratio tests. *Syst. Biol.* **53,** 793–808.

Schlosser, P. M., Lilly, P. D., Conolly, R. B., Janszen, D. B., and Kimbell, J. S. (2003). Benchmark dose risk assessment for formaldehyde using airflow modeling and a single-compartment, DNA-protein cross-link dosimetry model to estimate human equivalent doses. *Risk Anal.* **23,** 473–487.

Shi, L., Reid, L. H., Jones, W. D., Shippy, R., Warrington, J. A., Baker, S. C., Collins, P. J., de Longueville, F., Kawasaki, E. S., Lee, K. Y., *et al.* (2006). The MicroArray Quality Control (MAQC) project shows inter- and intra-platform reproducibility of gene expression measurements. *Nat. Biotechnol.* **24,** 1151–1161.

Swenberg, J. A., Gross, E. A., Martin, J., and Popp, J. A. (1983). Mechanisms of formaldehyde toxicity. In *Formaldehyde Toxicity* (J. E. Gibson, ed.), Hemisphere Publishing, New York.

Thomas, R. S., Rank, D. R., Penn, S. G., Zastrow, G. M., Hayes, K. R., Hu, T., Pande, K., Lewis, M., Jovanovich, S. B., and Bradfield, C. A. (2002). Application of genomics to toxicology research. *Environ. Health Perspect* **110**(Suppl. 6), 919–923.

Travis, C. C., Bishop, W. E., and Clarke, D. P. (2003). The genomic revolution: What does it mean for human and ecological risk assessment? *Ecotoxicology* **12,** 489–495.

Yu, X., Griffith, W. C., Hanspers, K., Dillman, J. F., III, Ong, H., Vredevoogd, M. A., and Faustman, E. M. (2006). A system-based approach to interpret dose- and time-dependent microarray data: Quantitative integration of gene ontology analysis for risk assessment. *Toxicol. Sci.* **92,** 560–577.

Zhang, B., Schmoyer, D., Kirov, S., and Snoddy, J. (2004). GOTree Machine (GOTM): A web-based platform for interpreting sets of interesting genes using gene ontology hierarchies. *BMC Bioinformatics* **5,** 16.

ATTACHMENT 4

ACB-PCR measurement of *p53* codon 271 CGT to CAT mutation in the nasal mucosa of rats exposed to formaldehyde

Meng, F.1, Bermudez, E.2, Andersen, M.E.2, Clewell, H.J. 3rd2, Parsons, B.L.1

1Division of Genetic and Reproductive Toxicology, National Center for Toxicological Research, Jefferson, AR 72079, USA
2The Hamner Institutes for Health Sciences, Research Triangle Park, NC 27709, USA

ACB-PCR measurement of *p53* codon 271 CGT to CAT mutation in the nasal mucosa of rats exposed to formaldehyde

Meng, F.[1], Bermudez, E.[2], Andersen, M.E.[2], Clewell, H.J. 3rd[2], Parsons, B.L.[1]

[1]Division of Genetic and Reproductive Toxicology, National Center for Toxicological Research, Jefferson, AR 72079, USA

[2]The Hamner Institutes for Health Sciences, Research Triangle Park, NC 27709, USA

Abstract

Formaldehyde is classified as a Group I human carcinogen with respect to the induction of nasopharyngeal cancers. Formaldehyde exposures are both occupational and environmental because formaldehyde is used in the manufacture of building materials, household products and industrial chemicals, is found in vehicle emissions, and is released indoors from building materials. To accurately assess the risk of formaldehyde exposures, sensitive and relevant biomarker data are needed to describe the formaldehyde mode of action (MOA) at different exposure levels. Mutation in the *p53* tumor suppressor gene has been implicated in the mechanism of formaldehyde-induced rat nasal tumor development because abnormal p53 protein accumulated in rat nasal mucosa following formaldehyde exposure and *p53* mutations were detected in several squamous cell carcinomas (SCC) generated in a two-year bioassay. The goals of this study were to: 1) determine the spontaneous level of *p53* mutation in rat nasal mucosa, 2) to describe the dose-dependence on the induction of *p53* mutation following 13 weeks of exposure to formaldehyde, and 3) to correlate the induction of *p53* mutation with other endpoints (*i.e.*, induction of cell proliferation and changes in gene expression). An allele-specific competitive blocker-PCR (ACB-PCR) was developed to quantify *p53* codon 271 CGT to CAT mutation in nasal mucosa of rats exposed to formaldehyde. Male Fisher 344 rats (6-7 weeks old, 5 rats/group) were exposed to formaldehyde via whole-body inhalation at target concentrations of 0.7, 2.0, 6.0, 10 and 15.0 ppm (0.86, 2.46, 7.38, 12.3, 18.5 mg/m^3) for 6 h/day, 5 days/week for 13 weeks. Formaldehyde concentrations of 6 ppm and above are carcinogenic in a two-year bioassay. DNA was isolated from sites of nasal mucosa where the incidence of SCC was greatest and *p53* codon 271 CGT to CAT mutant fraction (MF) was determined by three replicate ACB-PCR measurements. Only 8/30 samples had measurable levels of *p53* CGT to CAT MFs (>10^{-5}). The geometric mean MFs for the treatment groups were: 8.64 X 10^{-6}, 0 ppm; 2.89 x 10^{-6}, 0.7 ppm; 2.71 x 10^{-6}, 2 ppm; 8.49 x 10^{-6}, 6 ppm; and 2.67 x 10^{-6}, 10 ppm; 1.21 x 10^{-5}, 15 ppm. Further, the results indicated a large range of *p53* mutation exists in the nasal mucosa of control rats (from below 10^{-5} to 1.85 X 10^{-4}). Thirteen weeks of exposure to formaldehyde did not cause a significant induction of *p53* codon 271 CGT to CAT mutation at the doses tested, even though some of these doses have been shown to cause cytotoxicity, changes in gene expression, and to stimulate cell proliferation. This abstract does not necessarily reflect the views or policies of the US FDA.

Materials and Methods

Animals Male F344 rat (8 weeks of age, 5 rat/group) were exposed to formaldehyde via whole-body inhalation at target concentrations of 0.7, 2.0, 6.0, 10 and 15.0 ppm (0.86, 2.46, 7.38, 12.3, 18.5 mg/m^3) for 6 hours/day, 5 days/week for 13 weeks.

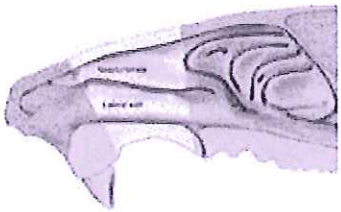

DNA isolation and first-round PCR Genomic DNA was isolated from nasal mucosa, at sites known to develop nasal tumors, and used as template for first-round PCR. A PCR product encompassing portions of *p53* intron 7 and exon 8 was amplified in 2-200 ul reactions. Each 200 ul PCR reaction contained: 1 ug genomic DNA, 200 nM primer P80-1 (5'-TTTCTTA CTGCCTTGTGCTG-3'), 200 nM primer P81 (5'-TTCTTTGTCCTGCCTGCTCA-3'), 200 nM dNTPs, 1X *PfuUltra* reaction buffer, and 10 units *PfuUltra* high-fidelity DNA Polymerase (Stralagene, La Jolla, CA). Cycling conditions were 94°C for 2 min, followed by 35 cycles of 94°C for 1 min, 58°C for 2 min, 72°C for 1 min, followed by a 7 min extension at 72°C. A first-round PCR product encompassing K-*Ras* exon 1 and part of intron 1 was amplified in 2-200 ul reactions. Each 200 ul PCR reaction contained: 1 ug genomic DNA, 100 nM primer RKR5 upstream (5'-ATATTTTATATTT TTATTATAAGGCTG-3'), 200 nM primer RKR2 (5'-CTGTACCGATGGTTCCCT-3'), 200 nM dNTPs, 1X *PfuUltra* reaction buffer, and 10 units *PfuUltra* high-fidelity DNA Polymerase (Stratagene, La Jolla, CA). Cycling conditions were 94°C for 2 min, followed by 35 cycles of 94°C for 1 min, 52°C for 1 min, 72°C for 1 min. PCR products were gel-purified. Aliquots of first-round PCR products were repeatedly quantified using a Nanodrop spectrophotometer (Nanodrop Technologies, Wilmington, DE), until three measurement that varied <10% from the group mean were obtained.

ACB-PCR PCR products corresponding to wild-type and mutant DNA sequence were prepared. These PCR products were identical in sequence composition to the first-round PCR products to be analyzed. The standards were mixed to generate samples with mutant fractions of 10^{-1}, 10^{-2}, 10^{-3}, 10^{-4}, and 10^{-5}. These standards and a no DNA control were analyzed in parallel with equal numbers of copies of the first-round PCR products. For the *p53* codon 271 CAT ACB-PCR, 4 x 10^8 copies were analyzed in each 50 ul reaction containing: 1X Stoffel buffer, 0.1 mg/ml gelatin, 1 mg/ml Triton X-100, 20 uM dNTPs, 1.6 mM $MgCl_2$, 70 nM mutant specific primer (MSP, 5'-fluorescein-CCCAGGACAGGCACAAACCT-3'), 500 nM block primer (BP, 5'-CCCAGGACAGGCACAAACCddC-3'), 85 nM upstream primer (UP P82, 5'-GCCTTGT-GCTGTGCCTCCTC-3'). Reactions were started with the addition of 3.1 units Stoffel fragment of *Taq* DNA Polymerase and 19 mUnits of PerfectMatch PCR Enhancer per reaction. Cycling conditions were 2 minutes at 94°C, followed by 36 cycles of 94°C for 30 sec, 41°C for 45 seconds, 72°C for 1 min. For the K-*Ras* codon 12 GAT ACB-PCR, 1 x 10^8 copies were analyzed in each 50 ul reaction containing: 1X Stoffel buffer, 0.1 mg/ml gelatin, 1 mg/ml Triton X-100, 60 uM dNTPs, 1.5 mM $MgCl_2$, 400 nM MSP (5'-fluorescein-CTTGTGGTAGTTGGAGCTTA-3'), 325 nM BP (5'-CTTGTGGTAGTTGGAGCTTG-3'), 400 nM UP (5'-AGCAGCATTTACCTCTATCG-3'). Reactions were started with the addition of 67 mU/ul Stoffel fragment of *Taq* DNA Polymerase and 36 mUnits/ul of PerfectMatch PCR Enhancer per reaction. Cycling conditions were 90 sec at 95°C, followed by 35 cycles of 94°C for 30 sec, 42°C for 45 sec, 72°C for 1 min. ACB-PCR products were analyzed on 8% polyacrylamide gels. Fluorescent bands were visualized and quantified using a PharosFX scanner with an external blue laser and quantified using QuantityOne software (Bio-Rad, Hercules, CA).

pACB-PCR Primer Design

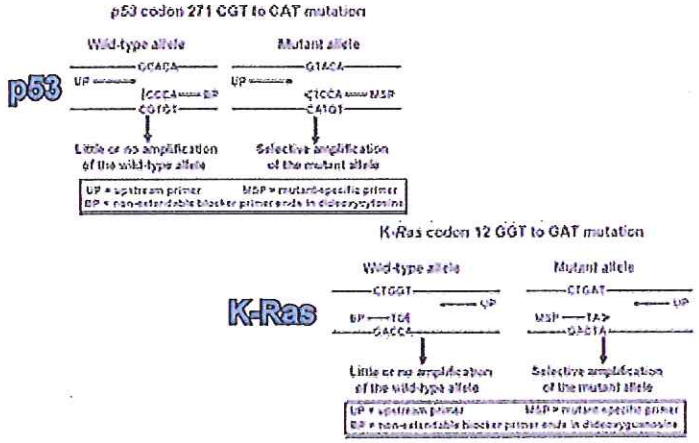

Data Analysis A standard curve was constructed from the mutant fraction (MF) standards and used to calculate the *p53* MFs in the unknown samples. Measurements were log-transformed. The average of the three independent ACB-PCR measurements for each nasal mucosa DNA sample was calculated. The log-transformed averages for the 5 animals in each treatment group were calculated and then converted back to scientific notation to derive a geometric mean MF for each treatment group. Statistical analysis of differences among treatment groups were analyzed using a one-sided analysis of variance on log-transformed MF data.

Results

p53 codon 271 CGT to CAT ACB-PCR

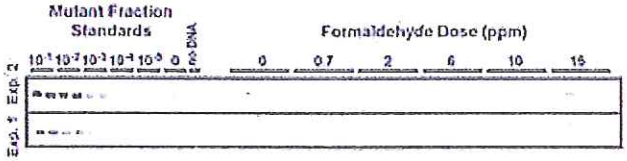

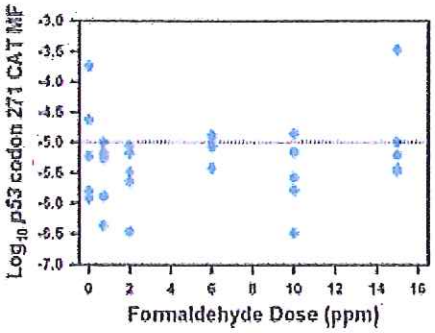

Formaldehyde Dose (ppm)	*p53* Geometric Mean MF
0	8.64×10^{-6}
0.7	2.89×10^{-6}
2	2.71×10^{-6}
6	8.49×10^{-6}
10	2.67×10^{-6}
15	1.21×10^{-5}

K-Ras codon 12 GGT to GAT ACB-PCR

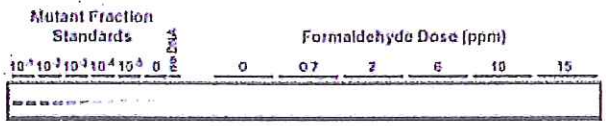

Discussion

- In 2-year studies using F344 rats, formaldehyde inhalation at 6 ppm and above causes nasal squamous cell carcinomas.
- Using ACB-PCR, it has been possible to demonstrate significant induction of cancer-relevant mutations at earlier times and lower doses than needed to induce tumors carrying the measured mutations.
- Because F344 rats exposed to formaldehyde develop tumors which carry *p53* mutations [Recio *et al.* (1992) *p53* mutations in formaldehyde-induced nasal squamous cell carcinomas in rats, *Cancer Research* 52: 6113-6116], an ACB-PCR was developed to quantify the levels of *p53* codon 271 CGT to CAT mutation and this assay was used to measure the induction of this *p53* mutation in rat nasal mucosa exposed to different levels of formaldehyde for 13 weeks.
- The F344 rat nasal mucosa contained low levels of spontaneous *p53* codon 271 CAT mutation. No significant differences among dose groups were observed (0, 0.7, 2, 6, 10, and 15 ppm formaldehyde, ANOVA, P = 0.405).
- Formaldehyde-induced changes in gene expression and unit length labeling index (a measure of cell proliferation) have been detected within 5 days of exposure at doses of 6 and 2 ppm formaldehyde, respectively [Andersen, M.E., Clewell, H.J. 3rd, Bermudez, E., Wilson, G.A., and R.S. Thomas (2008) Genomic signatures and dose-dependent transitions in nasal epithelial responses to inhaled formaldehyde in the rat, *Toxicological Sciences* 105:368-383].
- The lack of induction of *p53* mutation at a later timepoint than is needed to detect changes in cell proliferation and gene expression adds to the body of evidence that formaldehyde is not carcinogenic through a mutagenic mode of action.

ATTACHMENT 5

DNA Damage and Repair - Quantification of Sub-Cellular Events Using Automated Confocal Imaging

BD Biosciences
15010 Broschart Road, Rockville, MD 20850
For more information visit **bdbiosciences.com/bioimaging**
toll free: 800.245.2614 (US)
301.340.7320 (Outside the US)

APPLICATION NOTE

BD Biosciences

DNA Damage and Repair - Quantification of Sub-Cellular Events Using Automated Confocal Imaging

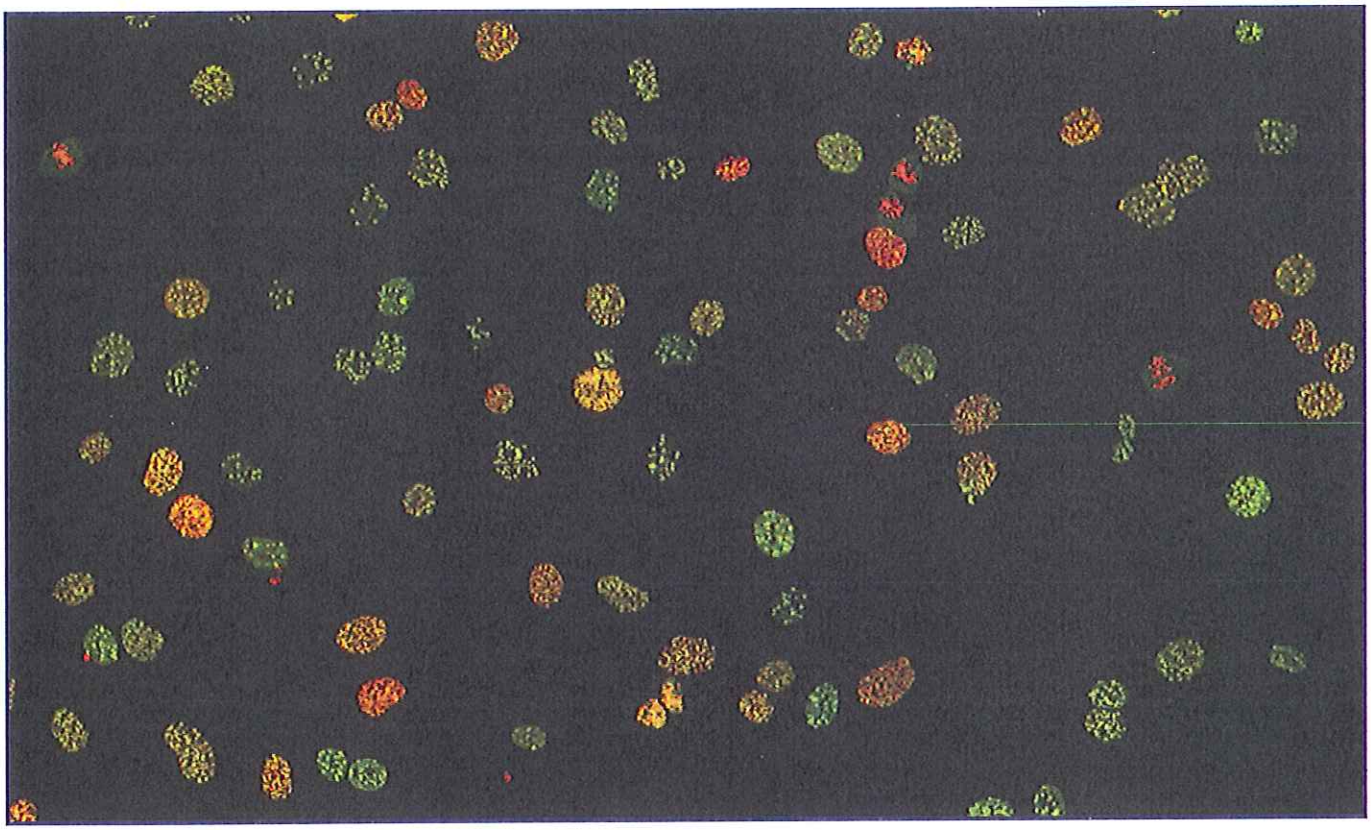

Introduction

Oxidative stress, radiation and other external insults have been shown to damage DNA molecules in cells derived from organisms as diverse as bacteria, yeast, drosophila, rodents and man (Friedberg *et al.* 2005). The presence of DNA damage may lead to cell cycle checkpoint arrest to allow time for DNA repair processes to occur. If however, the system becomes overwhelmed or the DNA repair mechanisms are impaired, the cell either enters the apoptosis pathway or become cancerous due to the accumulation of mutations resulting from replication of damaged DNA. Therefore, a complete understanding of DNA repair mechanisms is of great interest in the study of cancer prevention and treatment. In addition, this process has been implicated in cellular senescence and aging (Sedelnikova *et al.* 2004).

Following induction of DNA double strand breaks, the specialized histone protein H2AX becomes phosphorylated and rapidly (within minutes) accumulates at the sites of DNA damage forming distinct foci (Paull *et al.* 2000).

H2AX foci formation is followed by recruitment of many other proteins involved in the DNA repair process including the p53 binding protein 53BP1 (Schulz *et al.*, 2000). Over long time periods (hours), the number of foci declines with the progression of DNA repair. Detection and quantification of foci development as an indicator of DNA damage and repair is of great interest to groups investigating these pathways (Kim *et al.* 2005). The assay is generally performed using coverslips and chamber slides and imaged on fluorescence microscopes (Sedelnikova *et al.* 2004). The demands for high spatial resolution and sophisticated image analysis, however, have hindered the transfer of this assay into a multi-well plate format and thus into the drug screening arena. Our goal was to establish image acquisition and analysis methods allowing quantification of foci development both over time and with increasing concentrations of H_2O_2, a known inducer of DNA damage.

BD Biosciences
15010 Broschart Road, Rockville, MD 20850
For more information visit **bdbiosciences.com/bioimaging**
toll free: 800.245.2614 (US)
301.340.7320 (Outside the US)

BD

Methods

Cell Culture

HT1080 cells (ATCC, CCL-121, human fibrosarcoma derived cell line) were grown in 37°C, 5%CO_2 humidified incubators according to the supplier's protocol. Cells were seeded at 10,000 cell/well into 96 well plates (Cat. No. 353219) and incubated overnight. H_2O_2 (Sigma, H-1009) was used to initiate DNA double strand breaks. Immediately prior to the experiment, H_2O_2 was diluted in pre-warmed media and dose-response curves were obtained by serial dilution. Cells were exposed to chemical insult for 10 minutes at room temperature after which they were washed and replenished with fresh media. To allow for DNA repair processes to occur, the cells were returned to the incubator and left for 30, 90, or 180 minutes. In some experiments, cells were left to recover for 16 hours. At those time points, cells were fixed for 10 minutes with pre-warmed formaldehyde, 3.7% in phosphate-buffered saline (PBS), washed with PBS and permeabilized with ice-cold 90% methanol (10 minutes). Cells were washed twice with PBS and blocked using 1% BSA (in PBS) for 30 minutes. For the detection of phosphorylated H2AX, the mouse monoclonal anti-phospho serine 139 H2AX antibody (Chemicon, 05-636) at 2 µg/mL in 1% BSA block was used. 53BP1 was detected using the anti-53BP1 rabbit polyclonal antibody (Novus Biologicals, NB 100-304) diluted as described for H2AX.

After 1h at room temperature, the primary antibody was removed and cells were incubated with Tween 20 (0.05% in PBS, 10 minutes). Two PBS washes prepared the cells for the addition of the secondary antibodies, 5 µg/mL Alexa Fluor® 555-conjugated anti-mouse IgG (Cat. No. A21424) for H2AX and 5 µg/mL Alexa Fluor® 488-conjugated anti-rabbit IgG (Cat. No. A11034) for 53BP1, respectively. The DNA intercalating dye Hoechst 33342 (Invitrogen, H3570) was added at this point at 2 µg/mL and removed with the secondary antibodies after 1h at room temperature (light protected). Cells were washed as described above and wells replenished with 200 µL of PBS. Plates were sealed with adhesive foil and imaged on the BD Pathway™ Bioimager. Analysis of the image data was performed using BD IPLab™ for Pathway (Cat. No. 340989) and plotted using BD™ Image Data Explorer (Cat. No. 341039).

Results

Treatment of HT1080 cells with H_2O_2 rapidly induced the formation of phosphorylated H2AX and 53BP1 foci (***Figure 1***). There is a marked increase in the number and intensity of foci in H_20_2 treated cells compared to control cells. The two foci shared a high degree of co-localization within nuclei as observed in the merged images.

Preliminary results had shown that the nuclear foci were not evenly distributed in the same focal plane (***Figure 2***). We used the ability of the BD Pathway Bioimager to acquire 9 sections separated by 1.5 µm steps in confocal mode. To achieve the required spatial resolution, we used a 40× (NA 0.90) objective. Using the novel "collapsed-stack" acquisition feature, images were then automatically projected into a single focal plane with all objects appearing in focus.

This allowed segmentation and identification of objects within the nucleus using a customized image analysis routine written in BD IPLab for Pathway. The collapsed stack images were compared to images acquired in non-confocal mode (***Figure 2*** shows part of an image containing a single nucleus). The analysis tool generated specific parameters such as foci count, foci area as percent nuclear area, average foci intensity and average foci size. On the cellular level, the response appeared highly heterogeneous and cells could be found that showed very few foci next to cells containing a large number of foci (***Figure 1***). We therefore sampled on average 120 cells/well in a 3×3 montage. Data was imported into BD Image Data Explorer where dose-response curves and Z' data were generated (***Figures 3 and 4***).

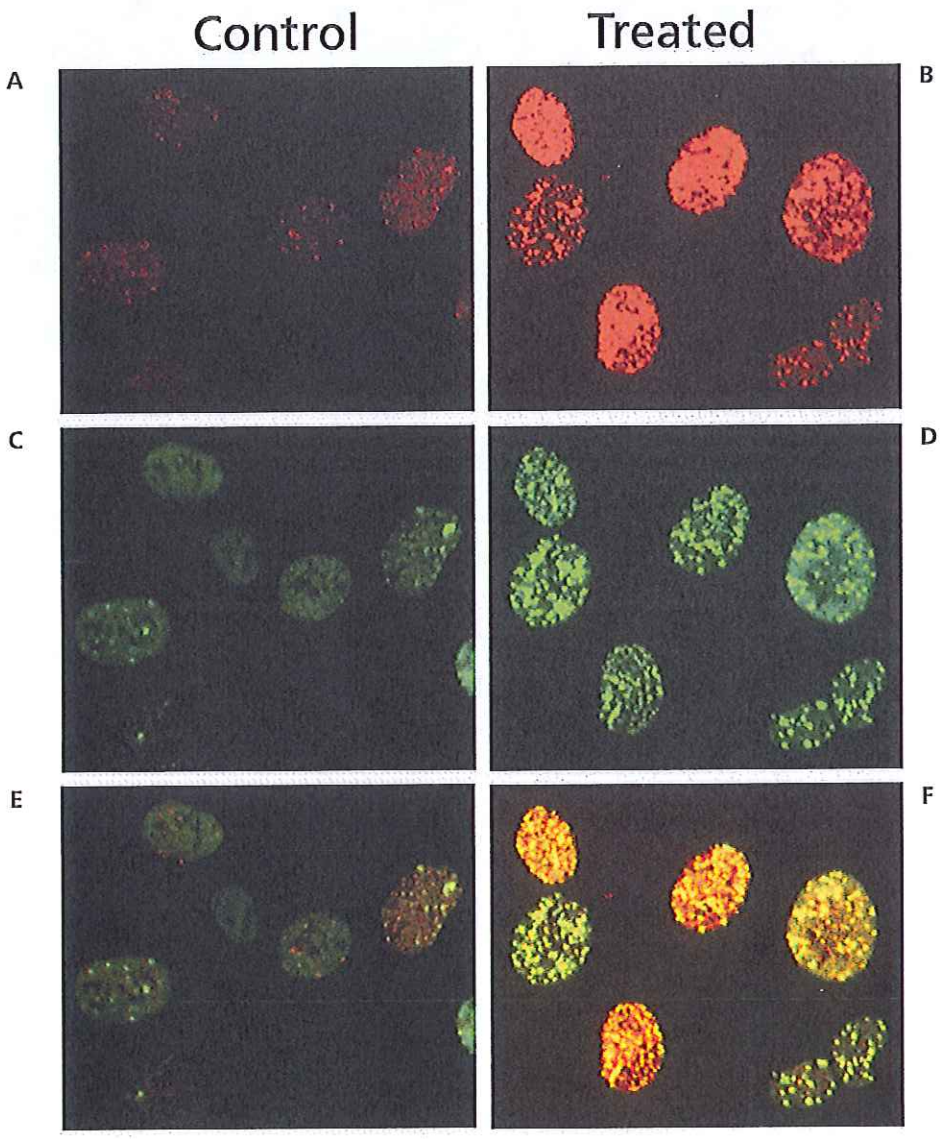

Figure 1. H_2O_2-induced H2AX and 53BP1 foci formation in HT1080 cells. Control (***panels A, C and E***) and H_2O_2 treated cells (250 µM, panels ***B, D and F***) are shown following a 30 min recovery time. The upper row (***A and B***) shows phosphorylated H2AX staining (red), the middle (***C and D***) shows 53BP1 staining (green) and the lower an overlay of both images (***E and F***). The images were acquired in confocal stack mode (see ***Figure 2***) and show the effect of H_2O_2 treatment on the number and intensity of foci at the locations of DNA damage. Note the high degree of spatial overlap between the 53BP1 and phosphorylated H2AX foci in panel F.

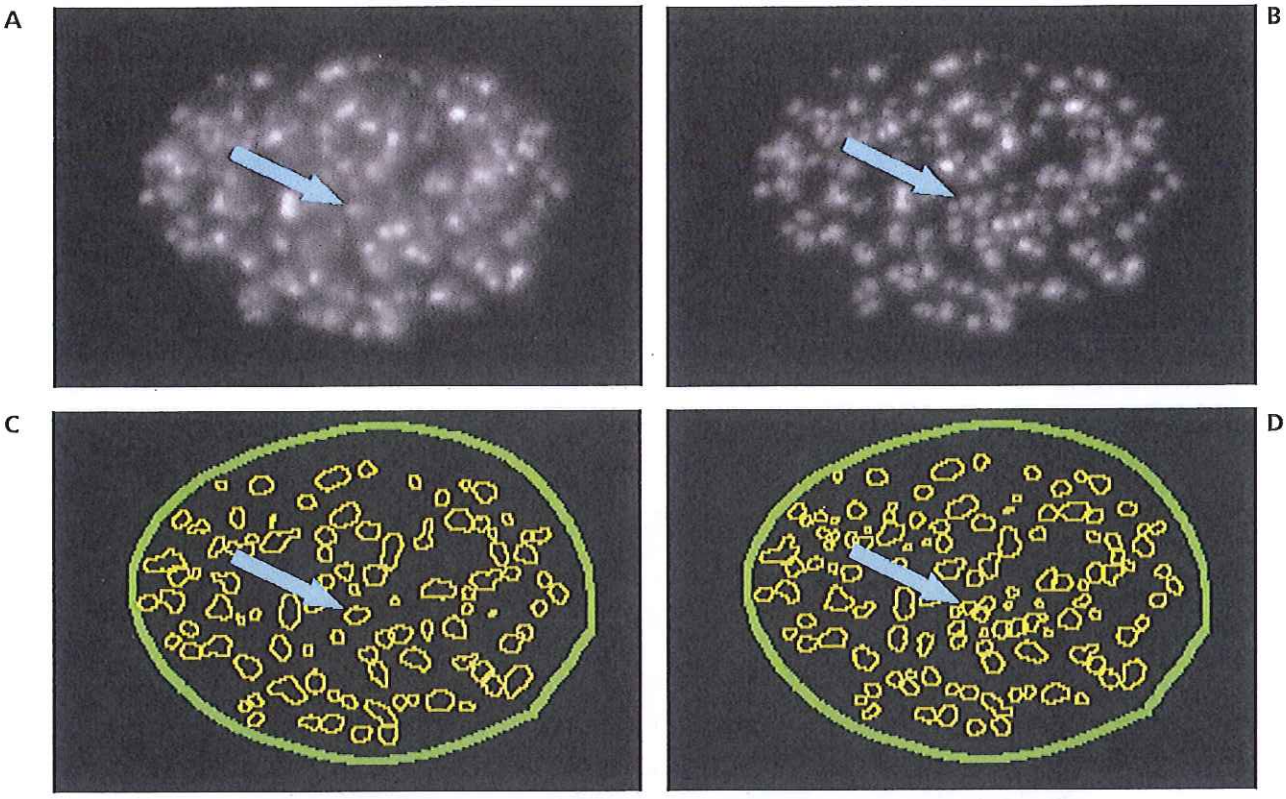

Figure 2. Comparison of images acquired in non-confocal or confocal mode. In non-confocal mode (***A***), the foci appeared fewer in number, larger and blurred (see arrows). The "collapsed-stack" feature of the BD Pathway Bioimager allowed acquisition of multiple Z positions and projection into a single image (***B***). The qualitative improvement seen with confocal over non-confocal imaging also translated into better assay performance (see ***Figure 3***). ***Panel C*** and ***D*** show the segmentation of the non-confocal **(A)** and confocal, collapsed stack ***(B)*** images, respectively. Note the greater number of foci (especially dim ones) identified by the image analysis algorithm (in the nucleus shown: 94 foci in non-confocal mode versus 118 in confocal collapsed stack mode corresponding to a 26% increase, panels C and D, respectively).

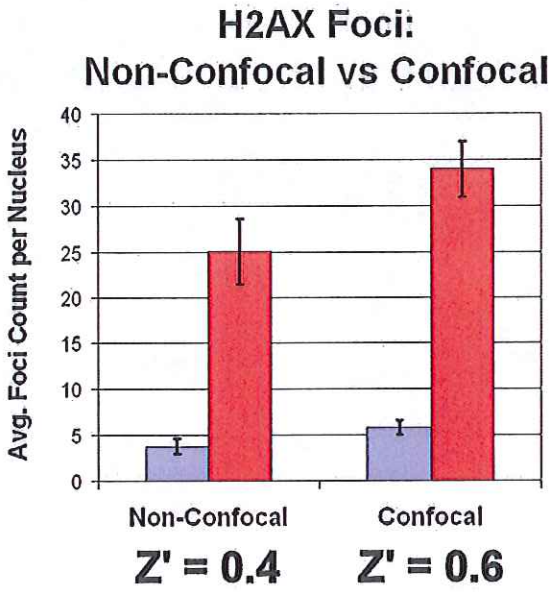

Figure 3. Comparison of assay performance under non-confocal and confocal collapsed stack acquisition conditions. The average number of H2AX foci per nucleus from control wells (blue bars) was compared to wells treated with 250 µM H_2O_2 (red bars). The data was averaged from 6 replicate wells from a 30 minute recovery time point. The statistical difference is expressed as the Z' and was 0.4 for non-confocal and 0.6 for confocal, collapsed stack.

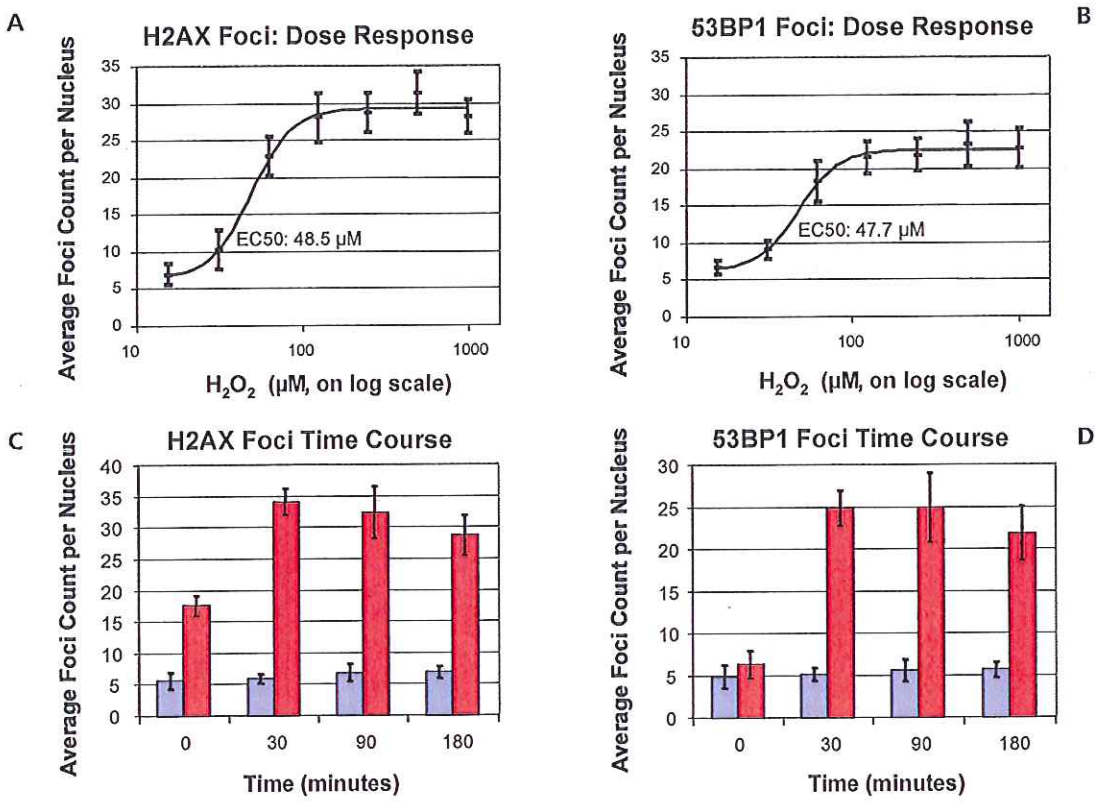

Figure 4. Dose-response relationship and time course of foci formation. Formation of H2AX foci (***panel A***) and 53BP1 (***panel B***) appears to plateau at 250 µM H_2O_2 for both proteins (shown at the 180 minute recovery time point). The dose response relationship generated an EC_{50} of 48.5 µM for H2AX and 47.7 µM for 53BP1.Time course of foci formation (***panels C and D***, blue bars = control, red bars = 250 µM H_2O_2 treated, n=6 wells) shows a distinct increase in the number of H2AX foci in cells allowed to recover for 30 minutes (***panel C***) whereas the increase of 53BP1 (***panel D***) lags behind and appears to peak between 30 and 90 minutes. The number of H2AX and 53BP1 foci slowly declined at longer time points (180 min). Overnight (16h) recovery further reduced the number of foci (data not shown) to approximately 2 fold of basal level.

Discussion

The ability to acquire confocal, collapsed stack images has allowed us to develop an automated assay relying on identification of small sub-nuclear features, namely foci of DNA damage and repair. The improved statistical performance of the assay in confocal, collapsed stack mode suggests that this assay indeed can be applied to a high-content screening environment.

We noted that even untreated cells contained some foci, suggesting that under basal conditions, some DNA double-strand breaks are present and repair occurs. Phosphorylated H2AX accumulation was seen immediately after chemical treatment confirming the rapid time course of the activation and recruitment of this protein to the sites of DNA damage. The subsequent accumulation of 53BP1 foci peaked between 30 and 90 minutes and is in agreement with published reports (Schultz *et al.* 2000). To our knowledge, the EC_{50} for H_2O_2-induced H2AX and 53BP1 foci formation has not been published and we believe that our assay can aid the characterization of other chemical agents and DNA repair proteins in a similar manner. The appearance of the 53BP1 foci in the same spatial location after 30 minutes confirms reports of rapid activation of the repair signaling cascade (Schultz *et al.* 2000).

Although we did not investigate the signaling properties between these two proteins, the assay is very suitable to investigate whether intermediate molecules are involved or whether 53BP1 is recruited by activated H2AX directly.

The comparatively straight-forward assay protocol using only 2 primary antibodies, 1 dye and a commercially available cell line allow this assay to be used in automated high-content screening applications where hands-off operation is required. The BD Pathway™ Bioimager with its confocal capability, white-light illumination and choice of 16 excitation filters allows development of multi-color assays and would even accommodate a 4th imaging channel. The complexity of change in the cellular phenotype in this assay mandate sophisticated and specialized image and data analysis algorithms. The combination of BD IPLab™ for Pathway and BD™ Image Data Explorer allows generation and analysis of high-content data in a drug screening environment.

References

1. Friedberg, E.C, Walker, G.C., Siede, *et al.* 2005 DNA Repair and Mutagenesis, ASM Press; 2nd edition *ISBN*: 1555813194
2. Kim, J-S, Krasieva, J_S, Kurumizaka, H, *et al.* 2005. Independent and sequential recruitment of NHEJ and HR factors to DNA damage sites in mammalian cells. *JCB,* 170, 341-347
3. Paull T.T., Rogakou E.P., Yamazaki V., Kirchgessner C.U., Gellert M., Bonner W.M..2000. A critical role for histone H2AX in recruitment of repair factors to nuclear foci after DNA damage. *Curr Biol.* 10, 886-95.
4. Schultz, L.B, Chehab, N.H., Malikzay, A., Halazonetis, T.H., 2000. p53 Binding Protein 1 (53BP1) Is an Early Participant in the Cellular Response to DNA Double-Strand Breaks. *JCB,* 7, 1381-1390
5. Sedelnikova O.A., Horikawa I., Zimonjic D.B., Popescu N.C., Bonner W.M., Barrett J.C. 2004. Senescing human cells and ageing mice accumulate DNA lesions with unrepairable double-strand breaks. *Nature Cell Biology.* 6, 168-70.

Notes

Regional Offices

Asia Pacific
BD Singapore
Tel 65.6861.0633
Fax 65.6860.1593

Australia/New Zealand
Australia
Toll Free: 1800 656 100
Tel 61.2.8875.7000
Fax 61.2.8875.7200
bd_anz@bd.com

New Zealand
Toll Free: 0800 572.468
Tel 64.9.574.2468
Fax 64.9.574.2469
bd_anz@bd.com

Europe
Belgium
Tel 32.53.720.550
Fax 32.53.720.549
customer_service_bdbelgium@europe.bd.com

Canada
BD Biosciences
Toll Free 888.259.0187
Tel 905.542.8028
Fax 888.229.9918
canada@bd.com

Japan
Nippon Becton Dickinson
Toll Free 0120.8555.90
Tel 81.24.593.5405
Fax 81.24.593.5761

United States
BD Biosciences
Customer/Technical Service
Toll Free 877.232.8995
Bioimaging Systems
Fax 301.340.9775
Discovery Labware
Fax 978.901.7493
Immunocytometry Systems
Fax 800.325.9637
Pharmingen
Fax 800.325.9637
bdbiosciences.com

Local Offices and Distributors

Argentina/Paraguay/Uruguay
Toll Free: 0800.444.5523
Tel 54.11.4551.7100
Fax 54.11.4551.7400
crc_argentina@bd.com

Austria
Tel 43.1.706.36.60.20
Fax 43.1.706.36.60.11
customerservice.bdb.at@europe.bd.com

Brazil
Toll Free: 0800.771.7157
Tel 55.11.5185.9995
Fax 55.11.5185.9895
biosciences@bd.com.br

CCA (Caribbean/Central America)
Tel 52.55.5999.8318
Fax 52.55.5999.8396
caribbean_customers@bd.com
centralamerica_customers@bd.com

Chile
Tel 56.2 482.7800 x16
Fax 56.2 482.7802

China
Tel 8610.6418.1608
Fax 8610.6418.1610

Colombia
Tel 57.1.572.4060 x244 / 258
Fax 57.1.572.3650 / 4250

Denmark
Tel 45.43.43.45.66
Fax 45.43.43.41.66
bdbnordic@europe.bd.com

East Africa
Tel 254.2.341157
Fax 254.2.341161
bd@africaonline.co.ke

Eastern Europe
Tel 49.6221.305.161
Fax 49.6221.305.418
bdb.ema@europe.bd.com

Egypt
Tel 202.268.0181
Fax 202.266.7562

Finland
Tel 358.9.88.70.7832
Fax 358.9.88.70.7817
bdbnordic@europe.bd.com

France
Tel 33.4.76.68.36.09
Fax 33.4.76.68.35.06
customerservice.bdb.france@europe.bd.com

Germany
Tel 49.6221.305.551
Fax 49.6221.303.609
customerservice.bdb.de@europe.bd.com

Greece
Tel 30.1.940.77.41
Fax 30.1.940.77.40

Hong Kong
Tel 852.2575.8668
Fax 852.2803.5320

Hungary
Tel 36.1.345.7090
Fax 36.1.345.7093
bdb.ema@europe.bd.com

India
Tel 91.124.238.3566.70
Fax 91.124.238.3225

Indonesia
Tel 62.21.577.1920
Fax 62.21.577.1925

Italy
Tel 39.02.48.240.1
Fax 39.02.48.20.33.36

Korea
Tel 822.3404.3700
Fax 822.557.4048

Malaysia
Tel 603.7725.5517
Fax 603.7725.4772

Mexico
Toll Free: 01.800.236.2543
Tel 52.55.5999.8296
Fax 52.55.5999.8288
bioscienciasmexico@bd.com

Middle East
Tel 971.4.337.95.25
Fax 971.4.337.95.51
bdb.ema@europe.bd.com

The Netherlands
Tel 31.20.582.94.20
Fax 31.20.582.94.21
customer_service_bdholland@europe.bd.com

North Africa
Tel 33.4.76.68.35.03
Fax 33.4.76.68.35.44
bdbiosciences_maghreb@europe.bd.com

Norway
Tel 47.73.59.12.00
Fax 47.73.59.12.01
norge@europe.bd.com

Pakistan
Tel 92.42.5718051
Fax 92.42.5718056
bdb_pak@bd.com

Peru/Bolivia/Ecuador
Tel 51.1.712.0160
Fax 51.1.712.0165

Philippines
Tel 632.815.8981
Fax 632.815.6644

Poland
Tel 48.22.651.75.88
Fax 48.22.651.75.89
bdb.ema@europe.bd.com

Portugal
Enzifarma
Tel 351.21.421.93.30
Fax 351.21.421.93.39

South Africa
Tel 27.11.603.2620
Fax 27.11.804.0544 / 46
bdb.ema@europe.bd.com

Spain
Tel 34.902.27.17.27
Fax 34.91.848.81.04

Sweden
Tel 46.8.775.51.10
Fax 46.8.775.51.11
bdbnordic@europe.bd.com

Switzerland
Tel 41.61.485.22.22
Fax 41.61.485.22.00
customerservice.bdb.ch@europe.bd.com

Taiwan
Tel 8862.2722.5660
Fax 8862.2725.1768

Thailand
Tel 662.646.1800
Fax 662.646.1801

Turkey
Tel 90.212.328.2720
Fax 90.212.328.2730
bdb.ema@europe.bd.com

United Kingdom & Ireland
Tel 44.1865.78.16.88
Fax 44.1865.78.16.27
BDUK_CustomerService@europe.bd.com

Venezuela
Tel 58.212.241.3412 x248
Fax 58.212.241.7389

West Africa
Sobidis
Tel 225.20.33.40.32
Fax 225.20.33.40.28

BD Biosciences
10975 Torreyana Road
San Diego, CA 92121-1106
Toll free 877.232.8995
bdbiosciences.com

06-A790030-6A

ATTACHMENT 6

K-Ras mutant fraction in A/J mouse lung increases as a function of benzo[a]pyrene dose

Meng, Fanxue; US Food and Drug Administration, National Center for Toxicological Research, Division of Genetic and Reproductive Toxicology

Knapp, Geremy; US Environmental Protection Agency, National Health and Environmental Effects Research Laboratory, Environmental Carcinogenesis Division

Green, Terry; US Environmental Protection Agency, National Health and Environmental Effects Research Laboratory, Environmental Carcinogenesis Division

Ross, Jeffrey; US Environmental Protection Agency, National Health and Environmental Effects Research Laboratory, Environmental Carcinogenesis Division

Parsons, Barbara; US Food and Drug Administration, National Center for Toxicological Research, Division of Genetic and Reproductive Toxicology

Environmental and Molecular Mutagenesis

K-*Ras* mutant fraction in A/J mouse lung increases as a function of benzo[*a*]pyrene dose

Journal:	*Environmental and Molecular Mutagenesis*
Manuscript ID:	draft
Wiley - Manuscript type:	Research Article
Date Submitted by the Author:	
Complete List of Authors:	Meng, Fanxue; US Food and Drug Administration, National Center for Toxicological Research, Division of Genetic and Reproductive Toxicology Knapp, Geremy; US Environmental Protection Agency, National Health and Environmental Effects Research Laboratory, Environmental Carcinogenesis Division Green, Terry; US Environmental Protection Agency, National Health and Environmental Effects Research Laboratory, Environmental Carcinogenesis Division Ross, Jeffrey; US Environmental Protection Agency, National Health and Environmental Effects Research Laboratory, Environmental Carcinogenesis Division Parsons, Barbara; US Food and Drug Administration, National Center for Toxicological Research, Division of Genetic and Reproductive Toxicology
Key Words:	Allele-specific competitive blocker PCR, risk assessment, B[a]P DNA adduct, mutation, lung cancer

Running title: K-*Ras* mutant fraction in A/J mouse lung
Key words: K-*Ras*, mutant fraction, lung, carcinogenesis, A/J mouse

K-*Ras* mutant fraction in A/J mouse lung increases as a function of benzo[*a*]pyrene dose

Fanxue Meng[1], Geremy W. Knapp[2], Terry Green[2], Jeffrey A. Ross[2], and Barbara L. Parsons[1]

[1]Division of Genetic and Reproductive Toxicology, National Center for Toxicological Research, Jefferson, AR 72079
[2]Environmental Carcinogenesis Division, National Health and Environmental Effects Research Laboratory, Environmental Protection Agency, Research Triangle Park, NC 27711

Corresponding Author

Fanxue Meng

Division of Genetic and Reproductive Toxicology,
HFT-120
3900 NCTR Road
Jefferson, AR 72079
Phone: 870-543-7082
Fax: 870-543-7393
Email: Fanxue.Meng@fda.hhs.gov

ABSTRACT

K-*Ras* mutant fraction (MF) was measured to examine the default assumption of low dose linearity in the benzo[*a*]pyrene (B[*a*]P) mutational response. Groups of ten male A/J mice (7-9 weeks-old) received a single *i.p.* injection of 0, 0.05, 0.5, 5, or 50 mg/kg B[*a*]P, and were sacrificed 28 days after treatment. K-*Ras* codon 12 TGT and GAT MFs in lung DNAs were measured using Allele-specific Competitive Blocker-PCR (ACB-PCR). The K-*Ras* codon 12 TGT geometric mean MF was 3.88 X 10^{-4} in controls, indicating an average of 1 mutation in every ~1,288 lung cells. The K-*Ras* codon 12 TGT geometric mean MFs were: 3.56 x 10^{-4}; 6.19 x 10^{-4}; 2.02 x 10^{-3}, and 3.50 x 10^{-3} for the 0.05, 0.5, 5, and 50 mg/kg B[*a*]P treatment groups, respectively. The 5 and 50 mg/kg dose groups had TGT MFs significantly higher than controls. Although 10^{-5} is considered the limit of accurate ACB-PCR quantitation, K-*Ras* codon 12 GAT geometric mean MFs were: 8.38 x 10^{-7}; 1.47 x 10^{-6}; 2.19 x 10^{-6}, 5.71 x 10^{-6} and 8.99 x 10^{-6} for the 0, 0.05, 0.5, 5, and 50 mg/kg B[*a*]P treatment groups, respectively. The K-*Ras* TGT and GAT MFs increased in a B[*a*]P-dose-dependent manner, with response approximately linear over the 0.05 to 5 mg/kg dose range. K-*Ras* MF increased with B[*a*]P adduct burden measured for identical doses in a separate study. Thus, ACB-PCR may be useful in characterizing the shape of a dose-response curve at low doses and establishing relationships between DNA adducts and tumor-associated mutations.

Keywords: Allele-specific competitive blocker PCR; risk assessment; mutation; lung cancer, B[*a*]P DNA adduct

Abbreviation: B[*a*]P, benzo[*a*]pyrene; MF, mutant fraction; ACB-PCR, allele-specific competitive blocker-PCR; TIDAL, Time-Integrated DNA Adduct Levels; PAH, polycyclic aromatic hydrocarbons; BPDE, 7,8-dihydroxy-9,10-epoxy-7,8,9,10-tetrahydro-benzo[*a*]pyrene; MOA, mode of action; UP, upstream primer; MSP, mutant-specific primer; BP, block primer; bp, basepair; EGFR, epidermal growth factor receptor; PI3K, Phosphoinositide 3 kinase; ERK, extracellular signal-regulated kinase; IGF, insulin-like growth factor; IRS, insulin receptor substrate; MAPK, Mitogen-activated protein (MAP) kinase; Shc, src homology 2 domain-containing.

INTRODUCTION

Lung cancer is the leading cause of cancer-related mortality in both men and women throughout the world, with a projected 161,840 deaths in the United States alone in 2008. Worldwide, the role of environmental air pollution in lung cancer causation is a significant health concern. Polycyclic aromatic hydrocarbons (PAHs) represent known carcinogenic environmental exposures. A mean total intake of 3.12 μg/day PAH was estimated in nonsmokers, of which food contributed 96.2%, air 1.6%, and water 0.2%. Smokers consuming one pack per day had an estimated additional intake of 2–5 μg/day (Menzie et al. 1992). A large body of epidemiological data suggests that approximately 85% of all lung cancer deaths in the United States are related to tobacco smoking (Reynolds and Anderson 1991).

PAHs occur as complex mixtures and 500 PAHs have been detected in air and water. B[*a*]P is frequently measured as the archetypical PAH. Concentrations of B[*a*]P in drinking-water have been shown to range from 0.2 to 24 ng/L (Europe 1987). The natural air background level of B[*a*]P is nearly zero. However, from June 1999 to May 2000, average B[*a*]P levels were 0.065 ng/m^3 in Los Angeles, California; 0.025 ng/m^3 in Houston, Texas; and 0.14 ng/m^3 in Elizabeth, New Jersey (Naumova et al. 2002). In the 1990's, typical annual mean levels for B[*a*]P varied between 0.1 and 1 ng/m^3 in European rural areas; between 0.5 and 3 ng/m^3 in European urban areas; and up to 30 ng/m^3 in European areas in the immediate vicinity of certain industrial installations (http://ec.europa.eu/environment/air/pdf/pp_pah. pdf). An annual average target value of 1 ng/m^3 for B[*a*]P (as the representative PAH) was proposed in the European Community's fourth Air Quality Daughter Directive (2005/107/EC)

(http://www.airquality.co.uk/archive/monitoring_networks_.php?n=_pah). The United Kingdom Air Quality Standards set an annual average standard for B[*a*]P at 0.25 ng/m^3 (Dimashki et al. 2001). No recommendation exists for the United States.

B[*a*]P is metabolized by cytochromes P-450 to form reactive intermediates. The mechanisms of B[*a*]P action are complex. There are two critical pathways of B[*a*]P metabolism; one pathway involves one-electron oxidation to form a radical cation (which then produces a BP-6-N7Gua adduct), while the other pathway operates through monooxygenation to form a diol epoxide [such as 7,8-dihydroxy-9,10-epoxy-7,8,9,10-tetrahydro-benzo[*a*]pyrene (BPDE)] (Baird et al. 2005; Banasiewicz et al. 2004). The B[*a*]P active intermediates covalently bind to DNA. Once formed, B[*a*]P-DNA adducts can be converted by DNA replication into the mutations that can cause tumors (Hakura et al. 1999; Ross et al. 1995). Although *in vivo* experiments showed B[*a*]P-DNA adducts were detectable in A/J mouse lung tissue at multiple time points (1 to 21 days) after exposure to doses ranging from 2 to 200 mg B[*a*]P/kg body weight, the relationship between administered dose and DNA adduct levels was non-linear (Ross et al. 1995).

Measurement of tumor-associated oncogene mutations is likely to be a sensitive endpoint with which to measure the low dose effects of B[*a*]P, because its DNA damaging effects may be amplified through the resultant growth advantage of mutant cells. K-*Ras* is an oncogene that functions in regulating cell cycle, cell proliferation, and differentiation. K-*Ras* mutations have been found in one third of human lung adenocarcinomas and are strongly associated with smoking (Ahrendt et al. 2001; Rodenhuis et al. 1988). Thus, K-*Ras* codon 12 mutation is the ideal mutational target with which to investigate the dose-dependence of B[*a*]P-induced mutation (Mass et al.

1993). In strain A/J mouse lung, K-*Ras* codon 12 mutations are found in 91% of spontaneous lung adenomas, with 59% of these mutants being GAT and 33% GTT (You et al. 1989). K-*Ras* codon 12 TGT mutation is the most frequent mutation observed in B[*a*]P-induced tumors (Mass et al. 1993; Tretyakova et al. 2002). The A/J mouse is sensitive in terms of lung tumor development; eventually, all A/J mice develop spontaneous lung tumors by 18-24 months of age, with the earliest tumors observed at 3-4 months of age (Tuveson and Jacks 1999).

Methodologies to quantify rare mutations accurately in tissue before tumors are evident have made it possible to use the measurement of somatic oncogene mutations as biomarkers of effect. Specifically, Allele-specific Competitive Blocker-PCR (ACB-PCR) has been used to detect the induction of H-*Ras* codon 61 CAA to AAA mutation in normal-appearing liver tissue from mice treated with 4-aminobiphenyl (Parsons et al. 2005) and K-*Ras* codon 12 GGT to GTT and GGT to GAT MFs in livers of Big Blue rats treated with N-hydroxy-2-acetylaminofluorene (McKinzie et al. 2006). ACB-PCR was used to describe the dose-response relationship between simulated solar light exposure and induction of a UV-specific *p53* codon 270 CGT to TGT mutation in mouse skin tissues and to relate those measurements to the induction of simulated solar light-induced mouse skin tumors (Verkler et al. 2008a; Verkler et al. 2008b). In this project, we developed ACB-PCR assays to quantify the levels of mouse K-*Ras* codon 12 GGT to TGT and GGT to GAT mutations. These assays were then used to measure levels of the two K-*Ras* mutations in untreated A/J mouse lung, as well as lung tissues of mice exposed to B[*a*]P at doses ranging from 0.05 mg/kg to 50 mg/kg body weight. The goals of this research were to: 1) explore the sensitivity of ACB-PCR in detecting the

mutagenicity of B[*a*]P in mouse lungs, 2) establish the shape of the dose response curve using low B[*a*]P doses, and 3) relate the induction of mouse lung DNA adducts, measured previously (Ross et al. 1995), to the induction of K-*Ras* mutations.

MATERIALS AND METHODS

Animals

Male A/J mice, 7 to 9 weeks old, were purchased from the Jackson Laboratory (Bar Harbor, ME). Animals were housed five per cage and maintained at 22 ± 2°C at 30 to 60% relative humidity, with a 12 h light/dark cycle. Water and food (Wayne Rodent Chow) were provided *ad libitum*. Four groups of mice (10 animals/group) were given a single *i.p.* injection of 0.05, 0.5, 5, or 50 mg/kg B[*a*]P as a uniform suspension in tricaprylin. Animals in the control group received tricaprylin alone. Twenty-eight days after treatment, all mice were killed by CO_2 asphyxiation and intact lungs were removed and immediately placed into liquid nitrogen.

Lung Tissue DNA Isolation and First-round PCR

To isolate DNA from A/J mouse lung tissue, whole lungs (38–50 mg) were homogenized in 1 ml of extraction buffer consisting of 0.2 mg/ml proteinase K, 100 mM NaCl, 25 mM EDTA, and 1% SDS. Samples were incubated ~16 hour at 37°C, then extracted with an equal volume of phenol/chloroform/isoamyl alcohol (25:24:1). Samples were resuspended in 200 µl of a RNAse buffer containing 10 mg/ml RNAse A (Sigma, St. Louis, MO), 600 units/ml Ribonuclease T1 (Sigma), 100 mM sodium acetate, and 50 mM Tris-HCl (pH 8). Samples were incubated ~16 hours at 37°C, then extracted

as described above. The DNA was precipitated and resuspended in 20 µl of TE buffer (5 mM Tris, 0.5 mM EDTA, pH 7.5) and 20 µg of each DNA sample was digested with Hind III according to the manufacturer's instructions (New England Biolabs, Beverly, MA). Finally, the digested DNAs were extracted and precipitated as described above and resuspended in 20 µl of TE buffer.

The genomic DNA was used for first-round PCR amplification of a K-*Ras* gene segment encompassing 5' flanking sequence, exon 1, and part of intron 1. Each 200 µl PCR reaction contained: 1 µg genomic DNA, 200 nM primer TR67 (5'-TGGCTGCCGTCCTTTACAA), 200 nM primer TR68 (5'-GGCCTGCTGAAAAT GACTGAGTATAAACTTGT), 200 nM dNTPs, 1X *PfuUltra* reaction buffer, and 10 units *PfuUltra* high-fidelity DNA Polymerase (Stratagene, La Jolla, CA). Cycling conditions were 94°C for 2 min, followed by 35 cycles of 94°C for 1 min, 58°C for 2 min, and 72°C for 1 min, followed by a 7 min extension at 72°C. The 170-bp PCR products were agarose gel-purified using a Geneclean® Spin Kit (Q-Biogene, Vista, CA). Aliquots of the first-round PCR products were prepared and repeatedly quantified using a Nanodrop spectrophotometer (Nanodrop Technologies, Wilmington, DE), until three measurements that varied by <10% from the group mean were obtained.

Plasmid A5, encompassing K-*Ras* 5' flanking sequence, exon 1, and part of intron 1 (including the wild-type K-*Ras* codon 12 DNA sequence, GGT), was digested by Hind III and used as the template to synthesize a wild-type DNA standard. Plasmid C5, encompassing the same K-*Ras* region but including a mutation at codon 12 (TGT), was digested by Hind III and used as template to synthesize a K-*Ras* codon 12 TGT mutant standard. The primers and PCR conditions used to synthesize the standards from plasmid

DNA were the same as those described above. Also, plasmid A5 was used as template for *in vitro* PCR mutagenesis to synthesize the K-*Ras* codon 12 GAT mutant standard. Primer TR72 (5'-GGCCTGCTGAAAATGACTGAGTATAAACTTGTGGTGGTTGG AGCTGATGGCGTAGGCAAGAGCGCCT) and primer TR 67 were used along with first-round PCR conditions as described above. Cycling conditions were 94°C for 2 min, followed by 35 cycles of 94°C for 1 min, 59°C for 2 min, and 72°C for 1 min, followed by a 7 min extension at 72°C. Wild-type, TGT and GAT mutant DNA standards were gel-purified and quantified as described above.

ACB-PCR

PCR products corresponding to K-*Ras* codon 12 wild-type (GGT) and mutant (TGT or GAT) DNA sequence were mixed to generate samples with mutant fractions of 10^{-1}, 10^{-2}, 10^{-3}, 10^{-4}, 10^{-5} and 0 (no-mutant control). These standards and a no-DNA control were analyzed in parallel with equal numbers of copies of first-round PCR products. Each K-*Ras* codon 12 TGT ACB-PCR reaction was prepared by placing 10 µl DNA (1×10^9 copies) and 35 µl of reaction mix into a 0.5 ml thin-walled microcentrifuge tube to which 40 µl of mineral oil were added. The reaction mix was prepared such that the final concentration of reagents in each 50 µl ACB-PCR reaction was 1X Stoffel buffer, 0.1 mg/ml gelatin, 1 mg/ml Triton X-100, 20 µM dNTPs, 1.5 mM $MgCl_2$, 200 nM mutant-specific primer (MSP, 5'-Fluorescein-ACTTGTGGTGGTTGGAGCCT-3'), 250 nM blocker primer (BP, 5'-ACTTGTGGTGGTTGGAGCCddG-3'), and 200 nM upstream primer (UP, 5'-TCGTAGGGTCGTACTCATC-3'). Reactions were initiated using a hot-start procedure, with the addition of 2.8 units/reaction Stoffel fragment of *Taq*

DNA polymerase (Applied Biosystems, Foster City, CA) and 56 mUnits/reaction of PerfectMatch PCR Enhancer (Stratagene, La Jolla, CA) that had been diluted into 5 µl of the reaction mix. Cycling conditions were 2 minutes at 94°C, followed by 37 cycles of 94°C for 30 sec, 41°C for 45 sec, and 72°C for 1 min.

Each K-*Ras* codon 12 GAT ACB-PCR reaction was prepared by placing 10 µl DNA (2 x 10^8 copies) and 35 µl of reaction mix into a 0.5 ml thin-walled microcentrifuge tube to which 40 µl mineral oil were added. The reaction mix was prepared such that the final concentration of reagents in each 50 µl ACB-PCR reaction was 1X Stoffel buffer, 0.1 mg/ml gelatin, 1 mg/ml Triton X-100, 20 µM dNTPs, 1.6 mM $MgCl_2$, 85 nM MSP (5'-Fluorescein-CTTGTGGTGGTTGGAGCTAA-3'), 500 nM BP (5'-CTTGTGGTGGT TGGAGCTAddG-3'), and 85 nM UP. Reactions were initiated using a hot-start procedure, with the addition of 3.4 units/reaction Stoffel fragment of *Taq* DNA polymerase (Applied Biosystems, Foster City, CA) and 63 mUnits/reaction of PerfectMatch PCR Enhancer (Stratagene, La Jolla, CA) that had been diluted into 5 µl of the reaction mix. Cycling conditions were 2 minutes at 94°C, followed by 37 cycles of 94°C for 30 sec, 43°C for 45 seconds, and 72°C for 1 min.

Gel Electrophoresis, Image Analysis, and Data Collection

Equal volumes of ACB-PCR products were analyzed on non-denaturing, 8% polyacrylamide gels. The fluorescent bands were visualized following excitation at 488 nm using a PharosFX™ Molecular Imager with an external blue laser (Bio-Rad Life Science, Hercules, CA). For each MF standard, the fluorescence of the correct-sized product (both TGT and GAT ACB-PCR products are 105 bp in length) was measured

using Quantity One software (Bio-Rad). Specifically, replicate boxes were drawn around individual bands and an average background pixel measurement (collected under the outline of each box) was subtracted from the total pixel count for each box. Log-linear plots relating fluorescence (in pixels) to MF were constructed and fit with an exponential function. This function was then used to calculate the MF in each unknown sample based on the fluorescence of the ACB-PCR product generated using that sample and the same quantitation methodology.

Data Analysis

The K-*Ras* MF for each sample was calculated and then the arithmetic average of replicate measurements was determined. In order to standardize the variability of measurements distributed over the log-scale, the average MF measurement for each sample was log-transformed. For each treatment group, the average of the log-transformed MF measurements was calculated then converted back to MF, to obtain the geometric mean MF.

Statistical differences in the average log-transformed K-*Ras* codon 12 GGT to TGT MFs among treatment groups were identified using log-transformed data and a one-sided analysis of variance (SigmaStat 3.11). K-*Ras* codon 12 GAT MF was analyzed by Fisher's Exact test (Graphpad Prism 5) based on mutation prevalence.

RESULTS

Mutant quantification by ACB-PCR is based on the parallel analysis of equal numbers of copies of first-round PCR products amplified from genomic DNA samples

and samples with defined mutant fractions (MFs). K-*Ras* codon 12 wild-type (GGT) and mutant (TGT or GAT) DNAs were generated by PCR. These DNAs were then combined to construct MF standards ranging from 10^{-1} to 10^{-5}. Using these standards, ACB-PCR reaction conditions were optimized, then used to measure the K-*Ras* codon 12 TGT or GAT MF in 50 A/J mouse lung samples, based on three replicate ACB-PCR measurements per sample. The primer strategy used in the mutant-specific amplification of the K-*Ras* codon 12 GGT to TGT ACB-PCR is shown in Figure 1A, that for the K-*Ras* codon 12 GGT to GAT mutant-specific amplification is shown in Figure 1B.

Twelve gels were used to quantify all of the study samples for K-*Ras* codon TGT MF, with 12 MF standards per gel (*i.e.* replicate 10^{-1}, 10^{-2}, 10^{-3}, 10^{-4}, 10^{-5}, and 0 standards). For the TGT MF measurements, one 10^{-4} standard was excluded as a technical failure because its pixel intensity was lower than the other 10^{-4} replicate, as well as 10^{-5}, and 0 MF replicates. The average r^2 value for the set of 12 TGT standard curves was 0.9599 (range 0.9097 to 0.9833). Results of two of the three replicate K-*Ras* codon 12 TGT ACB-PCR measurements are shown in Figure 2. Samples 1-25, along with MF standards, are presented in Figure 2A. Samples 26-50, along with MF standards, are presented in Figure 2B. The K-*Ras* TGT MF measurement of one sample in the 0.05 mg/kg dose group was based on two rather than three replicate ACB-PCR measurements, because one appeared to be a technical failure (negative pixel intensity following background correction). The A/J mouse lung contains a relatively high spontaneous level of K-*Ras* codon 12 TGT mutations. The K-*Ras* codon 12 GGT to TGT MF in every sample was above the limit of accurate ACB-PCR quantitation (10^{-5}). The lung tissues from control animals had a geometric mean MF of 3.88×10^{-4}, (Table 1). However, the

inter-animal variability in the K-*Ras* TGT geometric mean MF was large, with the control animals having MFs ranging from 3.50×10^{-5} to 3.24×10^{-3} (Figure 3A). The TGT geometric mean MFs for the B[*a*]P treatment groups were: 3.56×10^{-4}, 6.19×10^{-4}, 2.02×10^{-3}, and 3.50×10^{-3} for the 0.05, 0.5, 5, and 50 mg/kg dose groups, respectively (Table 1). Although statistically-significant differences between dose groups were observed (ANOVA, $P < 0.001$, with the Holm-Sidak method for multiple comparisons), only the 5 and 50 mg/kg dose groups were significantly higher than controls. A significant trend of increasing MF with increasing dose was observed (slope of linear regression line in log-log plot significantly non-zero, $P < 0.0001$, Figure 3B).

Figure 4A shows that the increase in K-*Ras* codon 12 GGT to TGT MF was approximately linear over the dose range of 0.05 to 5 mg/kg B[*a*]P, with a dampening of the response above 5 mg/kg. A small, non-significant decrease in K-*Ras* codon 12 GGT to TGT MF was seen in the 0.05 mg/kg treatment group relative to the control group. A transition in the shape of the dose-response curve was observed above 5 mg/kg B[*a*]P. Above 5 mg/kg B[*a*]P, a smaller increase in K-*Ras* codon 12 GGT to TGT MF with dose was observed compared to that seen below 5 mg/kg B[*a*]P.

Six gels were used to quantify GGT to GAT MF. Results of two of the three replicate K-*Ras* codon 12 GAT ACB-PCR measurements are shown in Figure 5. Because the ACB-PCR pixel intensities of all GAT unknowns were in the low range of the standard curve (all $<10^{-4}$), and the MF standard curves appear to be sub-linear above 10^{-2}, K-*Ras* GAT MF quantitation was based on ten standards per gel (*i.e.* replicate 10^{-2}, 10^{-3}, 10^{-4}, 10^{-5}, and 0 standards). The average r^2 value for the six GAT standard curves was 0.9729 (range 0.9555 to 0.9914). The K-*Ras* GAT MF measurement of one sample

in the 0.5 mg/kg dose group was based on two rather than three replicate ACB-PCR measurements, because one appeared to be a technical failure (negative pixel intensity following background correction). Compared to K-*Ras* codon 12 TGT mutation, much lower levels of the K-*Ras* codon 12 GAT mutation were detected (see Figures 3 and 6). In fact, all control samples had spontaneous K-*Ras* codon 12 GAT MFs below the lowest MF standard (10^{-5}) and the level of accurate quantitation. In the B[*a*]P-treated samples, the GAT MF was above the lowest MF standard (10^{-5}) in 1 of 10 mice in the 0.5 mg/kg B[*a*]P dose group, 2 of 10 mice in the 5 mg/kg B[*a*]P dose group, and 5 of 10 mice in the 50 mg/kg B[*a*]P dose group. Although most of the 50 K-*Ras* codon 12 GGT to GAT MF measurements were below the lowest ACB-PCR standard, the calculated ACB-PCR MFs were used to estimate the geometric mean MF for each treatment group. The lung tissue from control animals had a geometric mean MF of 8.38×10^{-7}. The GAT geometric mean MFs for the B[*a*]P treatment groups were: 1.47×10^{-6}, 2.19×10^{-6}, 5.71×10^{-6}, and 8.99×10^{-6} for the 0.05, 0.5, 5, and 50 mg/kg, respectively (Table 1). A significant trend of increasing GAT MF with increasing dose was observed (slope of linear regression line in log-log plot significantly non-zero, $P<0.0001$, Figure 6B).

An approximately linear increase in K-*Ras* codon 12 GAT MF was observed over the dose range of 0.05 to 5 mg/kg B[*a*]P, with a dampening of the response above 5 mg/kg (Figure 4B). Because the majority of the K-*Ras* GAT MFs measurements were below the limit of reliable ACB-PCR quantitation, treatment groups were compared based on proportion of measurement $>10^{-5}$ using Fisher's Exact test. A difference in distribution of samples above and below 10^{-5} was tested. The only statistically-

significant difference observed was between the 50 mg/kg dose group and the control group (one-tailed test, P=0.0163) (Figure 4B).

The total burden of DNA adducts (Time-Integrated DNA Adduct Levels, TIDAL value) had been measured in A/J mice treated with two of the same doses of B[*a*]P used in the current study (5 and 50 mg/kg B[*a*]P). This enabled a direct comparison of the levels of DNA adducts and levels of K-*Ras* mutations induced by particular B[*a*]P exposures 28 days after exposure (Ross et al. 1995). TIDAL values induced by a given dose of B[*a*]P were plotted against K-*Ras* codon 12 TGT and GAT MFs induced by the same B[*a*]P dose (Figure 7). Figure 7 shows that the levels of K-*Ras* mutation increased as a function of DNA adduct burden for both mutations. A greater yield of mutation relative to DNA adduct burden was apparent below 5 mg/kg B[*a*]P (DNA adduct level of 2456.24 attamole-days/ug DNA).

DISCUSSION

The potential lung cancer risk associated with B[*a*]P exposure through the environment and smoking is a significant health concern (DeMarini et al. 2001). In fact, the International Agency for Research on Cancer has recently characterized B[*a*]P as a known human carcinogen (Straif et al. 2005). Human exposure to B[*a*]P is generally long-term and variable. In human lung tumors, B[*a*]P-DNA adduct levels range from 0.5 to 9.9 adducts/10^8 bp, as measured by high performance liquid chromatography-fluorescence detection (HPLC-FD) (Alexandrov et al. 1992; Rojas et al. 1998) or 2-172 adducts/10^8 bp, as measured by high performance liquid chromatography-synchronous fluorescence spectroscopy (HPLC-SFS) (Andreassen et al. 1996; Boysen and Hecht

2003). Currently, epidemiological studies specifically linking B[*a*]P *per se* to carcinogenic effects are lacking, partly because B[*a*]P is just one component of PAH mixtures and it is difficult to separate carcinogenicity due to B[*a*]P from that potentially induced by other PAHs. However, the carcinogenic risk for B[*a*]P has been assessed in multiple animal studies (EPA 1994 or http://www.epa.gov/NCEA/iris/subst/0136.htm).

The lung carcinogenicity of B[*a*]P has been examined in one- and two-year tumor bioassays (Ross et al. 1995; Yan et al. 2006; Yan et al. 2005). A 50 mg/kg dose of B[*a*]P was shown to cause a significant increase in lung tumors eight months after treatment (Nesnow et al. 1995). To assess the risk of B[*a*]P exposure and inform B[*a*]P mode of action (MOA), the induction of DNA adducts at different B[*a*]P doses (from 5 to 200 mg/kg) has been measured. 100 mg/kg B[*a*]P greatly increased the level of B[*a*]P-DNA adducts (Mass et al. 1993). The most frequent B[*a*]P-DNA adduct is the one derived from BPDE. B[*a*]P-DNA adducts reach a peak level 3-5 days after treatment, then gradually decrease to 30-40% of the maximal level by 4 weeks (Banasiewicz et al. 2004; Ross et al. 1995). Such studies have not addressed the proportion of the DNA adducts that are converted to mutations or how that conversion is related to dose.

Using the ACB-PCR methodology, it was possible to measure the induction of K-*Ras* codon 12 GGT to TGT and GGT to GAT mutations at low doses of B[*a*]P and to characterize the relationships between B[*a*]P dose, DNA adducts, and K-*Ras* mutations. The K-*Ras* codon GAT mutation was examined because it is the most frequent spontaneous mutation observed in A/J mouse lung tumors and its role in lung carcinogenesis has been confirmed in transgenic models (Fisher et al. 2001; Jackson et al. 2001; Johnson et al. 2001). K-*Ras* codon 12 TGT mutation was examined because it is

the most common B[*a*]P-induced mutation in A/J mouse lung tumors (Ross and Nesnow 1999). Significant dose-related increases were observed for both mutations and the increases were approximately linear at low dose (0.05 - 5 mg/kg). Additionally, the induction of K-*Ras* MF was similar in magnitude for both mutations. The codon 12 TGT MF increased ~9-fold (from 3.88 X 10^{-4} in control group to 3.5 X 10^{-3} in the 50 mg/kg B[*a*]P dose group) and the K-*Ras* codon 12 GAT MF increases 10.7-fold (from 8.38 X 10^{-7} in control group to 8.99 X 10^{-6} in the 50 mg/kg B[*a*]P dose group).

Because B[*a*]P-induced K-*Ras* mutations were quantified as a function of administered B[*a*]P dose, these data can be evaluated relative to the DNA adduct levels induced by the same B[*a*]P exposures. BPDE-type B[*a*]P-DNA adduct levels of 420-430 or 600-830 amol/ug DNA were measured two and three days, respectively, after exposure in A/J mice exposed at low B[*a*]P dose (50 mg/kg) by *i.p.* injection (Banasiewicz et al. 2004). This damage level can also be expressed as ~1 adduct/10^7 nucleotides, an adduct level potentially induced by environmental exposures to PAHs (Banasiewicz et al. 2004). Ross *et al.* (Ross et al. 1995) performed a detailed timecourse analysis of B[*a*]P-induced DNA adducts by ^{32}P-postlabeling. They then integrated the area under the curve to calculate the time-integrated DNA adduct level (TIDAL) induced by different doses of B[*a*]P (5 – 200 mg/kg), as a measure of total DNA adduct burden. This study employed the same rodent model and route of exposure as the present study. Thus, the induced DNA adduct burden was directly relatable to the induced K-*Ras* MF measurements at doses of 0, 5, and 50 mg/kg (Figure 7). Figure 7 shows, for the first time, how the K-*Ras* codon 12 TGT and GAT mutations increased as a function of DNA adduct burden.. Figures 4 and 7 illustrate an apparent transition at ~5mg/kg B[*a*]P in the K-*Ras*

mutational response to B[*a*]P dose or B[*a*]P-induced DNA adduct level, with a dampening of the mutational response above 5 mg/kg.

The finding that the K-*Ras* codon 12 TGT and GAT mutations exhibit approximately the same fold increase relative to dose or DNA adduct burden may provide some insight into the mechanism of B[*a*]P-induced carcinogenesis. There are at least two mechanistic explanations for the B[*a*]P-induced increase in K-*Ras* MF. One possibility is that B[*a*]P adducts are induced at the first or second guanine of codon 12 in the K-*Ras* gene. A second possibility is that B[*a*]P adducts form at a variety of other sites that have phenotypic consequences, the non-K-*Ras* mutant cells then interact with pre-existing K-*Ras* mutants, and this interaction results in the clonal amplification of K-*Ras* mutant cells and progression toward carcinogenesis. Information about mutational specificity of B[*a*]P may be useful in distinguishing between these two possibilities. B[*a*]P has been shown to form adducts primarily at N-2 of guanine and to preferentially induce G to T mutations (Kohler et al. 1991; Mackay et al. 1992; Mass et al. 1993). Yet, in the current study, the codon 12 GGT to TGT and GGT to GAT mutations had strikingly similar dose-response curves, and approximately the same fold-increase between the control and 50 mg/kg treatment groups. This result is more consistent with the second possibility, where the K-*Ras* MF is a functional reporter (*i.e.*, reporter of tumor initiation or progression) of the B[*a*]P-induced mutational load within the tissue. However, the possibility that both mechanisms are operating simultaneously cannot be ruled out.

The fact that the K-*Ras* mutational response increases relative to the DNA adduct burden (TIDAL values at particular doses, see Figure 7) does not mean that B[*a*]P

induces tumors solely through a mutagenic MOA. A number of studies have shown that B[*a*]P and BPDE may also have epigenetic effects. Specifically, B[*a*]P exposure increases progression through the cell cycle, an effect mediated by active c-Jun via the *p*53-dependent PI3K/Akt/ERK pathway in human embryo lung fibroblasts (Jiao et al. 2008). B[*a*]P mimics the IGF-I receptor signal transduction pathway by inducing the phosphorylation of IGF-IRβ, IRS-1 and Shc, and increases cell survival by PI3K activation in human mammary epithelial cells (Tannheimer et al. 1998). BPDE increases the ERK1/2 and p38 MAPK activities resulting in the *p*53 accumulation in mouse epidermal cells (Mukherjee and Sikka 2006). BPDE also increases the intracellular Ca^{2+} concentration and induces phosphorylation of epidermal growth factor receptor (EGFR), which leads to the attenuation of apoptosis signaling in a human mammary epithelial cell line (Burdick et al. 2006). Therefore, in addition to inducing mutations in different tumor suppress genes or oncogenes (like *p53*, K-*Ras*, and EGFR), B[*a*]P may also alter the cell microenvironment by multiple mechanisms to initiate polyclonal tumor development (Ding et al. 2008; Fisher et al. 2001; Parsons 2008; Shimmyo et al. 2008).

One unexpected result was that the spontaneous K-*Ras* codon 12 TGT MF in A/J mice was remarkably high. It has been concluded that a spontaneous mutant frequency of ~10^{-7} per basepair is typically observed for neutral reporter genes in phenotypic selection assays (McKinzie et al. 2001). A similar frequency of spontaneous mutation was observed for the K-*Ras* codon 12 GAT mutation, 8.38 X 10^{-7}. However, the spontaneous frequency of the K-*Ras* codon 12 TGT mutation was several orders of magnitude higher at 3.88 X 10^{-4}, which translates into one mutant per every 1,288 lung cells. This was surprising because 59% of the K-*Ras* codon 12 mutations found in

spontaneous A/J mice lung adenomas are GAT mutations (Ross and Nesnow 1999). This result was not explained by technical error because multiple ACB-PCR assays performed on DNA isolated from the left and right lungs gave the same result, and the same first-round PCR products were used as template for both the TGT and GAT mutational analyses. Thus, the overrepresentation of GAT mutation in spontaneous lung tumors may indicate that the K-*Ras* codon 12 GAT mutation confers a greater selective advantage to mutant cells than the TGT mutation.

The A/J mouse is the most sensitive strain in terms of spontaneous and chemically-induced lung tumor development. This sensitivity is thought to arise due to a 37-basepair deletion in the second intron of K-*Ras* (Tuveson and Jacks 1999; You et al. 1992). The deleted K-*Ras* gene is expressed earlier in development than the wild-type gene, presumably providing a larger timeframe for the selection of K-*Ras* mutations during a period when cell proliferation rates are high. This may explain the high spontaneous K-*Ras* codon 12 TGT MFs observed in A/J mice. In future studies, it would be informative to compare the spontaneous levels of the K-*Ras* mutations in A/J mice to that of lung tumor-resistant mouse strains, such as C3H or C57BL/6.

Because only the highest dose used in the present study is sufficient to induce a significant increase in lung tumors in the strain A/J model, the K-*Ras* codon 12 TGT and GAT MFs cannot be plotted relative to tumor response. It is important to note, however, that a statistically-significant increase in K-*Ras* TGT MF was detected one month after treatment with a B[*a*]P dose of 5 mg/kg, whereas a statistically significant increase in adenomas was detected using 50 mg/kg, but not with 20 mg/kg, 8 months after exposure (Mass et al. 1993; Nesnow et al. 1995). Thus, if specific tumor-associated mutations are

selected based on known tumor etiology, such mutations should be stable and sensitive reporters of chemical effect and carcinogenic potential. Further, ACB-PCR measurement of tumor-associated mutations may provide a measure of carcinogenic potential at doses lower than are sufficient to demonstrate tumor response, as well as provide information on how dose and DNA adduct levels relate to the levels of particular tumor-associated mutations.

ACKNOWLEDGMENTS

The authors thank Drs. Frederick Beland and Robert Heflich for their critical review of this manuscript. We thank Dr. Page McKinzie and Tracie Verkler for their excellent technical assistance. This study was conducted as part of an Interagency Agreement between the Food and Drug Administration (FDA) and the Environmental Protection Agency (EPA). The contents of this manuscript do not necessarily reflect the views or polices of the U.S. EPA or the U.S. FDA, nor does the mention of trade names or commercial products constitute endorsement or recommendation for use.

REFERENCES

Ahrendt SA, Decker PA, Alawi EA, Zhu Yr YR, Sanchez-Cespedes M, Yang SC, Haasler GB, Kajdacsy-Balla A, Demeure MJ, Sidransky D. 2001. Cigarette smoking is strongly associated with mutation of the K-ras gene in patients with primary adenocarcinoma of the lung. Cancer 92(6):1525-30.

Alexandrov K, Rojas M, Geneste O, Castegnaro M, Camus AM, Petruzzelli S, Giuntini C, Bartsch H. 1992. An improved fluorometric assay for dosimetry of benzo(a)pyrene diol-epoxide-DNA adducts in smokers' lung: comparisons with total bulky adducts and aryl hydrocarbon hydroxylase activity. Cancer Res 52(22):6248-53.

Andreassen A, Kure EH, Nielsen PS, Autrup H, Haugen A. 1996. Comparative synchronous fluorescence spectrophotometry and 32P-postlabeling analysis of PAH-DNA adducts in human lung and the relationship to TP53 mutations. Mutat Res 368(3-4):275-82.

Baird WM, Hooven LA, Mahadevan B. 2005. Carcinogenic polycyclic aromatic hydrocarbon-DNA adducts and mechanism of action. Environ Mol Mutagen 45(2-3):106-14.

Banasiewicz M, Nelson G, Swank A, Grubor N, Ross J, Nesnow S, Kofeler H, Small GJ, Jankowiak R. 2004. Identification and quantitation of benzo[a]pyrene-derived DNA adducts formed at low adduction level in mice lung tissue. Anal Biochem 334(2):390-400.

Boysen G, Hecht SS. 2003. Analysis of DNA and protein adducts of benzo[a]pyrene in human tissues using structure-specific methods. Mutat Res 543(1):17-30.

Burdick AD, Ivnitski-Steele ID, Lauer FT, Burchiel SW. 2006. PYK2 mediates anti-apoptotic AKT signaling in response to benzo[a]pyrene diol epoxide in mammary epithelial cells. Carcinogenesis 27(11):2331-40.

DeMarini DM, Landi S, Tian D, Hanley NM, Li X, Hu F, Roop BC, Mass MJ, Keohavong P, Gao W and others. 2001. Lung tumor KRAS and TP53 mutations in nonsmokers reflect exposure to PAH-rich coal combustion emissions. Cancer Res 61(18):6679-81.

Dimashki M, Lim LH, Harrison RM, Harrad S. 2001. Temporal trends, temperature dependence, and relative reactivity of atmospheric polycyclic aromatic hydrocarbons. Environ Sci Technol 35(11):2264-7.

Ding L, Getz G, Wheeler DA, Mardis ER, McLellan MD, Cibulskis K, Sougnez C, Greulich H, Muzny DM, Morgan MB and others. 2008. Somatic mutations affect key pathways in lung adenocarcinoma. Nature 455(7216):1069-75.

Europe WHOROf. 1987. Polynuclear aromatic hydrocarbons (PAH). Air Quality Guidelines for Europe. Copenhagen. p 105-117.

Fisher GH, Wellen SL, Klimstra D, Lenczowski JM, Tichelaar JW, Lizak MJ, Whitsett JA, Koretsky A, Varmus HE. 2001. Induction and apoptotic regression of lung adenocarcinomas by regulation of a K-Ras transgene in the presence and absence of tumor suppressor genes. Genes Dev 15(24):3249-62.

Hakura A, Tsutsui Y, Sonoda J, Mikami T, Tsukidate K, Sagami F, Kerns WD. 1999. Multiple organ mutation in the lacZ transgenic mouse (Muta mouse) 6 months after oral treatment (5 days) with benzo[a]pyrene. Mutat Res 426(1):71-7.

Jackson EL, Willis N, Mercer K, Bronson RT, Crowley D, Montoya R, Jacks T, Tuveson DA. 2001. Analysis of lung tumor initiation and progression using conditional expression of oncogenic K-ras. Genes Dev 15(24):3243-8.

Jiao S, Liu B, Gao A, Ye M, Jia X, Zhang F, Liu H, Shi X, Huang C. 2008. Benzo(a)pyrene-caused increased G1-S transition requires the activation of c-Jun through p53-dependent PI-3K/Akt/ERK pathway in human embryo lung fibroblasts. Toxicol Lett 178(3):167-75.

Johnson L, Mercer K, Greenbaum D, Bronson RT, Crowley D, Tuveson DA, Jacks T. 2001. Somatic activation of the K-ras oncogene causes early onset lung cancer in mice. Nature 410(6832):1111-6.

Kohler SW, Provost GS, Fieck A, Kretz PL, Bullock WO, Sorge JA, Putman DL, Short JM. 1991. Spectra of spontaneous and mutagen-induced mutations in the lacI gene in transgenic mice. Proc Natl Acad Sci U S A 88(18):7958-62.

Mackay W, Benasutti M, Drouin E, Loechler EL. 1992. Mutagenesis by (+)-anti-B[a]P-N2-Gua, the major adduct of activated benzo[a]pyrene, when studied in an Escherichia coli plasmid using site-directed methods. Carcinogenesis 13(8):1415-25.

Mass MJ, Jeffers AJ, Ross JA, Nelson G, Galati AJ, Stoner GD, Nesnow S. 1993. Ki-ras oncogene mutations in tumors and DNA adducts formed by benz[j]aceanthrylene and benzo[a]pyrene in the lungs of strain A/J mice. Mol Carcinog 8(3):186-92.

McKinzie PB, Delongchamp RR, Chen T, Parsons BL. 2006. ACB-PCR measurement of K-ras codon 12 mutant fractions in livers of Big Blue rats treated with N-hydroxy-2-acetylaminofluorene. Mutagenesis 21(6):391-7.

McKinzie PB, Delongchamp RR, Heflich RH, Parsons BL. 2001. Prospects for applying genotypic selection of somatic oncomutation to chemical risk assessment. Mutat Res 489(1):47-78.

Menzie CA, Potocki BB, Santodonato J. 1992. Exposure to carcinogenic PAHs in the environment. Environmental Science & Technology 26:1278-1284.

Mukherjee JJ, Sikka HC. 2006. Attenuation of BPDE-induced p53 accumulation by TPA is associated with a decrease in stability and phosphorylation of p53 and downregulation of NFkappaB activation: role of p38 MAP kinase. Carcinogenesis 27(3):631-8.

Naumova YY, Eisenreich SJ, Turpin BJ, Weisel CP, Morandi MT, Colome SD, Totten LA, Stock TH, Winer AM, Alimokhtari S and others. 2002. Polycyclic aromatic hydrocarbons in the indoor and outdoor air of three cities in the U.S. Environ Sci Technol 36(12):2552-9.

Nesnow S, Ross JA, Stoner GD, Mass MJ. 1995. Mechanistic linkage between DNA adducts, mutations in oncogenes and tumorigenesis of carcinogenic environmental polycyclic aromatic hydrocarbons in strain A/J mice. Toxicology 105(2-3):403-13.

Parsons BL. 2008. Many different tumor types have polyclonal tumor origin: evidence and implications. Mutat Res 659(3):232-47.

Parsons BL, Beland FA, Von Tungeln LS, Delongchamp RR, Fu PP, Heflich RH. 2005. Levels of 4-aminobiphenyl-induced somatic H-ras mutation in mouse liver DNA correlate with potential for liver tumor development. Mol Carcinog 42(4):193-201.

Reynolds SH, Anderson MW. 1991. Activation of proto-oncogenes in human and mouse lung tumors. Environ Health Perspect 93:145-8.

Rodenhuis S, Slebos RJ, Boot AJ, Evers SG, Mooi WJ, Wagenaar SS, van Bodegom PC, Bos JL. 1988. Incidence and possible clinical significance of K-ras oncogene activation in adenocarcinoma of the human lung. Cancer Res 48(20):5738-41.

Rojas M, Alexandrov K, Cascorbi I, Brockmoller J, Likhachev A, Pozharisski K, Bouvier G, Auburtin G, Mayer L, Kopp-Schneider A and others. 1998. High benzo[a]pyrene diol-epoxide DNA adduct levels in lung and blood cells from individuals with combined CYP1A1 MspI/Msp-GSTM1*0/*0 genotypes. Pharmacogenetics 8(2):109-18.

Ross JA, Nelson GB, Wilson KH, Rabinowitz JR, Galati A, Stoner GD, Nesnow S, Mass MJ. 1995. Adenomas induced by polycyclic aromatic hydrocarbons in strain A/J mouse lung correlate with time-integrated DNA adduct levels. Cancer Res 55(5):1039-44.

Ross JA, Nesnow S. 1999. Polycyclic aromatic hydrocarbons: correlations between DNA adducts and ras oncogene mutations. Mutat Res 424(1-2):155-66.

Shimmyo T, Okada A, Hashimoto T, Kobayashi Y, Miyagi Y, Ishikawa Y, Nakagawa K, Osada H, Tsuchiya E. 2008. Etiologic value of p53 mutation spectra and differences with histology in lung cancers. Cancer Sci 99(2):287-95.

Straif K, Baan R, Grosse Y, Secretan B, El Ghissassi F, Cogliano V. 2005. Carcinogenicity of polycyclic aromatic hydrocarbons. Lancet Oncol 6(12):931-2.

Tannheimer SL, Ethier SP, Caldwell KK, Burchiel SW. 1998. Benzo[a]pyrene- and TCDD-induced alterations in tyrosine phosphorylation and insulin-like growth

factor signaling pathways in the MCF-10A human mammary epithelial cell line. Carcinogenesis 19(7):1291-7.

Tretyakova N, Matter B, Jones R, Shallop A. 2002. Formation of benzo[a]pyrene diol epoxide-DNA adducts at specific guanines within K-ras and p53 gene sequences: stable isotope-labeling mass spectrometry approach. Biochemistry 41(30):9535-44.

Tuveson DA, Jacks T. 1999. Modeling human lung cancer in mice: similarities and shortcomings. Oncogene 18(38):5318-24.

Verkler TL, Delongchamp RR, Couch LH, Miller BJ, Warbritton A, Mellick PW, Howard PC, Parsons BL. 2008a. Populations of p53 codon 270 CGT to TGT mutant cells in SKH-1 mouse skin tumors induced by simulated solar light. Mol Carcinog.

Verkler TL, Delongchamp RR, Miller BJ, Webb PJ, Howard PC, Parsons BL. 2008b. Simulated solar light-induced p53 mutagenesis in SKH-1 mouse skin: A dose-response assessment. Mol Carcinog.

Yan Y, Wang Y, Tan Q, Hara Y, Yun TK, Lubet RA, You M. 2006. Efficacy of polyphenon E, red ginseng, and rapamycin on benzo(a)pyrene-induced lung tumorigenesis in A/J mice. Neoplasia 8(1):52-8.

Yan Y, Wang Y, Tan Q, Lubet RA, You M. 2005. Efficacy of deguelin and silibinin on benzo(a)pyrene-induced lung tumorigenesis in A/J mice. Neoplasia 7(12):1053-7.

You M, Candrian U, Maronpot RR, Stoner GD, Anderson MW. 1989. Activation of the Ki-ras protooncogene in spontaneously occurring and chemically induced lung tumors of the strain A mouse. Proc Natl Acad Sci U S A 86(9):3070-4.

You M, Wang Y, Stoner G, You L, Maronpot R, Reynolds SH, Anderson M. 1992. Parental bias of Ki-ras oncogenes detected in lung tumors from mouse hybrids. Proc Natl Acad Sci U S A 89(13):5804-8.

Figure 1. Diagram of ACB-PCR priming strategy. The approximate position and partial sequences of the upstream primer (UP), the mutant-specific primer (MSP), and the block primer (BP) are depicted for the K-*Ras* codon 12 GGT to TGT ACB-PCR (A) and the K-*Ras* codon 12 GGT to GAT ACB-PCR (B).

Figure 2. ACB-PCR measurement of the K-*Ras* codon 12 GGT to TGT MF. PCR products generated from the 50 A/J mice lung DNA samples were analyzed in triplicate by ACB-PCR, along with MF standards, including a no mutant control and no DNA control. The ACB-PCR results of two of three replicate analyses (Exp. 1 and Exp. 2) are shown, samples 1-25 (A) and samples 26-50 (B)

Figure 3. An increasing trend in K-*Ras* codon 12 GGT to TGT MF with increasing B[*a*]P dose is evident despite considerable interanimal variability (A) The average of the replicate ACB-PCR measurements from each animal is plotted. The dash line denotes the geometric mean MF. (B) The base 10 log of K-*Ras* TGT MF is plotted relative to the base 10 log of dose. Error bars indicate the standard error of the geometric mean MF. Dash lines indicate the 95% confidence interval.

Figure 4. An approximately linear increase in K-*Ras* geometric mean MF occurs over the 0.05 to 5 mg/kg B[*a*]P dose range. (A) K-*Ras* TGT MF. (B) K-*Ras* GAT MF. Error bars indicate the standard error of the geometric mean, asterisks indicate treatment groups significantly different from control.

Figure 5. ACB-PCR measurement of the K-*Ras* codon 12 GGT to GAT MF. PCR products generated from the 50 A/J mice lung DNA samples were analyzed in triplicate by ACB-PCR, along with MF standards, including a no mutant control and no DNA control. The ACB-PCR results of two of three replicate analyses (Exp.1 and Exp. 2) are shown.

Figure 6. Mouse lung K-*Ras* codon 12 GGT to GAT MF increases as a function of B[*a*]P dose. (A) The average of the three replicate ACB-PCR measurements from each animal is plotted. The dash line denotes the geometric mean MF, the asterisk indicates the treatment group significantly different from control. (B) The base 10 log of K-*Ras* GAT MF is plotted relative to the base 10 log of dose. Error bars indicate the standard error of the geometric mean MF. Dash lines indicate the 95% confidence interval.

Figure 7. K-*Ras* codon 12 GGT to TGT and GGT to GAT MFs increases as a function of B[*a*]P-DNA adduct level. K-*Ras* codon 12 TGT MF (A) and GAT MF (B) are plotted as a function of B[*a*]P-induced TIDAL value (Ross et al. 1995)

Table 1. Summary of K-*Ras* codon 12 GGT to TGT mutation and GGT to GAT MF measurements in A/J mice lung DNA samples

B[*a*]P treatment (mg/kg)	K-*Ras* codon 12 TGT mutation			K-*Ras* codon 12 GAT mutation		
	Geometric Mean MF	Median MF	Mutation prevalence (%)[a]	Geometric Mean MF	Median MF	Mutation prevalence (%)[a]
Control	3.88×10^{-4}	3.97×10^{-4}	100	8.38×10^{-7}	1.15×10^{-6}	0
0.05	3.56×10^{-4}	4.63×10^{-4}	100	1.47×10^{-6}	1.44×10^{-6}	0
0.5	6.19×10^{-4}	9.89×10^{-4}	100	2.19×10^{-6}	1.95×10^{-6}	10
5	2.02×10^{-3}	3.81×10^{-3}	100	5.71×10^{-6}	5.33×10^{-6}	20
50	3.50×10^{-3}	5.32×10^{-3}	100	8.99×10^{-6}	9.18×10^{-6}	50

[a] **Mutation prevalence is the percentage of samples with K-*Ras* MF above the limit of reliable ACB-PCR quantitation, 10^{-5}.**

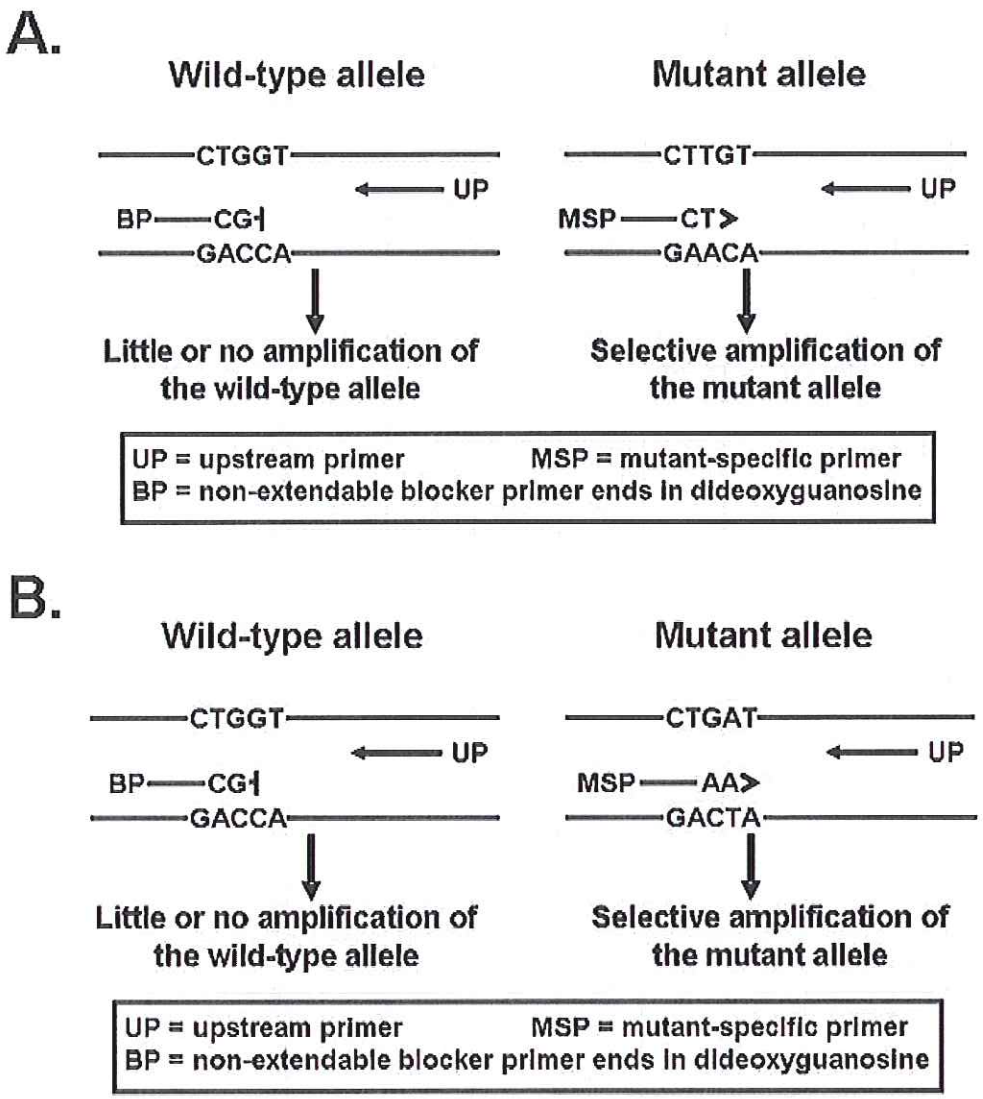

Figure 1
53x59mm (300 x 300 DPI)

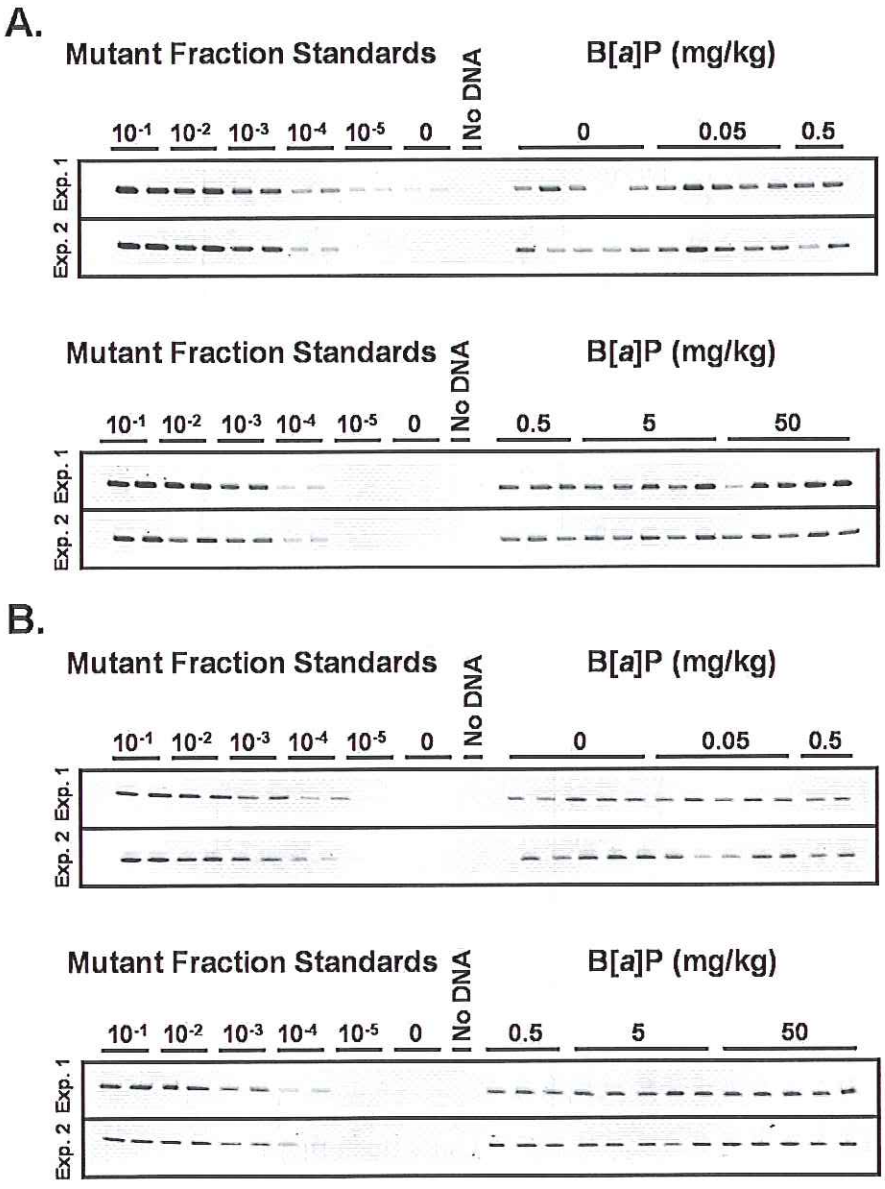

Figure 2
409x555mm (72 x 72 DPI)

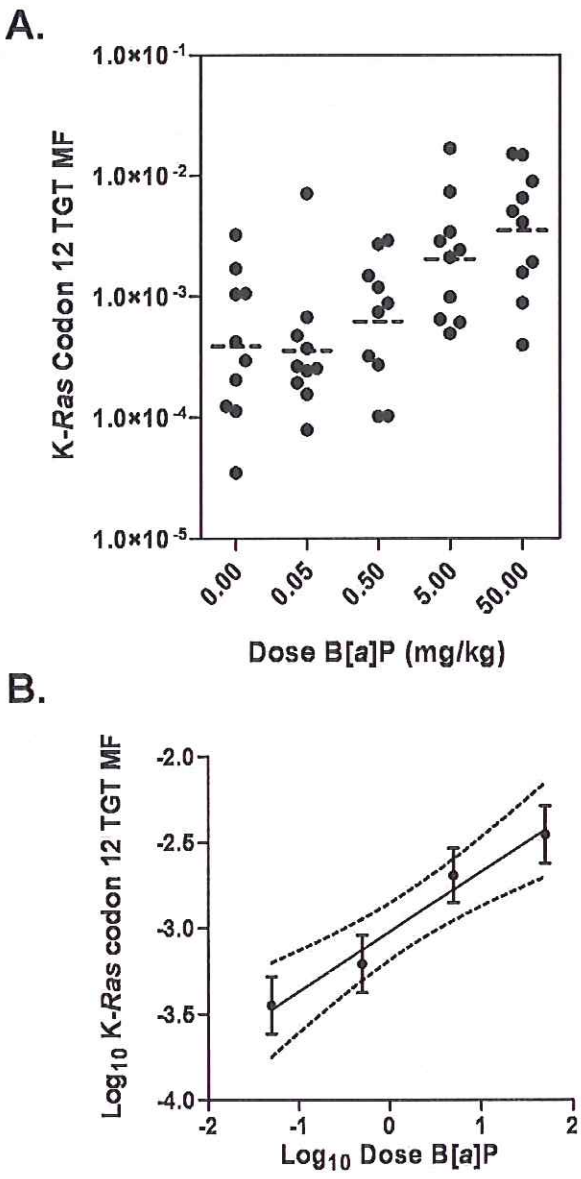

Figure 3
72x146mm (300 x 300 DPI)

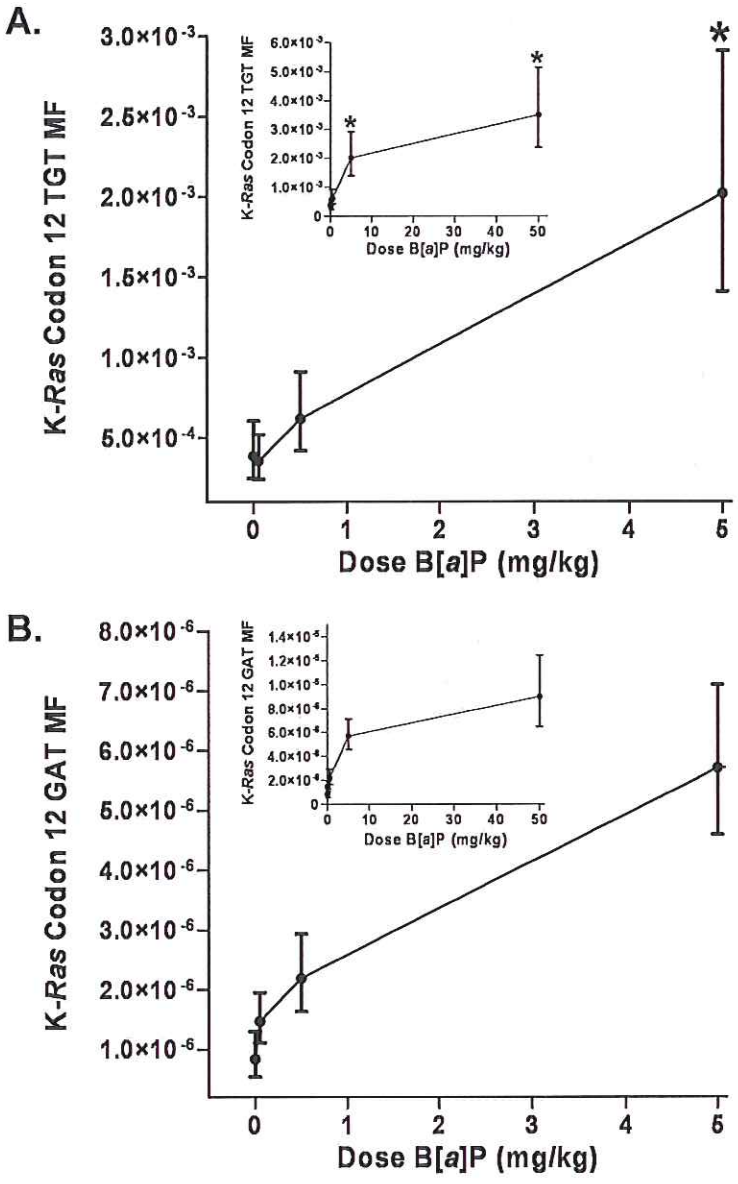

Figure 4
421x668mm (72 x 72 DPI)

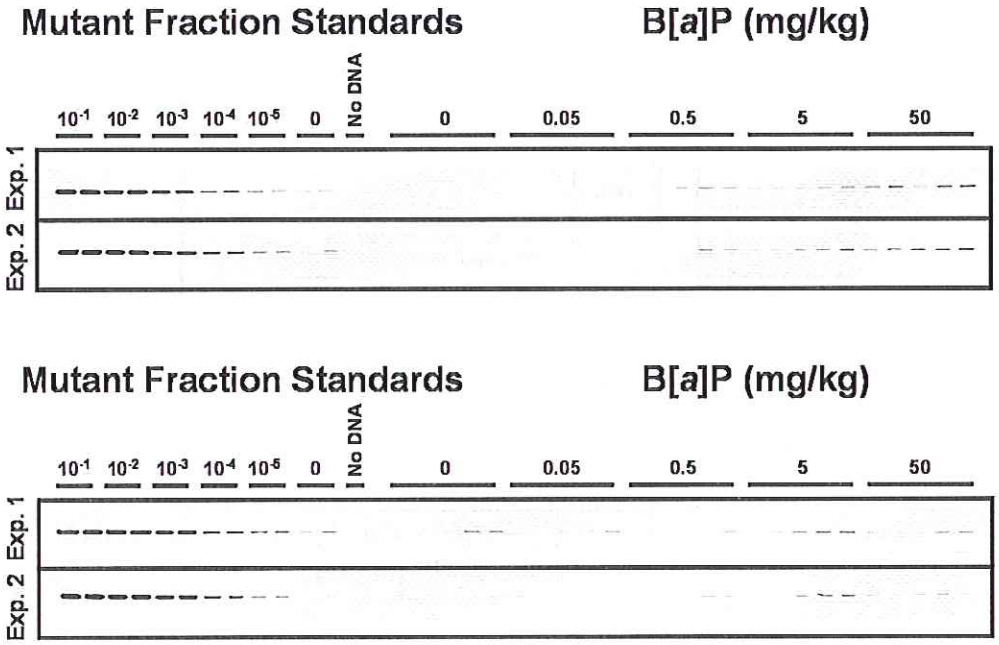

Figure 5
385x248mm (72 x 72 DPI)

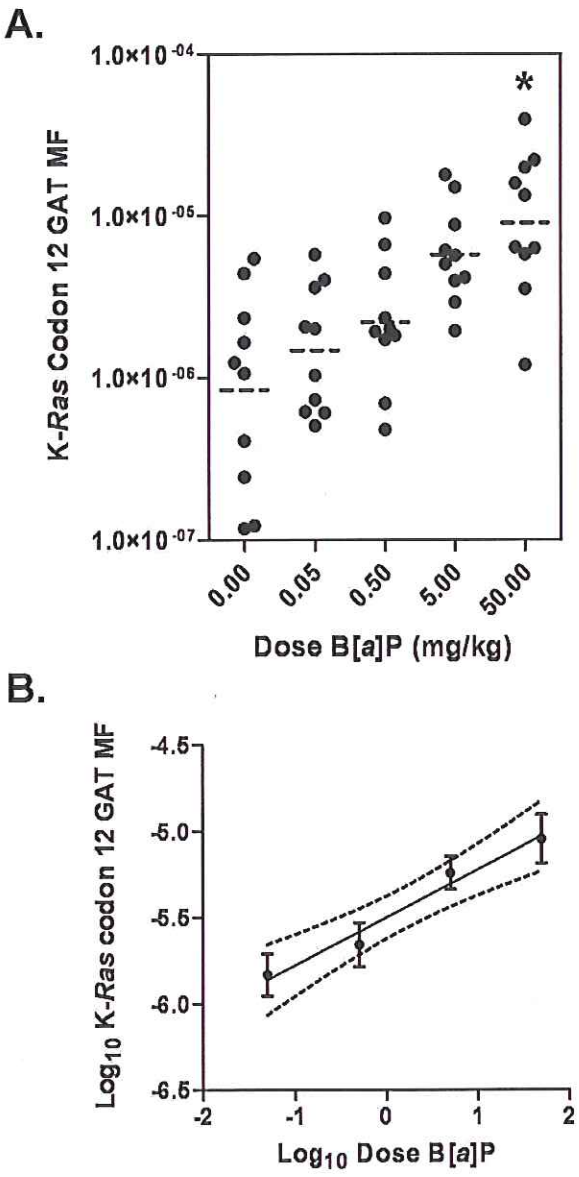

Figure 6
327x610mm (72 x 72 DPI)

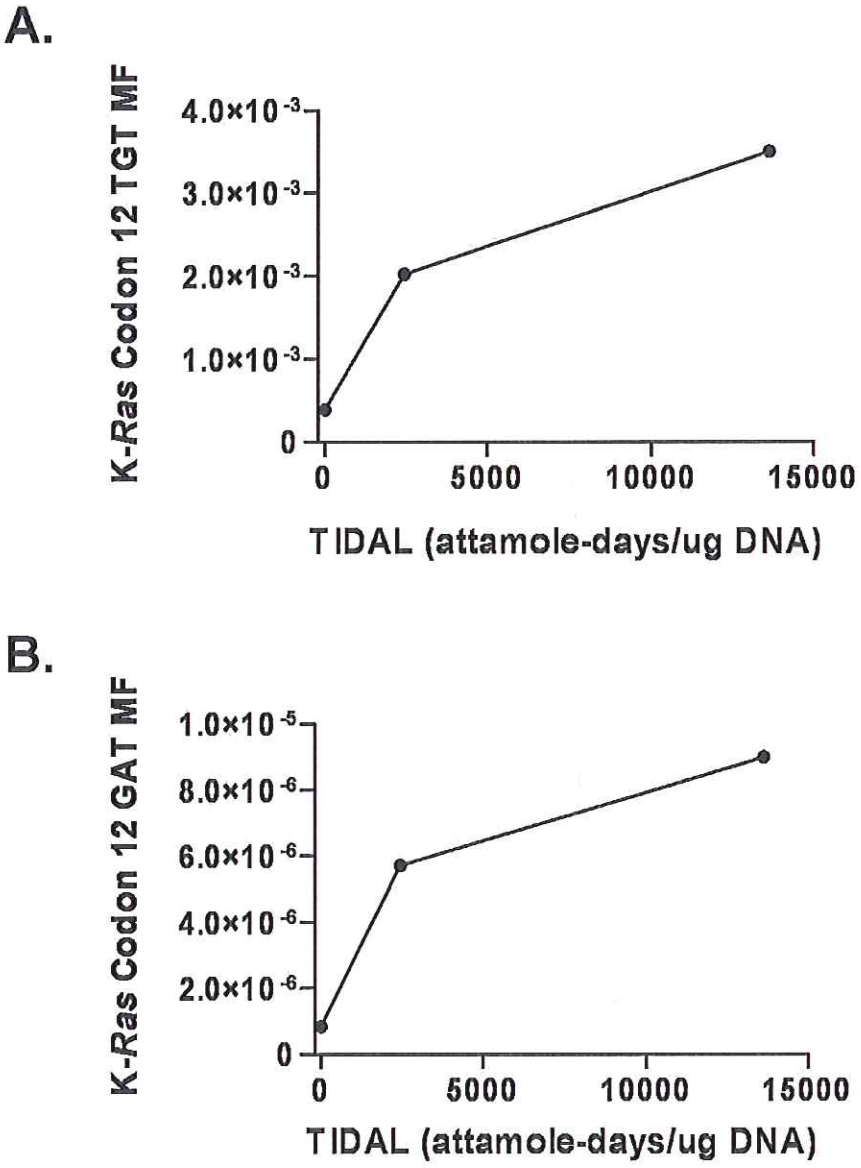

Figure 7
85x117mm (300 x 300 DPI)